Environmentally Friendly Flame-Retardant Composites

Vom Promotionsausschuss der Technischen Universität Hamburg

zur Erlangung des akademischen Grades
Doktor-Ingenieurin (Dr.-Ing.)

genehmigte Dissertation (Monographie)

von
Melissa Walter
aus Esslingen am Neckar

2026

Vorsitzender des Prüfungsausschusses:	Prof. Dr.-Ing. habil. Stefan Heinrich (Technische Universität Hamburg)
Gutachter:	Prof. Dr.-Ing. habil. Bodo Fiedler (Technische Universität Hamburg) Prof. Dr.-Ing. Hans-Peter Heim (Universität Kassel)
Tag der mündlichen Prüfung:	27.07.2026

Technisch-Wissenschaftliche Schriftenreihe

Herausgeber:
Prof. Dr.-Ing. habil. Bodo Fiedler

Anschrift:
Technische Universität Hamburg
Institut für Kunststoffe und Verbundwerkstoffe
Denickestraße 15
21073 Hamburg

Band 50:
Environmentally Friendly Flame-Retardant Composites
DOI: https://doi.org/10.15480/882.17730

Melissa Walter
https://orcid.org/0009-0009-0307-4594

1. Auflage
Hamburg 2026

ISSN 2625-6029

Copyright Melissa Walter 2026

Dieses Werk ist lizensiert unter einer Creative Commons Namensnennung 4.0 International Lizenz (https://creativecommons.org/licenses/by/4.0/).

Bibliographische Information der Deutschen Nationalbibliothek: Die deutsche Nationalbibliothek verzeichnet diese Publikation in der Deutschen Nationalbibliothek; detaillierte Informationen sind im Internet über dnb.de abrufbar.

Abstract

Fibre-reinforced polymers (FRP) offer enormous lightweight potential due to their outstanding specific mechanical properties and the possibility of load path-oriented design. Therefore, they are widely used in mobility applications. However, these applications usually demand high levels of flame resistance. Since typical matrix systems, such as epoxy resins, are highly flammable, this also applies to the resulting FRPs. Each polymer system reacts differently to modification with flame retardant additives. For example, reductions in mechanical, thermal or chemical properties are often reported, which may also have a negative impact on the composite. Furthermore, the systems used today are almost always harmful to the environment or health. Hence, there is an urgent need for the further development of FRPs that are both flame-retardant and environmentally friendly. This is the overarching aim of this work, from which the following research hypothesis is derived:

High-performance composites can be designed flame-retardant and eco-friendly with compatible thermo-mechanical properties.

Three different approaches are developed and addressed to confirm the hypothesis. The first chapter explores the approach of modifying only the outermost layers of an FRP with flame retardants, as the surfaces are most exposed in the event of a fire. The idea of combining partially pre-cured and flame-retardant modified laminate layers with a common infusion process not only allows affordable and variable manufacturing but also saves resources and preserves mechanical properties of the FRPs.

In order to achieve the objective of environmentally friendly composites, the matrix materials commonly used in FRPs themselves offer potential to reduce effects on the environment and health. Therefore, this work focuses extensively on the development of environmentally friendly matrix materials by replacing harmful chemical constituents with biomolecules. Among other findings, it has

been demonstrated that, e.g., amino acids can achieve competitive properties as curing agents for epoxies under appropriate conditions. This primarily involves the targeted use of thermokinetic methods to determine suitable material compositions and their curing processes. In this context, in-situ and ex-situ curing-state validation methods were applied. Furthermore, it has been demonstrated, that fine dispersion of the powdered amino acids in the liquid resin systems is an essential prerequisite for manufacturing.

By studying the thermo-mechanical behaviour of various stoichiometic variations, it has been possible to postulate likely reaction mechanisms. Finally, aging studies in water, solvents and oil demonstrate that the examined amino-acid cured epoxies show good long-term durability and media resistance, which is a requirement for many applications (e.g., mobility sector). Based on the long-term tests carried out, no reduction in performance under typical operating conditions was observed in comparison with conventional epoxy resins. Only when stored in water at 50 °C or above, excessive water absorption and a significant reduction in thermo-mechanical properties were determined.

Today, flame-retardancy in polymers is a much-discussed topic, as it often involves the use of hazardous and environmentally harmful substances. Apart from the ban of some halogenated flame retardants due to their negative impact on the environment, the currently preferred phosphorus-based flame retardants also raise some concerns. On the one hand, political dependencies must be critically examined, while on the other hand, mining of phosphate ores also poses risks to humans and the environment. Therefore, the third chapter combines the approaches of the other chapters and examines the use of suitable biomolecules as flame retardants. It is shown that amino acid-cured epoxy resins also stand out favourably in terms of their flame retardant properties. They perform better than unmodified commercial epoxies in flame tests and simultaneously exhibit synergies with additional flame retardants. Consequently, it is possible to reduce the amount of flame retardants required to achieve the necessary classifications, which in turn reduces the negative impact on thermo-mechanical properties as well.

Therefore, this thesis presents various approaches that can be used alone or in combination to achieve flame-retardant and environmentally friendly FRPs. Thus, the insights can serve as a toolbox for tailored composites.

Kurzfassung

Faser-Kunststoff-Verbunde (FKV) bieten aufgrund ihrer hervorragenden spezifischen mechanischen Eigenschaften und der Möglichkeit einer lastpfadorientierten Gestaltung ein enormes Leichtbaupotenzial. Daher werden sie häufig in Mobilitätsanwendungen eingesetzt. Diese Anwendungen erfordern jedoch in der Regel eine hohe Flammwidrigkeit. Da typische Matrixsysteme wie Epoxidharze leicht entflammbar sind, gilt dies auch für die daraus hergestellten FKVs. Jedes Polymersystem reagiert unterschiedlich auf die Modifizierung mit flammhemmenden Additiven. So können beispielsweise die mechanischen, thermischen oder chemischen Eigenschaften beeinträchtigt werden, was sich auch negativ auf den Verbundwerkstoff auswirken kann. Darüber hinaus sind die heute verwendeten Systeme fast immer umwelt- oder gesundheitsschädlich. Es kann demnach ein dringender Bedarf an der Weiterentwicklung brandgeschützter und zugleich umweltfreundlicher FKV festgestellt werden. Dies stellt das übergeordnete Ziel der Arbeit dar, aus dem sich die folgende Forschungshypothese ableitet:

Hochleistungsverbundwerkstoffe können flammhemmend und umweltfreundlich gestaltet werden und gleichzeitig kompatible thermo-mechanische Eigenschaften aufweisen.

Es werden drei verschiedene Ansätze entwickelt und bewertet, um die Forschungshypothese dieser Dissertation zu überprüfen. Das erste Kapitel befasst sich mit dem Konzept, nur die äußersten Schichten eines FKV mit Flammschutzmitteln zu modifizieren, da diese Oberflächen im Brandfall am stärksten exponiert sind. Die Idee, teilweise vorgehärtete und flammschutzmodifizierte Laminatschichten mit einem gemeinsamen Infusionsverfahren zu kombinieren, ermöglicht nicht nur eine kostengünstige und variable Fertigung, sondern spart auch Ressourcen und erhält die mechanischen Eigenschaften der FKV.

Um das Ziel umweltfreundlicher Verbundwerkstoffe zu erreichen, bieten die üblicherweise in FRPs verwendeten Matrixmaterialien selbst ein großes Potenzial zur

Verringerung der Auswirkungen auf Umwelt und Gesundheit. Daher konzentriert sich diese Arbeit intensiv auf die Entwicklung umweltfreundlicher Matrixmaterialien, indem risikobehaftete chemische Bestandteile durch Biomoleküle ersetzt werden. Unter anderem wurde nachgewiesen, dass beispielsweise Aminosäuren unter geeigneten Bedingungen als Härter für Epoxide wettbewerbsfähige Eigenschaften erzielen können. Dabei geht es in erster Linie um den gezielten Einsatz thermokinetischer Methoden zur Bestimmung geeigneter Materialzusammensetzungen und deren Aushärtungsprozesse. In diesem Zusammenhang wurden sowohl In-situ- als auch Ex-situ-Verfahren zur Validierung des Aushärtungszustands angewendet. Darüber hinaus wurde gezeigt, dass eine feine Dispersion der pulverförmigen Aminosäuren in den flüssigen Harzsystemen eine wesentliche Voraussetzung für die Fertigung ist.

Durch die Untersuchung des thermo-mechanischen Verhaltens verschiedener stöchiometrischer Variationen konnten wahrscheinliche Reaktionsmechanismen postuliert werden. Schließlich zeigen Alterungsstudien in Wasser, Lösungsmitteln und Öl, dass die untersuchten aminohärtenden Epoxide eine gute Langzeitbeständigkeit und Medienbeständigkeit aufweisen, wodurch sie für die meisten Mobilitätsanwendungen geeignet sind. Auf der Grundlage der durchgeführten Langzeittests wurde im Vergleich zu herkömmlichen Epoxidharzen keine Leistungsminderung unter typischen Betriebsbedingungen festgestellt. Nur bei Lagerung in Wasser bei 50 °C oder darüber wurden eine übermäßige Wasseraufnahme und eine signifikante Verringerung der thermo-mechanischen Eigenschaften beobachtet.

Heutzutage ist der Flammschutz von Polymeren ein viel diskutiertes Thema, da dabei oft gefährliche und umweltschädliche Substanzen zum Einsatz kommen. Abgesehen vom Verbot einiger halogenierter Flammschutzmittel aufgrund ihrer negativen Auswirkungen auf die Umwelt birgen auch die derzeit bevorzugten Flammschutzmittel auf Basis von Phosphor Risiken. Einerseits müssen politische Abhängigkeiten kritisch hinterfragt werden, andererseits birgt der Abbau von Phosphaterzen ebenfalls Gefährdungspotential für Mensch und Umwelt. Daher kombiniert das dritte Kapitel die Ansätze der anderen Kapitel und untersucht die Verwendung geeigneter Biomoleküle als Flammschutzmittel. Es wird gezeigt, dass auch mit Aminosäuren gehärtete Epoxidharze hinsichtlich ihrer flammhemmenden Eigenschaften positiv hervorstechen. Sie schneiden in Flammtests besser ab als unmodifizierte handelsübliche Epoxide und zeigen gleichzeitig Synergien mit zusätzlichen Flammschutzmitteln. Folglich ist es möglich, die Menge an

Flammschutzmitteln zu reduzieren, die zur Erreichung der erforderlichen Klassifizierungen erforderlich ist, was wiederum die negativen Auswirkungen auf die thermo-mechanischen Eigenschaften verringert.

Die vorliegende Arbeit präsentiert demnach verschiedene Ansätze, die alleinig oder in Kombination zur Erzielung umweltfreundlicher und flammgeschützter Faserkunstoffverbunde dienen. Die gewonnenen Erkenntnisse können als Werkzeugkasten für maßgeschneiderte Systeme dienen.

Contents

1. Introduction **1**
1.1. Aims and Scope 2
1.2. Thesis Outline 3

2. Materials and Methods **5**
2.1. Materials 5
2.1.1. Matrix Materials 5
2.1.2. Flame Retardants 7
2.1.3. Fibre Reinforcements 8
2.1.4. Supplementary Materials 9
2.2. Methods 9
2.2.1. Manufacturing 9
2.2.2. Specimen Preparation 11
2.2.3. Characterisation 11
2.2.4. Quality Control 15
2.2.5. Thermokinetic Methods 15

3. Efficient Use of Flame Retardants **21**
3.1. State of the Art 22
3.1.1. Development and Maintenance of Fires 22
3.1.2. Flame Retardants 24
3.1.3. Flame Tests 27
3.2. Materials 28
3.3. Methods 28
3.3.1. Manufacturing 28
3.3.2. Tailored Flame Tests 31
3.3.3. Mechanical Characterisation 32
3.3.4. Quality Control and Microscopic Examination 33
3.4. Results and Discussion 33
3.4.1. Partially Modified Handlaminates 33
3.4.2. Combined Prepreg and Infusion Technique 37
3.5. Conclusions 45

4. Sustainable Matrix Materials **47**
4.1. State of the Art . . . 47
4.1.1. Epoxidised Vegetable Oils . . . 48
4.1.2. Biobased Epoxy Curing Agents . . . 50
4.2. Amino Acid-Cured Epoxy Resins . . . 51
4.2.1. Methods . . . 51
4.2.2. Mixture and Shelf Life of Dispersions . . . 54
4.2.3. Characterisation . . . 56
4.2.4. Stoichiometric Variations . . . 61
4.2.5. Postulation of Occuring Reactions . . . 72
4.2.6. Postulation of Network Structures . . . 77
4.2.7. Aging in Various Environments . . . 79
4.2.8. Transfer to Fibre-Reinforced Amino-Acid-Cured Epoxies . 92
4.3. Fully Biobased Matrix Materials . . . 98
4.3.1. Methods . . . 98
4.3.2. Curing with Biobased Carboxylic Acids . . . 99
4.3.3. Curing with Biobased Anhydrids . . . 102
4.4. Conclusions . . . 104

5. Flame-Retardancy of Biomolecules **107**
5.1. Methods . . . 107
5.2. Flame Retardancy of Amino Acid-Cured Epoxies . . . 108
5.2.1. Flame Tests . . . 108
5.2.2. Thermogravimetric Analysis . . . 113
5.3. Biobased Flame Retardants . . . 117
5.3.1. Thermogravimetric Analysis . . . 118
5.3.2. Flame Tests . . . 119
5.3.3. Impact on Mechanical Properties . . . 122
5.4. Conclusions . . . 123

6. Summary and Outlook **125**

Bibliography **129**

A. Appendix **167**
A.2. Materials and Methods . . . 167
A.3. Partially Flame Retardant Composites . . . 169
A.4. Sustainable Matrix Materials . . . 172
A.5. Flame-Retardancy of Biomolecules . . . 179

List of Abbreviations

ACE	Active chain end
AHEW	Amine hydrogen equivalent weight
AM	Activated monomer
APP	Ammonium polyphosphate
ASTM	American Society for Testing and Materials
ATR	Attenuated total reflectance
BDDGE	1,4-Butanediol diglycidyl ether
CA	Citric acid
CAI	Compression after impact
CNC	Computerized numerical control
CNT	Carbon nanotube
CP	Cross-ply
CPI	Combined prepreg and infusion technology
CR	Char residuum
CS	Chitosan
DBU	1,8-Diazabicycloundec-7-ene
DCB	Double cantilever beam
DEA	Dielectric analysis
DGEBA	Diglycidyl ether of bisphenol A
DGEBF	Diglycidyl ether of bisphenol F
DIN	Deutsche Institut für Normung e.V.
DIPEA	N,N-diisopropylethylamine
DMA	Dynamic mechanical thermal analysis
DMC	2,20-Dimethyl-4,40-methylene-bis-(cyclohexylamine)
DOPO	9,10-Dihydro-9-oxa-10-phosphaphenanthrene-10-oxide
DSC	Differential scanning calorimetry
DTG	Derivative mass loss
EEW	Epoxy equivalent weight
ELO	Epoxidised linseed oil
ENF	End-notch flexure
ESBO	Epoxidised soybean oil
FM	Friedman
FR	Flame retardant
FRP	Fibre-reinforced polymer
FTIR	Fourier transform infrared spectroscopy

GF	Glass-fibre
GFRP	Glass-fibre-reinforced polymer
HDDGE	1,6-Hexanediol diglycidyl ether
IAH	Itaconic anhydride
IFR	Intumescent flame retardant
IP6	Inositol hexaphosphate
IPDA	Isophorone diamine
IR	Infrared
IRM	Impregnation roll mill
KAS	Kissinger-Akahira-Sunose
L-Arg	L-Arginine
LOI	Limited oxygen index
L-Phe	L-Phenylalanine
L-Trp	L-Tryptophan
MIR	Mid-infrared
NaPh	Sodium phytate
NW	Non-woven
OFW	Ozawa-Flynn-Wall
OI	Oxygen index
PA	Phytic acid
POPA	Polyoxypropylenediamine
PTFE	Polytetrafluoroethylene
QI	Quasi-isotropic
RP	Red phosphorus
RTM	Resin transfer moulding
SE	Secondary electron
SEM	Scanning electron microscopy
SENB	Single-edge notch bending
TGA	Thermogravimetric analysis
THF	Tetrahydrofuran
tti	time-to-ignition
UD	Unidirectional
UL	Underwriters Laboratories
UV	Ultraviolet radiation
VO	Vegetable oil
3PB	Three-point bending

1. Introduction

Fibre-reinforced polymers (FRPs) consist predominantly of a matrix polymer and fibres. The matrix in FRPs serves to protect and embed the fibres in the desired direction and evenly distribute loads across the fibre-matrix interphases. The fibres provide an orientation-dependent reinforcement effect. In the direction of the fibres, the mechanical properties of the fibres exceed those of the matrix many times, but in the transverse direction, the fibres have limited reinforcing effect. The loads occurring in each application determine the layer structure, so that the directional dependence of the properties can be used efficiently [1]. According to Puck [2], certain conditions must be met for a reinforcement effect to be achieved. The fibres must have higher stiffness and strength than the matrix, but the matrix should exhibit a higher elongation at break, ensuring that it does not break before the fibres.

Glass fibres are most commonly used for reinforcement due to their good cost-benefit ratio. Carbon fibres offer even better specific mechanical properties with most available manufacturing methods [3], but due to their cost, they are usually only used when enormous cost savings through lightweight design are possible (e.g., aviation). Natural fibres and fibres of other material classes (e.g., aramid, basalt) can also be used in FRPs [4].

In the case of thermosetting matrix systems, such as epoxy resins, the reaction between the resin and the curing agent forms a three-dimensional network. Compared to non-crosslinked polymers (thermoplastics), this generally results in higher temperature resistance as well as higher stiffness and strength. However, specific properties are highly dependent on the selected constituents and the curing conditions.

In addition to the advantages of great design freedom, easy-to-implement functional integrations, and corrosion resistance, FRPs are used in a wide range of applications primarily because of their high specific stiffness and strength. The

resulting potential for lightweight design helps to save fuel in mobility applications or, specifically in the case of rail transport, to reduce damage to the rails and extend the service life of components such as brakes. This is beneficial not only from an ecological point of view, but also from an economic perspective [5].

Looking at the application in railways as an example, GFRP is used as top layers of sandwich components. A structure with a foam or honeycomb core is not only an excellent way to improve the potential for lightweight design, but also helps to meet a wide range of other requirements. In addition to safety-related criteria, such as crash behaviour, acoustic and thermal insulation demands must also be taken into account, which can be met by using suitable core materials [6, 7].

Particularly in mobility applications, the protection of humans must also be prioritised, which is why the issue of flame retardancy is also of central importance. By selecting suitable materials, sufficient evacuation time can be ensured in the event of a fire by maintaining structural integrity and preventing dripping of the polymers used. Furthermore, the smoke produced should be as low in toxicity as possible, so that short-term exposure does not cause long-term damage to health. There are a number of ways to achieve this, for example, through the additional use of flame retardants in matrix polymers [8].

1.1. Aims and Scope

Although research into flame retardants for polymers and FRPs has been conducted for decades, new areas of research are constantly emerging. For example, halogen-based flame retardants have been investigated for a long time because they have been shown to be very effective. However, halogens raise significant environmental concerns that are currently in contrast to the growing interest in sustainable solutions. Reasons for this trend include increased regulatory adjustments due to rising awareness of environmental and health risks, as well as growing awareness of the scarcity of resources and the resulting geopolitical dependencies [9, 10].

Therefore, this dissertation, entitled *'Environmentally Friendly Flame-Retardant Composites'*, deals with approaches to save resources through the efficient use of flame retardants. In addition, it also examines the substitution of synthetic

chemicals with natural raw materials to reduce environmental and health hazards. It should be emphasised that biomolecules can generally be obtained from biomass at low cost using large-scale industrial processes. Direct competition with the food industry can often be avoided by using waste streams. Thereby, cost-effective availability is particularly relevant, as sustainable solutions must be applied industrially to have a real impact on the environment, and ecological advantages are often neglected in the industrial context if they conflict with economic goals [11].

The focus on bio-based resources for use in polymers raises many questions, even without the addition of flame retardants. As is customary in the development of polymers, the curing conditions must initially be determined. For this purpose, thermokinetic methods with appropriate experimental validation are used. In addition, for example, the long-term properties of the bio-based materials examined in this thesis have not yet been sufficiently investigated, although an equivalent service life is of central importance for the sustainability of parts. At the same time, the feasibility of traditional FRP manufacturing processes and compatibility with commercial sizings requires investigation for deployment in industrial applications. With regard to the use of additional flame retardants and their dependence on the degradation processes of the polymer, it must also be clarified whether these flame retardants can be effective without disadvantages or even offer advantages. In addition, reports have generally indicated a reduction in thermo-mechanical properties due to the use of flame retardants [12, 13], which is why these effects must also be taken into account.

The following section provides an overview of the outline of this thesis, which thoroughly examines the overarching hypothesis:

High-performance composites can be designed flame-retardant and eco-friendly with compatible thermo-mechanical properties.

1.2. Thesis Outline

Firstly, the materials and methods commonly used in the investigations are listed in Chapter 2. A brief overview of fundamental knowledge is provided in the respective chapter.

Chapter 3 examines concepts for the efficient use of the flame retardant additive red phosphorus in a commercially available epoxy resin system. It contains,

e.g., a proof of concept for the pre-curing of modified plies based on thermokinetic methods using heterogeneously modified hand laminates. Furthermore, this chapter includes the development of tailored and qualitatively comparable flame tests, as well as a transfer to industrial methods using a combined prepreg and infusion process with residual strength testing after customised flame tests.

The first part of Chapter 4 deals with the development of biomolecule cured thermosets. In detail, amino acids are used as curing agents for epoxy resins and substitute classical petro-chemicals. Alongside kinetic analysis to determine curing conditions, thermo-mechanical properties for several stoichiometric reactions, as well as under different environmental influences, are under investigation. Furthermore, the feasibility of composite manufacturing and their mechanical performance are evaluated. The second part addresses fully biobased systems based on vegetable oils.

The third approach deals with the use of biomolecules to achieve flame-retardancy. In Chapter 5, the amino acid-cured epoxies investigated in Chapter 4, as well as selected biomolecules are tested regarding their flame retardant effects and their influences on mechanical properties. In addition, it is examined whether results of thermogravimetric analysis can predict flame-retardancy without time- and material consuming flame tests.

Finally, a summary and outlook (Chapter 6) follows, describing the findings as a toolbox for tailored systems. Parts of this thesis have been previously published [14–18]. If permitted by the publisher, CRediT author statements are provided in the publications describing the contributions of individual authors.

2. Materials and Methods

2.1. Materials

2.1.1. Matrix Materials

This work focuses mainly on epoxy resins as matrix materials for use in fibre-reinforced polymers. Epoxy resins consist of at least two components. The A-component includes epoxy-groups, the curing agent, e.g., amine or anhydride functionalities.

The following A-components are used:

- DGEBA resin 827 (Epikote™ 827, Westlake, Houston, USA)
- DGEBA-based resin 135 (Epikote™ MGS™ RIMR 135, Westlake, Houston, USA), includes 10 - 20 % 1,6-hexanediol diglycidyl ether (HDDGE) as reactive diluent
- Partially biobased epoxy resin SR810 (SR Infugreen 810, Sicomin, Chateauneuf les Martigues, France, 38 wt % bio-C), containing DGEBA, diglycidyl ether of bisphenol F (DGEBF) and 1,4-butanediol diglycidyl ether (BDDGE) as reactive diluent
- Fully biobased A-component ELO (epoxidised linseed oil, Merginat ELO, HOBUM Oleochemicals GmbH, Hamburg, Germany)

The petrobased amine curing agent 137H (EPIKURE™ MGS™ RIMH 137, Westlake, Houston, USA) contains 50 - 75 % polyoxypropylenediamine (POPA) and 25 - 50 % isophorone diamine (IPDA). If not otherwise specified, curing with this hardener takes place for 8 h at 50 °C followed by post-curing for 16 h at 80 °C.

Furthermore, in Chapter 4, the following biomolecules are used as curing agents. The generated curing profiles are discussed later on.

- L-Arg (L-Arginine base, Buxtrade GmbH, Buxtehude, Germany)
- L-Phe (L-Phenylalanine, Harrison Sport Nutrition S.L., Peligros, Spain)
- L-Trp (L-Tryptophan, Buxtrade GmbH, Buxtehude, Germany)
- CA (Citric acid, Buxtrade GmbH, Buxtehude, Germany)
- IAH (Itaconic anhydride, 95%, Th.Geyer GmbH & Co. KG, Renningen, Germany)

Partially, the accelerator UR500 (Dyhard® UR500, Alzchem Group AG, Trostberg, Germany) is added at 1 pph. The chemical structures of the introduced materials are shown in Figure 2.1.

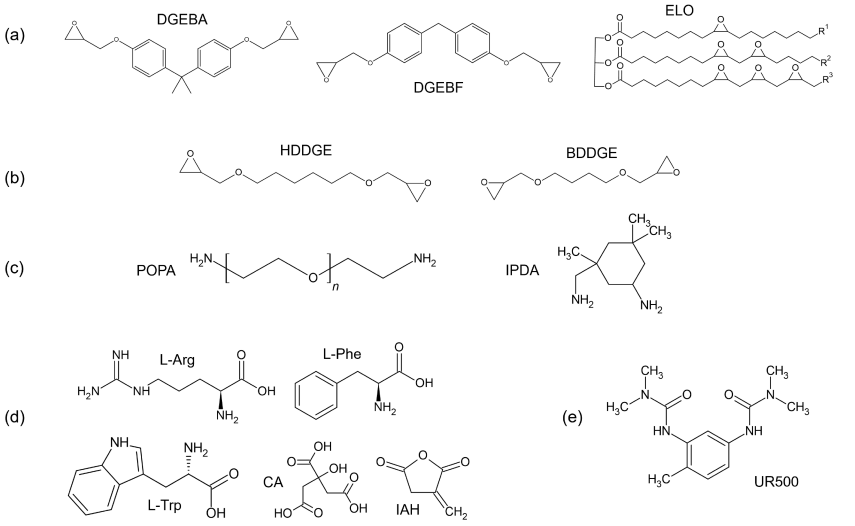

Figure 2.1.: Chemical structures of used Materials. (a) A-components: DGEBA, DGEBF and ELO with (b) reactive diluents: HDDGE and BDDGE. (c) Constituents of 137H: POPA and IPDA and (d) biobased curing agents: L-Arg, L-Phe, L-Trp, CA and IAH. (e) Accelerator UR500.

In the following chapters, epoxy systems are abbreviated using the sequence XX/YY/ZZ, where XX is the introduced short form of the A-component, YY that of the curing agent, and ZZ that of the accelerator. The mixing ratios used are taken from the data sheets or calculated via epoxy equivalent weights

(EEW) and amine hydrogen equivalent weights (AHEWs), which are summarised together with the bio-C fractions in Table 2.1. The AHEWs of the amino acids are theoretically calculated. Therefore, the molecular weight is divided by the amount of active hydrogen atoms in the molecular structure. The stoichiometric ratio was calculated under consideration of the respective EEW. The EEW of 827 was taken from the data sheet, while the EEW of SR810 and ELO was titrated according to standard DIN EN ISO 3001 [19].

Exemplarily, Equation 2.1 displays this calculation for the system 827/L-Arg, where the molecular weight of L-Arg (M_W = 174 g/mol) is divided by seven, the amount of active hydrogen atoms in the molecular structure. The stoichiometric mass ratio (1) was calculated considering the epoxy equivalent weight (EEW) of 827 (EEW = 182 g/mol) with m_i as the respective component mass:

$$\frac{m_{827}}{m_{L-Arg}} = \frac{100\ g}{100\ g \cdot \frac{AHEW}{EEW}} = \frac{100\ g}{100\ g \cdot \frac{25\ g/mol}{182\ g/mol}} = \frac{100\ g}{13.74\ g} \tag{2.1}$$

Table 2.1.: Mixing ratios and biobased fractions of all used epoxy systems.

System	Resin (wt. %)	Hardener (wt. %)	Accelerator (wt. %)	Biobased fraction (wt. %)
135/137H	76.90	23.10	0	0
827/137H	77.78	22.22	0	0
827/L-Arg	87.92	12.08	0	12.08
827/L-Arg/UR500	87.05	11.96	0.99	11.96
827/L-Trp/UR500	77.34	21.67	0.99	21.67
827/L-Phe/UR500	76.03	22.98	0.99	22.98
SR810/137H	76.25	23.75	0	28.98
SR810/L-Arg	86.98	13.02	0	46.07
ELO/CA	78.67	21.33	0	100
ELO/IAH	75.96	24.04	0	100

2.1.2. Flame Retardants

Red phosphorus (RP, Exolit RP 607, Clariant, Muttenz, Suisse) and ammonium polyphosphate (APP, FLACAVON 114, Schill+Seilacher GmbH, Böblingen, Germany) are added as commercially available flame retardants. As biobased flame retardants, chitosan (CS, DAC 90%, Food Grade, MarkNature, Fullerton,

CA, USA), phytic acid (PA, rice bran inositol hexaphosphate (IP6), MarkNature, Fullerton, CA, USA) and sodium phytate (NaPh, Food Grade, MarkNature, Fullerton, CA, USA) are explored. The chemical structures of all flame retardants used are shown in Figure 2.2.

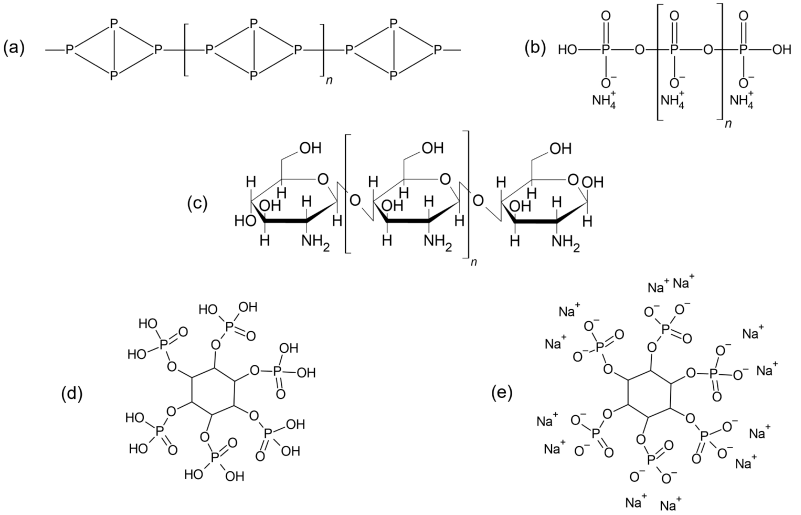

Figure 2.2.: Chemical structures of used flame retardants: (a) RP, (b) APP, (c) CS, (d) PA, (e) NaPh.

2.1.3. Fibre Reinforcements

In Section 3.3.1, composites are manufactured using 600 gsm unidirectional glass fibre fabrics with 10 % backing fibres (UD600, R&G Faserverbundwerkstoffe GmbH, Waldenbuch, Germany), while in Section 3.3.1, biaxial E-glass fibre fabrics (X-E-610, 610 gsm, SAERTEX GmbH & Co. KG, Saerbeck, Germany) are utilised. A 30 gsm non-woven (NW, R&G Faserverbundwerkstoffe GmbH, Waldenbuch, Germany) was partly added to the surfaces.

In Chapter 4.2, unidirectional composites are manufactured with the E/ECR glass fibre fabric HP-U600E (HP-Textiles, Schapen, Germany) consisting of 608 gsm fibres in 0° direction, 40 gsm fibres in 90° direction, and 15 gsm stitching yarn. For comparison with other matrix materials, the fracture toughness

of composites is tested with unidirectional non-crimp fabrics HP-U400E (HP-Textiles, Schapen, Germany) with 440 gsm areal weight and epoxy sizing. For quasi-isotropic (QI) laminates, X-E-610 fabrics are used.

2.1.4. Supplementary Materials

As release agent, Mikon® W64+ (Münch Chemie International GmbH, Weinheim, Germany) was used. Demineralised water, isopropanol (Ing. G. Linker GmbH, Sprockhövel, Germany), acetone (Lohmann Laborservice GmbH, Marxen, Germany) and hydraulic oil (Mobil Nuto H 46, Exxon Mobil Corporation, Irving, Texas, USA) serve as immersion media in Chapter 4.2.7.

2.2. Methods

In this section, test methods and machines that are used in several investigations are listed. Specific methods, used only once, are described in the respective chapter. The same applies to specific parameters.

2.2.1. Manufacturing

Mixing and Degassing

Mixing and degassing are performed with a Thinky Mixer ARE-250 (THINKY U.S.A., INC., Laguna Hills, USA) and a vacuum stirrer at 200 min^{-1}. Flame retardants are mixed into the epoxy system prior to degassing.

For an appropriate dispersion of solid curing agents, a three-roll mill 120E (EXAKT Advanced Technologies GmbH, Norderstedt, Germany) is used. The process parameters are determined according to [20] (see Table A.2.1, Appendix). For comparison (see Section 4.2), dispersions of solid curing agents in epoxy are prepared 2 x 3 min with a planetary centrifugal mixer ARE-250 (THINKY U.S.A., INC., Laguna Hills, USA) and 2 x 10 min with an ultrasonic bath SONOREX RK 510S (BANDELIN electronic GmbH & Co. KG, Berlin, Germany). Furthermore, the ultrasonic homogeniser SONOPULS 2200.2 (BANDELIN electronic GmbH & Co. KG, Berlin, Germany) with the sonotrode KE 76 in the rosette RZ 3 are compared (10 x 1.5 min intervals, ice bath).

Casting Process

If not described otherwise, resin plates of the size 200 x 250 mm^2, respectively 100 x 150 mm^2 are manufactured in aluminium moulds (see Figure A.2.1, Appendix). Different thicknesses are achieved with frames.

Wet Lay-up / Handlaminates

Vacuum-assisted hand lamination is a simple process to manufacture composites. Moltoprene Rollers (R&G Faserverbundwerkstoffe GmbH, Waldenbuch, Germany) are used to prepare wet lay-ups. The vaccuum bag set-up contains peel plies, perforated films, and absorbent fleeces. Curing takes place in a convection oven (UF 450plus, Memmert GmbH & Co. KG, Büchenbach, Germany) or using a silikon heating mat (msquare GmbH, Stuttgart, Germany).

Resin Transfer Moulding

Resin transfer moulding (RTM) is conducted in a closed aluminium mould with dimensions of 600 mm x 300 mm x 4 mm (see Figure A.2.1, Appendix) using a heat press. Infusion takes place at a vacuum of 0.01 bar. After infusion, a pressure of 2 bar is applied. Post-curing takes place in a convection oven (UF 450plus, Memmert GmbH & Co. KG, Büchenbach, Germany).

DirectPreg / Autoclave Process

Prepreg manufacturing is conducted partially through handlaminates or with a prototype impregnation roll mill (IRM, EXAKT Advanced Technologies GmbH, Norderstedt, Germany) using an overfilled gap to ensure uniform resin distribution (see Figure A.2.1, Appendix). The two rollers rotate in opposing directions at 30 rpm. Fibre-volume ratios can be adjusted with a changing gap.

The prepregs are laminated and packed in a vacuum bag set-up between two metal plates for good surface qualities, as shown in Figure A.2.1 (Appendix). Curing takes place in an autoclave (Maschinenbau Scholz GmbH & Co. KG, Coesfeld, Germany), operating under 7 bar pressure using nitrogen.

2.2.2. Specimen Preparation

A F45 circular saw (Altendorf GmbH & Co. KG Maschinenbau, Minden, Germany) with diamond saw blade is used for edging the manufactured plates. A CNC-saw Brillant 265 (ATM Qness GmbH, Mammelzen, Germany) with a diamond saw blade and water cooling is utilised to cut the test specimens according to the respective standards. For SENB specimens, a CNC-saw of type Brillant 220 (ATM Qness GmbH, Mammelzen, Germany) is used. Dogbone specimens are milled with an EUROMOD®-MP (Isel Germany AG, Eichenzell, Germany). To ensure representativity and reproducibility, test specimens were extracted from at least two different plates at defined locations.

2.2.3. Characterisation

Rheological Characterisation

Uncured resins are tested rheologically with an ARES rheometer (TA Instruments Inc., New Castle, USA) in plate-plate mode according to DIN EN ISO 3219 [21] (20-50 °C, 2 K/min, plate diameter: 40 mm, gap: 0.5 mm, frequency: 5 Hz, shear strain: 10 %).

Fourier Transform Infrared Spectroscopy

FTIR measurements in the MIR range (4000 to 500 cm^{-1}) are performed on a Tensor II (Bruker Corporation, Billerica, USA) in Attenuated Total Reflectance (ATR) using a MIRacle™ Single Reflection Horizonal ATR Accessory from PIKE Technologies (Fitchburg, Wisconsin, USA). The resolution is set to 2 cm^{-1}, for background and sample spectra, the mean values of 40 measurements are used. Validation of the predicted curing profiles is performed in transmission mode in the NIR range (7500 cm^{-1} to 2500 cm^{-1}) with a resolution of 2 cm^{-1}. The background spectrum is generated via the mean value of 40 measurements, while for the sample spectra eight measurements are performed. Processing of raw data includes a baseline correction and normalisation of the spectra on the constant aromatic peak (1605 cm^{-1}, C=C stretching). Gaussian fitting is used to determine the positions of the peaks.

Thermogravimetric Analyses

Thermogravimetric analyses (TGA) are performed according to DIN EN ISO 11358 [22] on a TGA Q500 (TA Instruments Inc., New Castle, USA) or on a TGA/DSC 1 Star system (Mettler-Toledo, Columbus, Ohio, USA) from 20 to 800 °C resp. 1000 °C with 10 K/min for three samples per configuration under nitrogen as well as synthetic air atmosphere. The decomposition temperatures (T_ds) are determined by the maximum in the differentiated mass loss-temperature curves.

Glass-Transition Temperatures and Cross-Linking Densities

Glass transition temperatures (T_gs) are determined by DSC 204 F1 Phoenix (Erich NETZSCH GmbH & Co. Holding KG, Selb, Germany) according to DIN EN ISO 11357-2 [23] by midpoint analysis. Therefore, samples are heated twice from 5 °C to 300 °C with a heating rate of 10 K/min. Furthermore, T_gs are determined by dynamic mechanical thermal analysis (DMA) on a GABOEPLEXOR®500N (Erich NETZSCH GmbH & Co. Holding KG, Selb, Germany) in accordance with DIN EN ISO 6721-1 [24] via onset analysis (1 Hz, 2 K/min, e.g., -130 °C to 230 °C). These measurements can simultaneously be used to calculate the cross-linking density ν_C using Equation (2.2), with the universal gas constant $R = 8.3145\ \mathrm{J/(mol \cdot K)}$ [25].

$$\nu_C = \frac{E'_{T_g+40K}}{3 \cdot R \cdot (T_g + 40K)} \tag{2.2}$$

Quasi-Static and Dynamic Tensile Tests

Mechanical testing was performed according to DIN EN ISO 527-2 [26] on different specimen geometries, listed together with the crosshead speeds in the respective chapter. For testing matrix properties, dogbone specimens are either tested on a Z010 (Zwick Roell GmbH und Co. KG, Ulm, Germany) or on a GABOEPLEXOR®500N (Erich NETZSCH GmbH & Co. Holding KG, Selb, Germany). Composites are tested with reference to DIN EN ISO 527-4 [27] standard using rectangular specimens of 250 mm length and 15 mm width for longitudinal tests resp. 25 mm width for transverse tests with 1 mm GFRP taps on a Z100 (Zwick Roell GmbH und Co. KG, Ulm, Germany) equipped with

hydraulic clamps. Transverse tensile strengths are determined as the strength at the knee point of the stress-strain diagram.

Fatigue tests were performed on fibre-reinforced polymers according to the DIN EN ISO 527-5 [28] standard with sinusoidal cyclic loading on a universal hydraulic testing machine (100 kN load cell, Instron GmbH, Darmstadt, Germany) in tension-tension mode with a load ratio $R = \sigma_{min}/\sigma_{max}$ of 0.1 and 20 %, 30 % as well as 40 % of the ultimate tensile strength.

Three-Point Bending Tests

Three-point bending (3PB) tests are performed according to DIN EN ISO 14125 [29] on a universal testing machine Z010 (Zwick Roell, Ulm, Germany) with 3 mm/min. The 3PB samples investigated have a geometry of 120 mm x 15 mm and a test length of 80 mm, while the supports have a diameter of 10 mm.

Compression Tests

Compression tests are conducted according to DIN EN ISO 14126 [30] on Z400 (Zwick Roell, Ulm, Germany). The composite specimens have geometries of 140 mm x 10 mm x 4 mm. According to the fourth Euler buckling case, the free test length is calculated to 10 mm. GFRP tabs (± 45°) are applied with UHU PLUS Endfest 300 (Uhu Holding GmbH, Bühl,Germany) at 60 °C. Ten specimens are tested per configuration.

Fracture Toughness

For neat epoxy, fracture toughness in Mode I is determined using single-edge notch bending (SENB) tests according to ASTM D5045 [31]. A razor blade is utilised to insert a sharp crack immediately before testing. The critical-stress-intensity factor at fracture initiation $K_{I,c}$ is calculated as displayed in (2.3), where F is the fracture load, b the width and w the height of the specimens. f(a/w) is a correction factor based on the geometry and crack length of the sample. The energy per unit area of crack surface at fracture initiation $G_{I,c}$ is calculated according to Equation (2.4).

$$K_{I,c} = \frac{F}{b \cdot \sqrt{w}} \cdot f(a/w) \tag{2.3}$$

$$G_{I,c} = \frac{(1-\nu^2)\cdot K_{I,c}^2}{E} \tag{2.4}$$

The interlaminar fracture toughness of unidirectional fibre-reinforced polymers is determined using double cantilever beam (DCB) tests (Mode I, G_I) and end-notch flexure (ENF) tests (Mode II, G_{II}) in accordance with ASTM D5528 and ASTM D7905. A thin polytetrafluoroethylene (PTFE) film (38 µm) is inserted in the neutral plane as intrinsic crack start. The compliance calibration method is used to evaluate energy release rates.

SENB, DCB, and ENF tests are performed on a Z010 (Zwick Roell, Ulm, Germany) with hinged load introduction, respectively, 3PB setup.

Optical Analysis

A digital microscope of type VHX-6000 (Keyence Corporation, Osaka, Japan) is used for optical examination. For quality control of manufacturing, parts of the plates for several configurations were embedded in KEM 15 plus (ATM Qness GmbH, Mammelzen, Germany) and polished with a polishing machine of type Saphir 550 (ATM Qness GmbH, Mammelzen, Germany) prior to microscopy. Microscopic fracture analysis after mechanical testing is conducted without embedding. Particle sizes and diffusion lines are investigated with transmitted light.

Furthermore, fracture surfaces are analysed via scanning electron microscopy (SEM). The images were acquired with a SUPRA 55VP (Zeiss, Germany) using secondary electron (SE) detection with an accelerating voltage of 3 kV. All samples were provided with silver conductive paint at the edge of the sample carrier and vaporised with gold for 30 s at 40 mA with a BALTEC SCD 050 SPUTTER (BALTIC Präparation e.K., Germany), creating an electrically conductive layer of a few nanometre thickness on the surface.

Flame Tests

All flame tests are conducted in an HVFAA Horizontal Vertical Flame Chamber (Atlas Material Testing Technology, Mount Prospect, Illinois, USA). The Limited Oxygen Index (LOI) is determined according to ISO 4589-2 [32] using an Oxygen Index Analyzer LOI 901 (NETZSCH TAURUS Instruments GmbH,

Weimar, Germany). In addition, vertical UL 94 tests [33] are performed. Furthermore, tailored flame tests were developed that are specified in Chapter 3.

2.2.4. Quality Control

Density Determination

Densities are measured with a precision scale AT261 DeltaRange equipped with a density determination kit (Mettler Toledo, Columbus, Ohio, USA), following Archimedes' principle for eight samples per configuration. Firstly, the mass of the specimen is weighed in air, followed by a measurement in ethanol. The difference between the two values corresponds to the buoyancy. Formula (2.5) is used to determine the density of the composite ρ_c, with A: weight in air, B: weight in ethanol, and ρ_0: density of ethanol (at 21 °C: 0.78849 g/cm^3).

$$\rho_c = \frac{A}{A-B} \cdot \rho_0 \tag{2.5}$$

Fibre Volume Ratio

Fibre volume ratios V_f are analysed at 600 °C in a muffle furnance (Heraeus Deutschland GmbH & Co. KG, Hanau, Germany). V_f is calculated as shown in (2.6), where V_f is the volume of the fibres and v_c the volume of the composite. According to data sheet information, the fibre density is $\rho_f = 2.62$ g/cm^3. The mass of the fibres (m_f) corresponds to the mass of the residuum after calcination and m_c/ρ_c is taken from density measurements for at least four specimens.

$$V_f = \frac{v_f}{v_c} = \frac{\frac{m_f}{\rho_f}}{\frac{mc}{\rho_c}} \tag{2.6}$$

2.2.5. Thermokinetic Methods

Theoretical Background

In the development of new reactiv matrix materials, an understanding of the respective curing kinetics is crucial to exploit the full potential of the investigated polymers.

Curing can be achieved with many different temperature profiles composed of the parameters temperature, time and heating as well as cooling rates. In each case, the conversion rate differs. To determine a suitable temperature profile, there are analytical methods of varying complexity that describe the reaction kinetics by solving the kinetic equation (2.7) [34], where α is the degree of conversion, t the time, T the temperature, k(T) the reaction rate constant, and f(α) the conversion function. Equation (2.7) includes the Arrhenius equation [35] to determine k(T). A is the pre-exponential factor, E_A the activation energy, and R the universal gas constant.

$$\frac{d\alpha}{dt} = \Phi(T,\alpha) = k(T) \cdot f(\alpha) = A \cdot exp\left(\frac{-E_A}{RT}\right) \cdot f(\alpha) \tag{2.7}$$

Different methods can be used to determine the parameters A, f(α), and E_A. Fundamentally, a distinction is made between isoconversional and isokinetic methods. The first mentioned requires knowledge of the temperatures at which an equivalent reaction stage occurs for different heating rates, while the second depends on the reaction model [36, 37]. In this study, isoconversional methods are used because they are considered comparatively superior for the accurate determination of kinetic parameters [37]. They can again be differentiated into differential (e.g., Friedman (FM)) and integral methods (e.g., Kissinger-Akahira-Sunose (KAS) and Ozawa-Flynn-Wall (OFW)). Necessary data can be generated by different experimental methods such as Differential Scanning Calorimetry (DSC), Dielectric Analysis (DEA), Thermogravimetric Analysis (TGA), or rheological measurements.

In the FM method [38], the main kinetic equation is logarithmised (Equation (2.8) and the so-called FM plot is applied. For this purpose, measurement data are transformed into a coordinate system with ln(dα/dt) over 1,000/T. Points with the same degree of conversion are then connected linearly (see, e.g., Figure A.4.6, Appendix) and evaluated as a linear function as shown in Equation (2.9).

$$ln\left(\frac{d\alpha}{dt}\right) = \ln((A \cdot f(\alpha)) - \frac{E_A}{RT} \tag{2.8}$$

$$y = b + a \cdot x \tag{2.9}$$

Considering Equation 2.8, the parameters can be determined with y = ln(dα/dt); x = −1/T; a = E_A/R and b = ln(A · f(α)) using multiple linear regression analysis. For the KAS method [39], the kinetic equation (1) is converted to Equation (2.10), where β is the linear heating rate. This equation is then integrated (Equation (2.11)) and logarithmised, resulting in Equation (2.12) [39].

$$\frac{d\alpha}{dT} = \frac{1}{\beta} \cdot \Phi(T,\alpha) = \frac{1}{\beta} \cdot k(T) \cdot f(\alpha) = \frac{A}{\beta} \cdot exp\left(\frac{-E_A}{RT}\right) \cdot f(\alpha) \tag{2.10}$$

$$\beta \cdot \int_0^a \frac{d\alpha}{f(\alpha)} = A \cdot \int_{T_0}^T exp\left(\frac{-E_A}{RT}\right) dT \tag{2.11}$$

$$ln\left(\frac{\beta}{T^2}\right) = ln\left(\frac{A}{F(\alpha)}\right) - \frac{E_A}{RT} - ln\left(\frac{E_A}{R}\right) \tag{2.12}$$

Measurement data for different heating rates are transferred into a so-called KAS plot, with a coordinate system with ln(β/T^2) over 1,000/T. As with the FM method, the points with the same α are connected and the relevant parameters are evaluated by Equation (2.9) with y = ln(β/T^2); x = −1/T; a = E_A/R and b = ln(A/F(α)) − ln(E_A/R) (see Equation (2.12). The Doyle approximation [40] is used within the OFW method [41], resulting in Equation (2.13).

$$ln(\beta) = 5.3305 + ln\left(\frac{A}{F(\alpha)}\right) - 1.052 \cdot \frac{E_A}{RT} \tag{2.13}$$

Using the OFW plot with the ordinate ln(β) over 1,000/T, the required parameters can also be determined by isoconversional linear functions with y = ln(β); x = −1/T; a = 1.052 · E_A/R and b = 5.3305 · ln(A/F(α)) (see Equation (2.13)).

The described methods can represent multiple-step reactions without parallel reaction steps although there is no detailed knowledge about the reactions [42, 43]. If parallel and independent reactions occur, only the mean values of E_A are considered. The FM method can be applied to isothermal and dynamic measurements, while the KAS and OFW methods require dynamic measurement data [44]. Despite simplifying assumptions, the presented isoconventional methods can represent epoxy reactions well in many cases [36, 37, 43]. Especially, the FM method is often particularly suitable [45–47]. Over time, further methods were developed. For example, the Kamal-Sourour method [48] considers non-catalytic and autocatalytic reactions with two constants, but assumes that

primary and secondary amines have the same reactivity and no etherification reaction occurs [49]. In addition to the methods mentioned, there are also simpler approaches, e.g., Kissinger (ASTM E2890) [50–52] or Ozawa (ASTM E698) [53, 54], which determine only one value of E_A and A without dependence on α. However, these cannot adequately represent epoxy reactions, which are often autocatalytic [55].

Implementation and Experimental Validation

For the determination of curing profiles for new epoxy systems via thermokinetic methods as described in Section 2.2.5, DSC measurements at 1, 2, 5, 10, 20 and 40 K/min from 5 °C to 300 °C provide the basis. In this work, the analysis was performed software-based with Kinetics Neo (Erich NETZSCH GmbH & Co. Holding KG, Selb, Germany). The approaches that show the best correlation with the experimental results are chosen from the introduced thermokinetic methods to predict a temperature profile for curing. When generating curing profiles, a constant and slow conversion rate avoids excessive exothermic heat development [56], thus preventing thermal degradation [57]. Therefore, the following boundary conditions were set:

- Constant conversion rate of 0.25 %/min, which is in the range of commonly used curing profiles [58, 59].
- Max. heating rate: 5 K/min
- Max. temperature: 180 °C

The profiles are linearised for subsequent curing in convection ovens. Ex-situ FTIR and DSC measurements are used to validate the predictions. For this purpose, the FTIR device introduced in Section 2.2.3 is used. Measurements are performed between two glass slides (Menzel Gläser, Braunschweig, Germany), which are glued together with double-sided adhesive tape (Tesa GmbH, Norderstedt, Germany) forming a measuring cell with a gap of 185 µm. The decrease in the area of the epoxy peak between 4560 and 4497 cm^{-1} is evaluated at various times of the temperature profile. Processing of raw data includes a baseline correction and normalisation of the spectra on the constant aromatic peak (4681 cm^{-1}). DSC measurements (25 – 300 °C, 10 K/min) are performed on several prepared crucibles, which are successively removed from the oven during the run of the material-specific temperature profile. α is determined from

the decrease in the exothermic peak. Figure 2.3 illustrates this procedure using experimental results obtained for the system 827/137H.

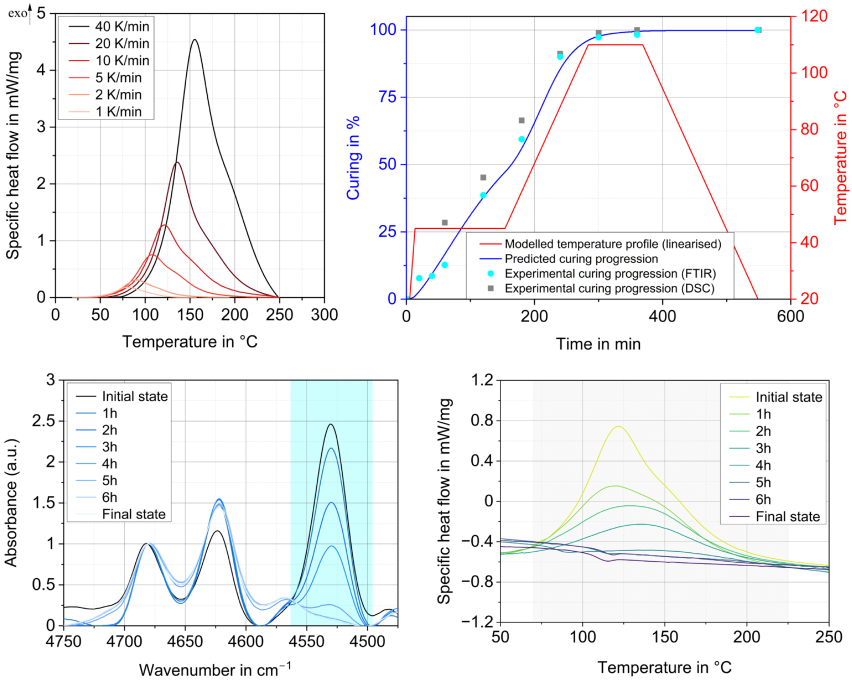

Figure 2.3.: DSC measurements at various heating rates (top left) for the generation of temperature profiles for curing (top right: linearised) and the associated prediction of curing progression (top right, blue), as well as validation points. Underlying results of the experimental validation procedure using FTIR (bottom left) and DSC (bottom right). Exemplified for 827/137H (own data).

3. Efficient Use of Flame Retardants

In recent decades, composites have become a key factor to realise lightweight design, e.g. to safe energy in mobility applications. As FRPs are usually combustible, flame retardants (FRs) are necessary to fulfil critical requirements. In addition to the challenges with filtration effects, described in Section 3.1.2, particles in the micrometre range often influence thermo-mechanical properties. Although toughness can be improved due to their implementation, most other properties, such as glass-transition temperature or strength, often decrease [12, 13, 60, 61]. This is because particles of this size can act as defects [62, 63], 'disturb' the structure of the polymer network and also worsen the fibre-matrix bonding in FRPs [64]. Therefore, minimal use is desirable in order to minimise the impact on thermo-mechanical properties.

In order to minimise the proportion of flame retardants required in composites, current studies often focus on combining different flame retardants [65–68] to exploit synergistic effects (see Section 3.1.2), e.g., via microencapsulations [69, 70] to make flame retardants more efficient. Especially when using carbon and natural fibres, surface modifications for fibres [71, 72] or interlayer nanofibre methods [73] are also under investigation.

In the case of FR-particles, implementation in fire-exposed sections, e.g., on component surfaces, is most effective. The use of gel-coats or coatings is one way to achieve surface flame retardancy in industrial practice [74]. However, the use of additional material can limit the potential for lightweight design [75] and is sometimes not possible due to restricted mounting circumstances [76] or cause adhesion challenges [77]. Consequently, the working hypothesis is:

An efficient use of flame retardants in appropriate locations can save material, contribute to lightweight design and minimise the impact on mechanical properties at the same time.

This chapter presents the approach to reduce the global amount of FR through a heterogeneous distribution of FR particles within the laminate, using the FR modification only in individual layers of the FRP. The following chapter is divided into two parts, where the first one uses handlaminated wet lay-ups and serves as preliminary study and proof-of-concept for the second part, where a transfer to industrially applicable methods follows.

3.1. State of the Art

For the development of environmentally friendly flame retardant composites, it is relevant to know how fires develop and how flame retardants can interrupt or delay this process. The following section gives an overview of the basic principles and innovative approaches that can be found in the literature for a more sustainable use of flame retardants.

3.1.1. Development and Maintenance of Fires

The factors required for the development and maintenance of a fire can be visualised in a fire tetrahedron (Figure 3.1, left). A fire is caused by an external heat source that decomposes the polymer as soon as the thermal energy exceeds the binding energies. In linear thermoplastic polymers, depolymerisation to oligomers is observed [78, 79]. Because of the cross-linked structure of thermosets, these polymers are decomposed more irregularly through fragmentation of polymer chains.

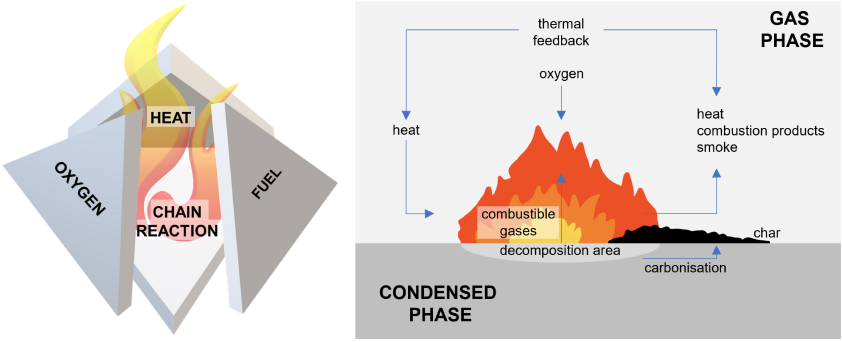

Figure 3.1.: Left: Fire tetrahedron. Right: Schematic representation of polymeric combustion process, adjusted from [80]

In the condensed phase, a solid, carbon-rich residue (char) forms via dehydration, cross-linking, and aromatisation processes during thermal or flame treatment. Possible reactions depend heavily on the specific composition of the polymer. In neat epoxy resins, it is reported that char formation is initiated at temperatures of approximately 300 °C by homolytic cleavage of thermally unstable bonds, such as ether bonds (C-O-C), which produce radicals (e.g., phenoxy radicals). Molecular rearrangements and dehydration or dehydrogenation reactions increase the carbon content, and conjugated double bond systems can form. Radical recombination, disproportionation, and cyclisation reactions further create new C-C bonds. This is described as secondary cross-linking. The resulting polycyclic aromatic structures are more thermally stable than the original polymer network. If temperatures continue to rise, further condensation reactions can take place, causing the carbon content to increase and resulting in graphite-like domains [81–84].

According to Schartel et al. [81], the reactions that occur not only differ between different classes of polymers but also depend on the specific choice of the constituents. Thus, diglycidyl ether of bisphenol A (DGEBA) cured with 2,20-dimethyl-4,40-methylene-bis-(cyclohexylamine) (DMC) forms a graphitic residue containing mainly aromatic–allylic or cyclic ethers and strongly unsaturated hydrocarbons, while the decomposition of methylene-bis-(2,6-diethylaniline)/ methylenebis-(2,6-diisopropylaniline)-cured tetraglycidyl methylene-dianiline results in a polyaromatic residue with included amino groups. Consequently, differences in the formed char influence the flame-retardant effect.

In these condensed phase processes, short-chain pyrolysis gases are produced, which serve as fuel for the combustion process. The volatile components form a highly flammable air-gas mixture with atmospheric oxygen. Heat is released in the process and is partially fed back into the polymer material. The process produces highly reactive OH· and H· radicals, which again generate new radicals (chain reaction). By reaching the auto-ignition temperature, the polymer ignites itself, which results in new heat, and the process progresses. This thermal feedback is shown in Figure 3.1 (right).

Consequently, a fire involves simultaneous pyrolysis (thermal decomposition without oxygen) in the condensed phase and combustion reactions in the gas phase (oxidation with flame) [85]. Over time, the pyrolysis zone continuously moves through the polymer material. Thereby, aromatic structures in polymers sim-

plify the charring reactions because the aromatic rings can act as precursers in the building of the cycloaromatic structure, resulting in a higher char yield. This char is a physical barrier for heat and mass transfer. If there is a lack of fuel or oxygen, or if heat is removed from the system, one of the necessary factors is no longer present and the fire extinguishes itself.

Nevertheless, neat epoxy is reported to be combustible. The resulting char has only a low degree of graphitisation [86] and therefore low protective properties, insufficient for an effective heat barrier. Consequently, additional flame retardants are used to interrupt the combustion process by suppressing at least one of the necessary parameters displayed in the fire tetrahedron (Figure 3.1, left).

3.1.2. Flame Retardants

In the past, flame retardancy was mainly achieved using halogenated substances because they are highly efficient. However, due to the release of toxic gases during thermal degradation and the associated risk to organisms and the environment, the use of some of these flame retardants has already been banned by law [9, 10]. For this reason, compounds containing phosphorus, nitrogen and silicon or inorganic substances such as metal hydrides or zinc borates are being increasingly used [87]. Nevertheless, the use of these substances can also pose potential risks. For example, zinc borates are highly toxic to aquatic organisms.

Flame retardants (FRs) can be categorised into solid and liquid substances or in reactive and non-reactive additives [88]. Furthermore, FRs can be classified according to their mode of action. The mechanisms of FR are based on chemical and/or physical processes that occur in the gas and/or solid phase [74, 89]. The oxidising agent (oxygen) can be limited by the release of non-combustible gases in the gas phase. In the condensed phase, flame retardants can limit the fuel source and the release of combustible gases by charring with an acid and a carbon source. In addition to shielding the fuel source from the oxidising agent, this protective layer also impairs heat transfer (limiting the heat source), which is considered another important flame-retardant mechanism [9]. Intumescent flame retardants (IFRs) additionally consist of a blowing agent which foams the char, resulting in an effective insulation layer, particularly protecting the underlying layers from the spread of flames [87].

Phosphorus-containing FRs can act in the condensed phase and/or the gas phase. The mode of action depends on the composition of the system, as several interactions with other components are conceivable within the combustion process [10, 89]. During thermal decomposition, most of the phosphorus in the system is oxidised to phosphorus pentoxide (P_2O_5), which removes water from the pyrolysing substrate, producing polyphosphoric acid ($H_xP_yO_z$). In the solid phase, the phosphoric acid and the polymer substrate esterify, resulting in a dense char [88, 90, 91]. In the gas phase, phosphorus-containing radicals ($PO\cdot$, $HPO\cdot$) act as radical scavengers by intercepting combustible radicals ($H\cdot$, $OH\cdot$) and thus interrupting the chain reaction of combustion [92].

In particular, red phosphorus (RP), which is used in the Chapters 3 and 5, forms a particularly dense and stable carbon layer by acting as a strong acid source, allowing efficient catalysis of carbonisation. RP can therefore also be used as an acid source in intumescent systems [93]. Ammonium polyphosphate (APP) (Chapter 5) can even act as an acid source and blowing agent simultaneously in intumescent systems and forms a multicellular char [94].

Synergistic Effects

Synergistic effects are exploited to enable more efficient flame-retardancy. Here, several additives work together to improve the overall effect of flame-retardancy, thus reducing the total amount of additives required [65–68]. This can be achieved, for example, by simultaneously using APP with aluminium hydroxide [95] or with montmorillonite [96]. According to Yang et al. [97], boron-containing APP enhances not only flame resistance but also smoke release.

Besides, intumescence systems containing different components as acid source and blowing agent, microencapsulations [69, 70, 91, 98] are also used to realise synergetic effects efficiently, since the synergistic components are locally present together. Bi et al. [98] dilutes flammable gases by releasing non-combustible gases such as NH_3 through surface modification of APP with Schiff base covalent organic frameworks, while Cheng et al. [91] improve the compatibility between RP and epoxy through polydopamine/melamine microencapsulated RP.

Filtration Effects in Infusion Processes

Infusion processes are widely used manufacturing methods for large composite parts with the advantage of relatively low tooling costs and high surface qualities [99, 100]. The addition of particle fillers to the matrix is used to enhance or provide supplementary properties, e.g., flame retardancy [101, 102]. The distribution of the particles in the laminate is usually decisive for these properties.

In infusion processes, particles of the size of tens of microns lead to filtration effects [103–106] with an inhomogeneous particle distribution or, in the worst case, to an inadequate filled final component [107, 108]. In general, larger particle sizes or agglomerations, as well as higher fibre-volume contents, increase filtration effects [108]. Filtration effects can be divided into different types, where cake filtration and deep bed filtration are the most common phenomena [105, 109, 110]. Figure 3.2 displays a schematic representation of these filtration effects.

When particle sizes are larger than the available space between fibres, macroscopic cake filtration occurs where deposited particles build-up ahead of the fibres as soon as the dispersion enters the mould. Throughout the length of the reinforcement, microscopic cake filtration may appear due to different scales of the inter- and intra tow channels [107]. If particles dimensionally smaller than the accessible channels are captured, deep bed filtration occurs, resulting not only in particle gradients but also in extended infusion times [107].

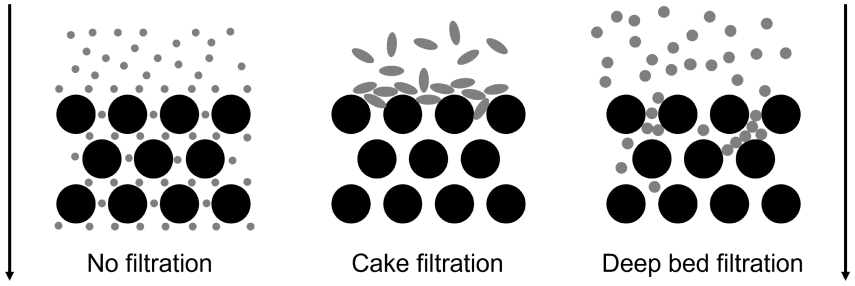

Figure 3.2.: Schematic representation of most common filtration effects compared to desired uniform particle distribution.

3.1.3. Flame Tests

Various tests can be performed to assess fire behaviour. However, the real fire behaviour of materials depends on many other factors, such as ventilation, heat transport, the component itself, or storage conditions. However, realistic room fire tests are very time-consuming and expensive. The fire behaviour of small test specimens can be tested on lab scale under ideal conditions. The influencing parameters of specimen geometry, ignition source, oxygen supply, and heat yield can be controlled to allow meaningful comparisons between materials. UL 94 flame tests [33] are frequently used, in which samples are flamed twice for ten seconds with a defined bunsen burner flame, e.g., in a vertical flame test. After each flame treatment, the after-flame time is noted and the dripping of the material is analysed, allowing different classifications of the material as a result, where V0 is the classification with the best flame resistance. The determination of the Limited Oxygen Index (LOI) is another standardised test procedure [32, 111]. The share of oxygen in the test atmosphere is adjustable by using varying ratios of nitrogen and oxygen. The LOI describes the minimum concentration of oxygen that will support the combustion of the material.

For composites, cone calorimetry [112] is a frequently used flame test, where a sample is exposed horizontally to a constant heat flow for the duration of the test. In addition, a spark igniter is used, which ignites the material as soon as an ignitable mixture is created in the gas phase. The aim is to determine the heat release rate through oxygen consumption. Besides, the time-to-ignition (tti) and mass loss of the sample, as well as the total amount of heat released and the maximum heat release rate, are determined. In contrast to the UL 94 test, in which flammability and burning behaviour are examined, the fire process is investigated energetically. In general, specific tests must be passed to certify materials for various applications. For instance, in aircraft construction, test specimens are tested for their flame resistance following the "Aircraft Materials Fire Test Handbook" [113]. For example, samples are clamped horizontally over a Bunsen burner and flamed for 15 seconds. The burn rate is determined. A metal mould with specified internal dimensions is used as a holder, which itself is non-combustible and corrosion-resistant. When positioning the mould, the side that is exposed to the flames in the real application must be placed towards the flame. Other standards, such as DIN EN 60695-11-10 [114], also provide methods for the analysis of composite specimens, in which different fire lengths are examined.

3.2. Materials

In the following, the epoxy system 827/137H is used. RP is added as a flame retardant (see Chapter 2), as RP is visually distinguishable due to its red colour. Given percentages of RP refer to the relative mass of RP related to the total mass of the resin and curing agent. In Section 3.4.1, composites are manufactured using the introduced UD600 glass fibre fabrics to manufacture unidirectional lay-ups, while in Section 3.4.2, X-E-610 glass fibre fabrics are utilised for quasiisotropic laminates. The NW was partly added to the surfaces.

3.3. Methods

3.3.1. Manufacturing

Handlaminates

The handlaminated, 4 mm thick and unidirectional wet lay-ups which are investigated in the first part of this chapter, are cured vacuum-assisted with a heating mat and post-cured in a convection oven. Table 3.1 gives an overview of the manufactured plates and their nomenclature.

As can be seen in Figure 3.3 (left), one typical problem while curing plies with and without flame retardants is the convey of particles into unmodified layers. As a result, the desired particle content on the surface is lower than intended. By pre-curing the modified plies, it is possible to ensure that the RP remains in the desired layers so that the filler content could be kept as low as necessary (Figure 3.3, right). In order to investigate any potential influence of pre-curing independent of additional particle loading, an unmodified plate was also pre-impregnated and pre-cured with neat resin.

Commercial prepregs are pre-cured to $\approx 25 - 35$ % which is described in the literature as B-stage [115, 116]. Various temperatures can be selected to realise the desired degree of curing. In this work, pre-curing is carried out at 50 °C, analogous to the complete curing, introduced before. Thermokinetic methods were conducted and validated via FTIR and DSC as described in Section 2.2.5 to determine the required time for pre-curing. After an initial study, 90 min at 50 °C ($\approx$ 40 % pre-curing) is necessary to achieve a prepreg that is easy to process.

Table 3.1.: Manufactured Configurations with their amount of RP per plate (250 mm x 250 mm). NW: Non-woven fabric, *: pre-cured, x %: mass-related amount of RP.

Configuration	Scheme	Absolut RP content in g	Global RP fraction in wt %
$[0]_8$		0	0
$[\mathrm{NW}, 0_8, \mathrm{NW}]$		0	0
$[\mathrm{NW}^*, 0^*, 0_7, \mathrm{NW}]$		0	0
$[\mathrm{NW}, 0_8, \mathrm{NW}]^{3\%\mathrm{RP}}$		4	3
$[\mathrm{NW}, 0_8, \mathrm{NW}]^{12\%\mathrm{RP}}$		16	12
$[\mathrm{NW}^{12\%*}, 0^{12\%*}, 0_7, \mathrm{NW}]$		2.8	2.1

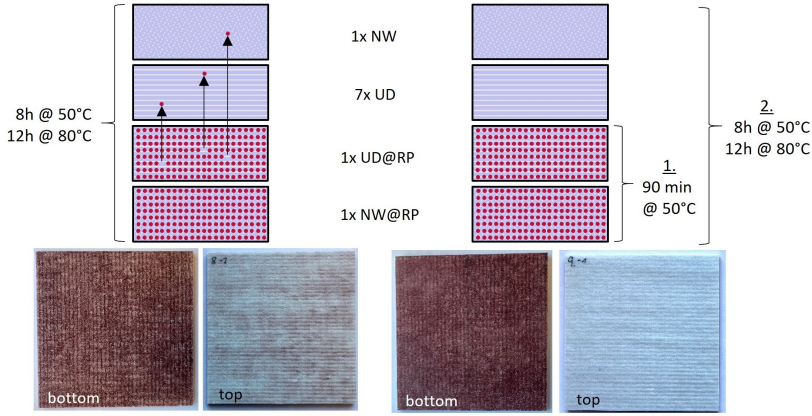

Figure 3.3.: GFRPs containing partially modified layers without pre-curing (left) and pre-cured (right). NW: Non-woven fabric, UD: Unidirectional glass-fibre fabric; RP: Red Phosphorus.

Combined Prepreg and Infusion Technique

Figure 3.4 displays the manufactured and investigated quasiisotropic $[\pm 45°, 90°, 0°, \pm 45°, 90°, 0°]_s$ laminates, partially containing NWs on the surface. In order to distinguish between the results of both manufacturing methods within a glance, a different nomenclature is used in this section (see Figure 3.4), but the schemes are consistent. For unmodified configurations, manufacturing is conducted via RTM process as described in Chapter 2. Due to occurring filtration effects mentioned in Chapter 3.1.2, it is not possible to manufacture panels with RP-loaded epoxy resin via infusion processes (see Figure 3.5).

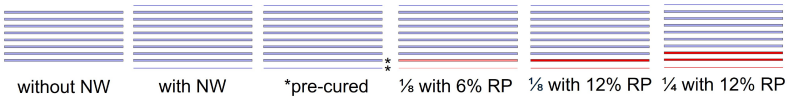

Figure 3.4.: Schematic illustrations of investigated heterogeneously modified laminates manufactured via *Combined Prepreg and Infusion Technique*. (Thick line: Biaxial glass-fibre fabric; thin line: NW; blue: unmodified; light red: 6 wt. % RP; dark red: 12 wt. % RP. All modified plies are pre-impregnated and pre-cured. Unmodified plies are infused in their dry state, except plies marked with *.)

This is why this study uses a *Combined Prepreg and Infusion Technology* (CPI) to manufacture GFRPs containing heterogeneous distributed RP. Before the RTM process with unmodified epoxy resin, the modified plies are impregnated by hand and pre-cured, as illustrated in Figure 3.5.

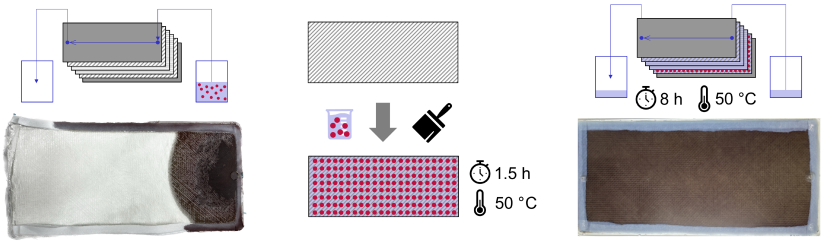

Figure 3.5.: Incompletely infused plate due to the filtration effect during the RTM process with RP-loaded resin (left), wet lay-up of the modified layers (centre) and combined prepreg and infusion process to avoid filtration effects (right).

Originally, the CPI-method is used for highly stressed components that are large and have complex geometries. In this context, prepregs are used for geometrically simple areas exposed to high mechanical loads, while complex structures such as stringers or frames are manufactured using infusion processes (e.g., RTM). Both parts are combined in the same curing cycle, increasing integration and cost efficiency. Thus, the advantages of both processes can be achieved. However, the quality of the interface between prepreg and the infusion part is relevant for the mechanical performance of the component [117–119].

Two plates are manufactured for each configuration to ensure reproducibility. For tracability and comparability, test specimens are uniformly extracted and labelled. Figure 3.6 shows a schematic overview of the uniform division of plates into test specimens and their labelling for traceability.

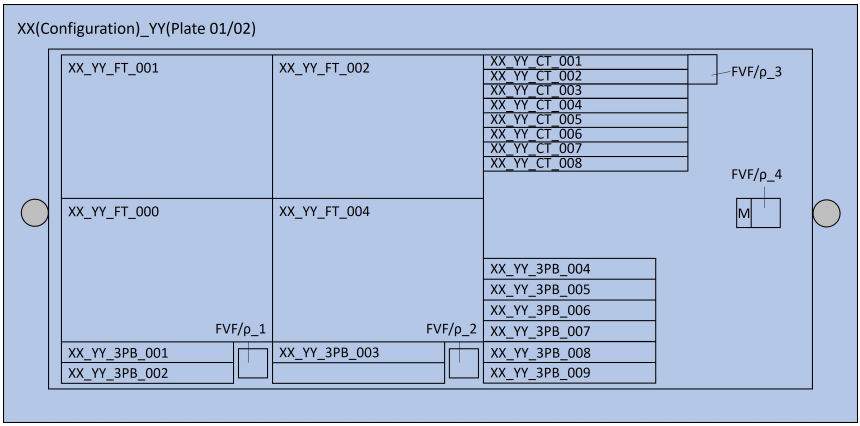

Figure 3.6.: Uniform plate division into test specimens and labelling for traceability. XX: Configuration; YY: Platenumber (01/02); FT: Flame test; 3PB: Three-point bending; CT: Compression Test; FVF/ρ: Fibre-volume fraction and density analysis, M: Microscopy.

3.3.2. Tailored Flame Tests

The flame tests conducted are tailored to the flame-retardant surface modifications of the laminates considering methodical approaches of conventional test methods (see Chapter 3.1.3).

The 40 mm flame of a bunsen burner (0,7 kW, methane gas, technical grade) is applied centrally to the respective test specimens. To prevent the flame from

spreading over the edges, a horizontally aligned steel frame is utilised. In addition, three temperature sensors (type K, TC Mess- und Regeltechnik GmbH, Mönchengladbach, Germany, see Figure 3.7, left, 1-3) are installed to measure the temperature development during flame treatment on the top (centrally) and bottom (edge area) of the test specimen and on the frame every five seconds. Videos are recorded during the tests. Herewith, the time-to-ignition and afterflame time is analysed. Furthermore, mass loss is tracked.

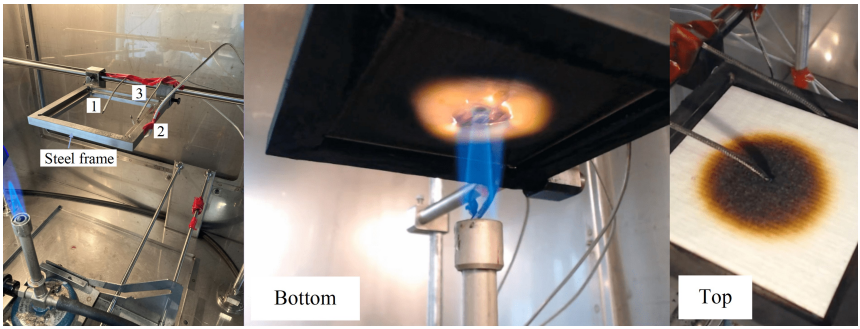

Figure 3.7.: Set-up of the flame test.

For handlaminated specimens, the flame is applied at a distance of 25 mm to the surface of 100 mm x 100 mm specimens. Test A used ten flame applications of 60 s. A 180 s flame treatment was added afterwards. As a second test (Test B), a single flame treatment was performed over 180 s.

Taking into account thereby generated results, the burner distance is enlarged to 35 mm for the second part of this chapter (Section 3.4.2) and the flame treatments are set to 180 s and 300 s. Furthermore, the specimens were enlarged to 100 mm x 150 mm specimens to allow the determination of residual compressive strengths after flame treatments. Four specimens are flamed for each configuration and length of flame treatment.

3.3.3. Mechanical Characterisation

Three-point bending (3PB) tests are performed with the pre-cured part on the tensile side as well as on the compression side. For each configuration, ten specimens are tested in both orientations.

To evaluate the residual strength after different types of damage, the mechanical properties of damaged specimens are compared with the initial undamaged state. In the following, a compression after impact (CAI) setup (ASTM D7137) is used to investigate the residual strength of flamed specimens with a Z400 (Zwick Roell, Ulm, Germany) at 1.25 mm/min. For each flame test and configuration, three specimens are analysed. To exclude the influence of particle modification on mechanical properties, the residual strength was standardised to the compressive strength of unflamed specimens of the respective configuration (see Section 2.2.3).

3.3.4. Quality Control and Microscopic Examination

Densities and fibre volume fractions for four (handlaminates) or eight (RTM / CPI) samples per configuration, as well as digital microscopy and SEM images of the various configurations, are analysed for the purpose of quality control. Furthermore, samples are partially cut in the centre after flame treatment in order to examine their cross-sections. ImageJ was used to process and analyse these images.

3.4. Results and Discussion

3.4.1. Partially Modified Handlaminates

Figure 3.8 (left) shows the results of the eleven flame treatments of Test A, while Figure 3.8 (right) displays the single 180 s flame treatment of Test B. The dots demonstrate the time-to-ignition (tti) within the flaming time (60 s or 180 s, grey column). On top of this column, the after-flame time is shown.

Firstly, the influence of the NW is analysed by comparing the configurations $[0_8]$ and $[\mathrm{NW}, 0_8, \mathrm{NW}]$. In addition to the positive influence on the surface quality, the non-woven fabric is beneficial for the GFRPs behaviour against fire, because it prevents the after-flame time after A3, while without NW, six flame treatments lead to an after-flame time.

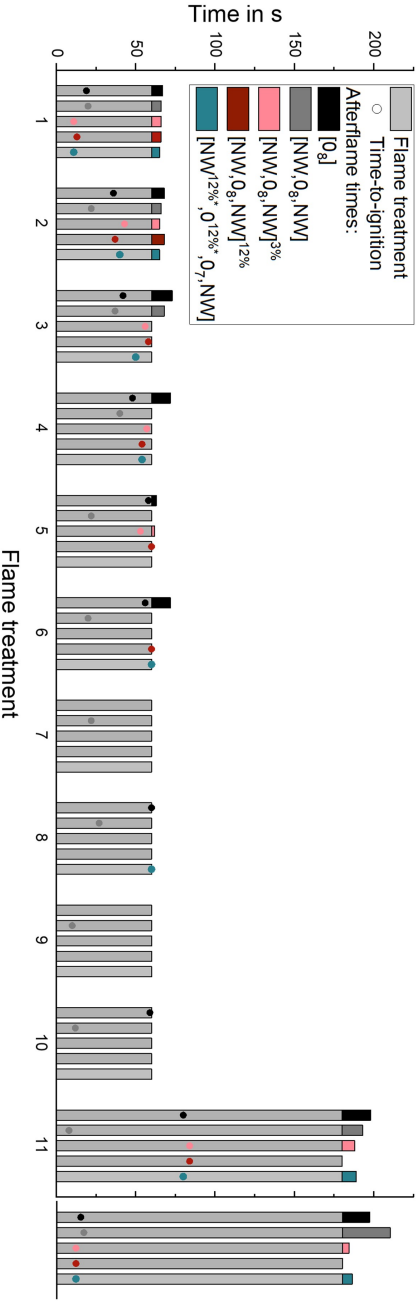

Figure 3.8.: After-flame times and tti in Test A with several flame treatments (left) and Test B (right).

Considering the images of the flame-treated surface of the specimens (Table 3.2), it is noticeable that the fibres without the NW are already exposed after the first flame treatment.

Table 3.2.: Flamed surfaces after first, fifth, and last flame treatment of Test A and after Test B.

Configuration	A1	A5	A11	B
	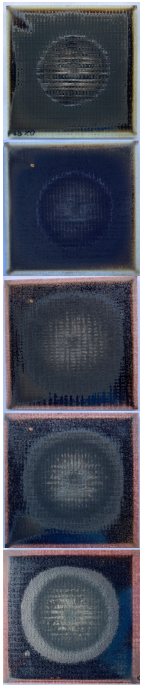	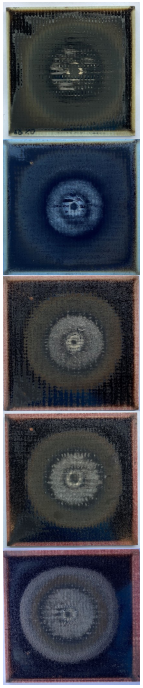	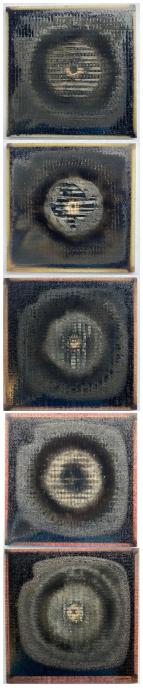	

Consequently, the matrix of the lower layers is more freely accessible, while the NW forms a closed layer above the load-bearing fibre layers. The matrix content is comparatively high in the NW, so more carbon is present, which can carbonise and form a char. If the number of flame treatments increases, the NW cannot withstand any more, which is also noticeable in an after-flame time of 13 s after A11. It is also noticeable that the ttis with NW are significantly lower than those without NW. However, this does not have a negative influence on the after-flame times.

When using RP, no after-flame times can be observed for any of the configurations analysed from the third flame treatment onwards. The configurations only differ in the three-minute flame treatments. While no after-flame times can be determined for the 12 % modified configuration in Test A11 and B, the configuration modified with 3 % RP throughout burns for eight seconds (A11) respectively four seconds in Test B. The only locally modified configuration is in a comparable range in terms of after-flame times. However, Table 3.2 shows that fewer fibres are exposed after A11 than with $[\mathrm{NW}, 0_8, \mathrm{NW}]^{3\%}$. On the other hand, Test B leads to comparable surfaces. Table 3.2 also shows that the modified configurations have a different char structure than the unmodified configurations due to the reaction of the RP described in the introduction. In general, Test B leads to a different visual impression. The load-bearing fibres are less exposed without prior flame treatment for all configurations with NW.

Figure 3.9 shows the temperature development over three minutes (A11 and B) exemplary for the configuration $[\mathrm{NW}, 0_8, \mathrm{NW}]$. However, in qualitative terms, the curve can be observed in the same way for all configurations. The temperature on the upper side initially rises more slowly, but the maximum measured value then exceeds that of test B as the flame exposure time increases.

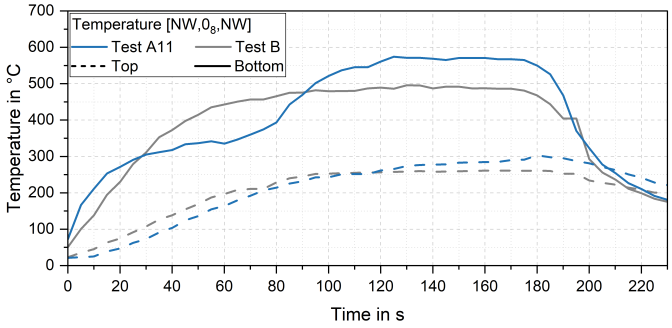

Figure 3.9.: Temperatures on the flamed surface (bottom) and the top of the specimen $[\mathrm{NW}, 0_8, \mathrm{NW}]$. 180 s flame treatment after 10 x 60 s (Test A11) and Test B.

As described in Chapter 3.1, the shielding caused by the formation of a char by the individual flame treatments leads to a change in heat conduction. As the duration of the flame treatment increases, the heat conduction across the cross-section appears to increase proportionately more. The reason for this may be the 'failure' of the NW and, thus, the loss of the char built up on it. On the

bottom side, the temperature is measured at the edge as described. In contrast to Test B, in Test A11 a plateau is formed at a comparatively lower temperature level. In this case, the temperature also increases to a higher maximum value with further flame treatment.

3.4.2. Combined Prepreg and Infusion Technique

Quality Control of Manufacturing

By using the introduced CPI-method, filtration effects are avoided. As Figure 3.10 shows, RP particles remain in the desired plies, which can be detected by the red colour of the entire layers. Individual RP particles are visible in Figure 3.10 in white, as the particles scatter the light of the microscope. According to the specifications of the manufacturer, the median particle size distribution is $D_{50} \approx 24$ µm. Larger particles are present mainly between the fibre layers and infiltrate the fibre bundles less frequently (see Figure A.3.1, Appendix). Due to the production of the prepregs via wet lay-up by hand, some pores are present in the prepreg layers. Porosity increased by a factor of ≈ 2.4, determined by analysing digital microscopy images [15] (see Appendix, Figure A.3.2).

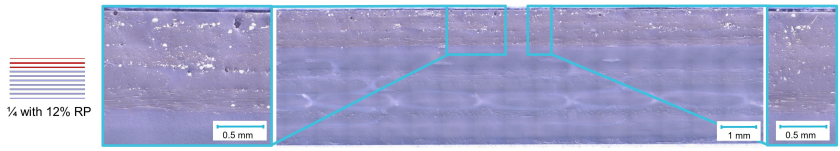

Figure 3.10.: Exemplary microscopic evaluation of CPI-process.

The densities and fibre-volume ratios are displayed in Table A.3.1 (Appendix). Due to the closed RTM-mould with a predetermined thickness of 4 mm, the fibre-volume ratios are ≈ 45 % for all lay-ups. The densities remain unchanged at ≈ 1.82 g/cm^3. The standard deviations within each configuration are very low, indicating good reproducibility. Hence, the manufacturing quality is adequate for the following investigations. For comparison, the handlaminates discussed in the previous section (Chapter 3.4.1) achieved fibre-volume ratios of ≈ 40 %.

Impacts of Process and Particle Loading on the Bending Strength

Figure 3.11 displays the bending strengths for all investigated lay-ups. The plates manufactured with standard RTM-process are shown in blue. The NW reduces the bending strength due to a different fibre distribution over the cross-section resulting in a shifted Steiner term.

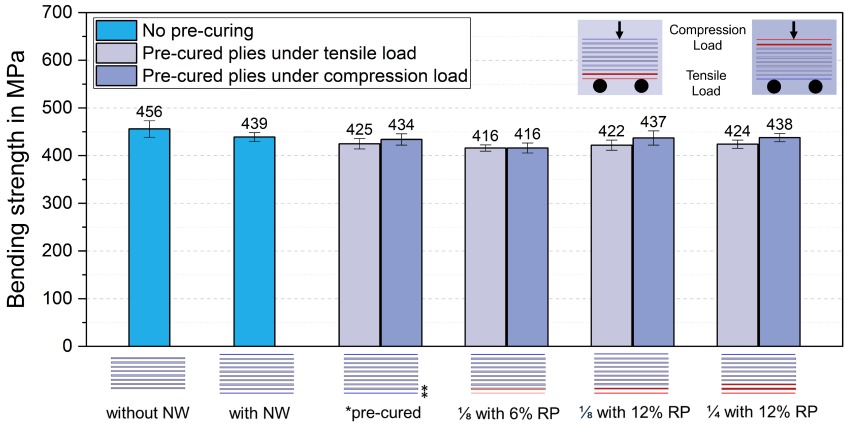

Figure 3.11.: Bending strengths for all configurations with the pre-cured side under tensile as well as under compressive load.

Within the lay-ups containing NWs, no difference exceeding the standard deviation could be found. In general, it is visible, that the bending strength measured with the pre-cured side under tensile load is slightly lower. Because this is the case for the unmodified but pre-cured configuration too, the decrease is supposed to be due to the occurring pores (see section 3.4.2) rather than because of the implemented particles. No further damage induced by the modified layers (e.g., delaminations during bending) was observed.

Flame Tests

The relative mass loss due to the flame treatment is shown in Figure 3.12. The unmodified configuration without NW exhibits the greatest mass losses. The use of the NW already reduces mass losses. This can be explained by the aforementioned higher matrix content in the NW, resulting in a denser char.

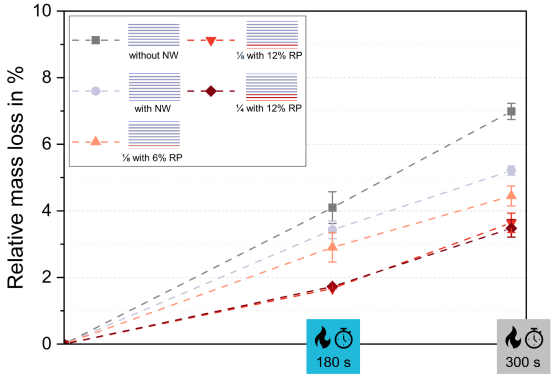

Figure 3.12.: Relative mass loss in % for different lay-ups and 180 s as well as 300 s of flame treatment.

The modification of the NW and ⅛ of the load-bearing plies with 6 wt. % RP only reduces the mass loss by a further small proportion. It is noticeable that the mass loss increases almost linearly with the flaming time, whereby the two configurations modified with 12 wt. % show less mass loss after 180 s, which may be an indicator of a desired delay. Another positive aspect is that the standard deviation is relatively low, ensuring that the flame test provides reproducible results. Table 3.3 sums up the time-to-ignition and after-flame times after 180 s and 300 s flame treatment for different configurations.

The trends are in line with the mass losses displayed in Figure 3.12. The NW already delays the tti, while the after-flame times for both flame treatments were shortened. Compared to the unmodified configurations, 12 wt. % RP significantly improve the tti (≈ 250 % for ¼ 12 % RP) and further reductions in afterburning times (≈ –32 % for ¼ 12 % RP) are observed, although the global RP content is still very low. By modifying the NW and ⅛ of the load-bearing layers with 6 wt. %, the analysed parameters, like the mass loss in Figure 3.12, fall between the unmodified and the 12 wt. % modified values. The tti is retarded by 25 % and the after-flame time nearly halved. It is remarkable, that the after-flame time after 300 seconds has already been reduced to a very low level. This may be due to the fact that a large part of the available matrix has already been carbonised over the entire cross-section and no further carbon source is available, causing the flame to fade. The unmodified test specimens also show lower afterburning times after 300 s than after 180 s, while the 12 wt. %

Table 3.3.: Time-to-ignition and after-flame times after 180 s resp. 300 s flame treatment for n = 4 specimens of different configurations.

Configuration	Time-to-ignition in s	After-flame time in s (180 s flame)	After-flame time in s (300 s flame)
without NW	14.6 ± 1.2	55.0 ± 17.1	27.5 ± 4.0
with NW	16.0 ± 2.8	50.0 ± 16.1	30.3 ± 2.9
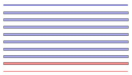 ⅛ 6% RP	20.4 ± 2.4	32.5 ± 2.5	18.0 ± 5.4
⅛ 12% RP	24.6 ± 10.1	23.0 ± 6.8	22.3 ± 4.9
¼ 12% RP	37.3 ± 2.5	20.3 ± 2.9	18.7 ± 0.5

modified lay-ups each show similar afterburning times in the range of 20 s. Figure 3.13 visualises the 180 s flame test, showing the significant improvement of the partially modified compared to the unmodified configuration.

The discussed trends are predominantly beyond the standard deviations of the investigated parameters (see Table 3.3). While the standard deviations of the unmodified configurations show higher deviations, e.g., in their after-flame times after 180 s flame treatment, the configuration with the highest degree of modification (¼ 12% RP) shows very repeatable results in their time-to-ignition and after-flame times. Despite the simplicity of the tests and the complexity of fire development processes, the tailored flame tests can be classified as representative and reproducible.

In Figure 3.14, cross-sections after flame treatment are shown which confirm, that the whole cross-section is affected for the unmodified and 6 wt. % configurations. The higher mass loss for unmodified specimens (Figure 3.12) is due to a broader affected area without RP.

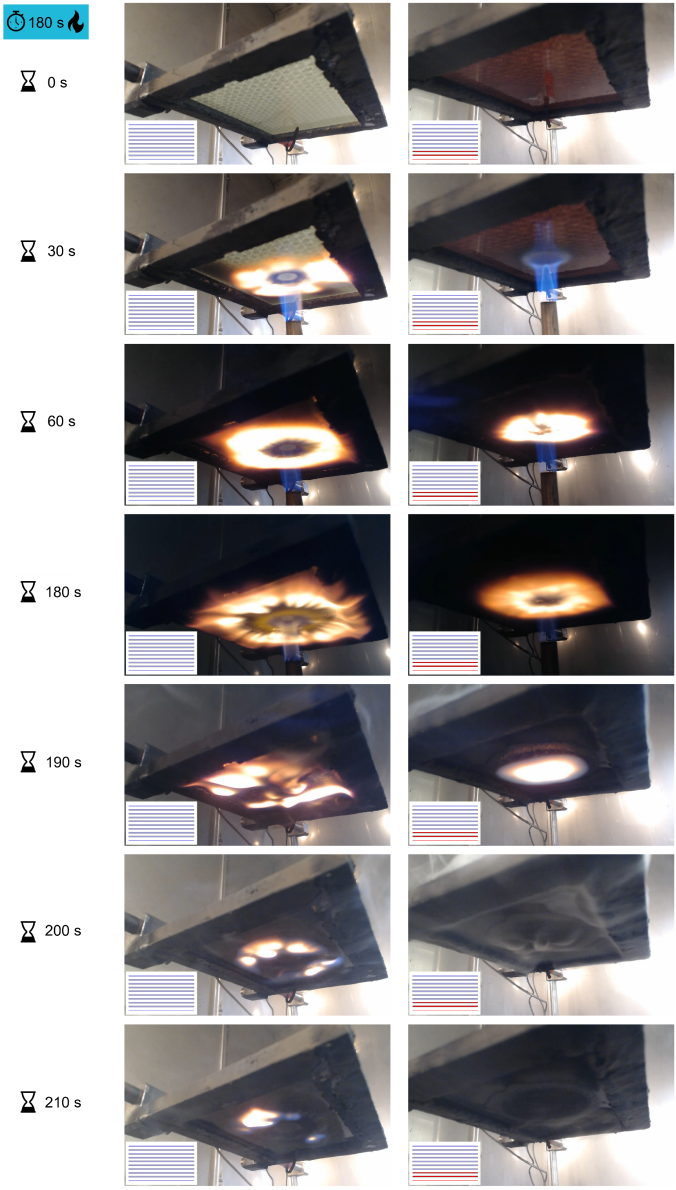

Figure 3.13.: Comparison between unmodified (left) and partially RP-modified (right) configurations manufactured via CPI-process during 180 s flame tests.

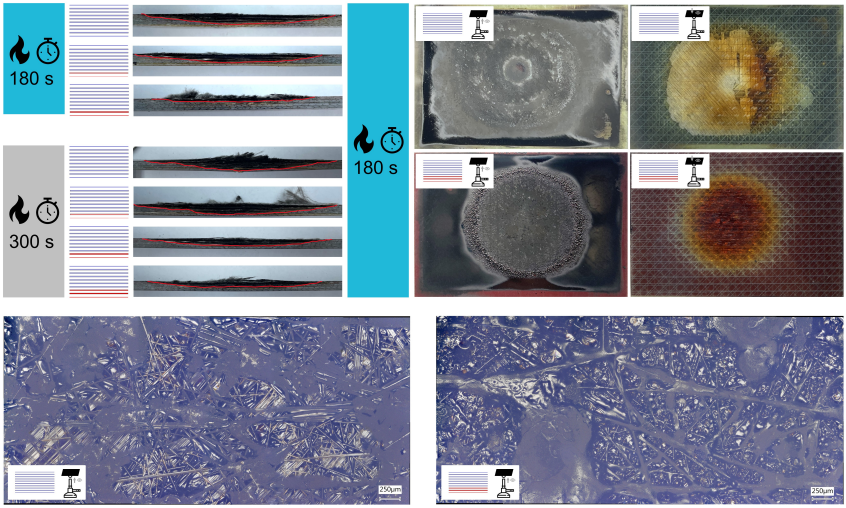

Figure 3.14.: Left: Cross-sections of relevant configurations after flame tests. Influenced plies are marked. Right: Flamed and opposite surfaces of specimens after 180 s flame treatment. Bottom left: Blank NW without RP modification. Bottom right: NW with char of condensed phosphoric acid.

Figure 3.14 (right) shows the affected areas of test specimens from the flamed and non-flamed side. The modification leads to a typical reaction of RP with O_2 and H_2O from the air on the flamed side to condensed phosphoric acid at $\approx 300\ ^\circ C$, forming a protective layer (see Figure 3.14, bottom right). The unflamed side is already damaged for unmodified specimens after 180 s of exposure to flame, while the modified configuration under consideration shows brown discolouration in a limited area due to heat exposure. The fibres are still intact as visible in the cross-sections in Figure 3.14 (left).

In Figure 3.15, the temperature progression over time is displayed for the flamed surface aside from the flame. It can be seen that the measured temperature decreases with an increase in the amount of RP. As described, the char built with RP slows the heat transfer, resulting in lower temperatures at the edge of the specimen. Consequently, the area with critical high temperatures for matrix degradation decreases with the use of RP.

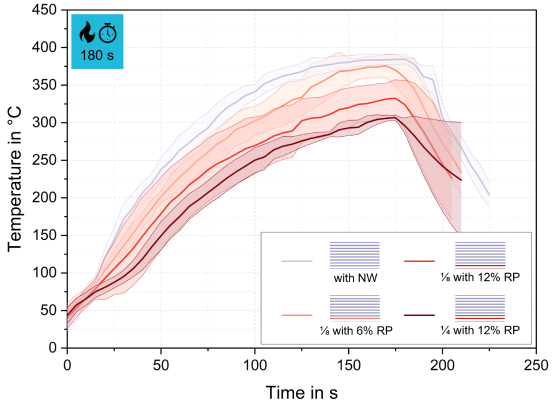

Figure 3.15.: Temperature of sensor on the flamed side during 180 s flame test for different lay-ups.

Residual Compressive Strength after Flame Tests

Figure 3.16 shows the residual strength of the different lay-ups standardised to their compressive strength (see Table A.3.2, Appendix A.3). To exclude influences from manufacturing, the unmodified specimens are also manufactured via the CPI-method.

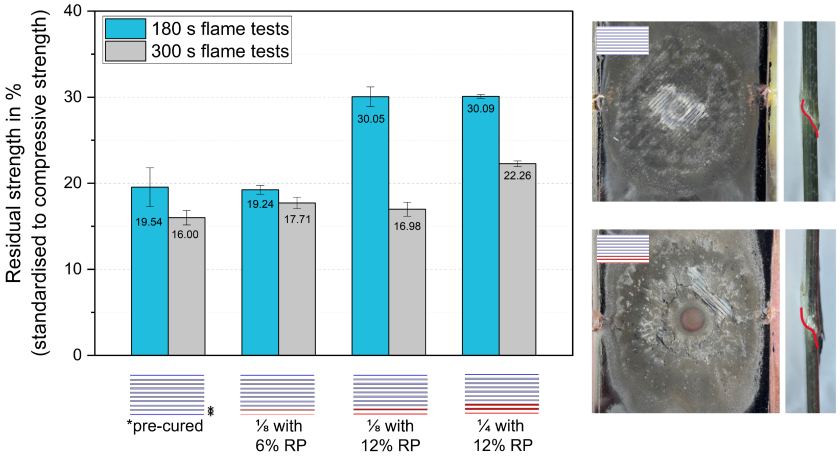

Figure 3.16.: Compressive strength retention of n = 3 specimens after flame tests and specimens after testing.

The residual strength of the specimens modified with 6 wt. % RP is at the same low level as that for the unmodified specimen. This observation is in line with the affected plies shown in Figure 3.14, where for both lay-ups similar levels of damage are visible. Modification of ⅛ of load-bearing plies with 12 wt.% RP significantly improves the residual strength after 180 s of flame treatment, while after 300 s of fire load, the compressive strength drops to the low values of the configurations first discussed.

The residual compressive strength of the composites containing 12 wt. % RP is up to 54 % higher after 180 s flame tests compared to the non- and low-modified composites, while the highest modification grade (¼ 12 %) also increased the residual strength after flame treatment of 300 s by approximately 40 %. These results highlight the significant improvement due to the local modification. The differences in the residual compressive strengths of the different configurations fall outside the standard deviations and are therefore reproducible for several specimens (n=3). As compressive strength retention is highly influenced by sample destruction by the flame treatment (see cross-sections in Figure 3.14), the standard deviation for compressive strength retention is slightly higher for specimens, where the standard deviations in Table 3.3, e.g., after-flame times, were also higher.

As the pictures in Figure 3.14 show, the char which is built during flame test with RP-modification cracks under compressive load and unembedded fibres become visible below, where load transfer is limited resulting in lower compressive strengths. A micrograph of a char crack is shown in Figure A.3.3 (Appendix), showing that cracks occur in the condensed phosphoric acid char in the NW (also see Figure 3.14). Accordingly, this char layer initially bears minimal loads compared to the blank NW without RP modification, where no cracks occur. However, compared to fibres with intact matrix, this is expected to be only a very small proportion.

Consequently, the proportion of plies with degraded matrix is decisive for the residual strength. Of course, ≈ 30 % residual compressive strength is generally not sufficient for further operation. However, in contrast to, e.g., impact damages [120], fires are easily noticeable and components are replaced after the fire. Nevertheless, an improved residual strength increases the probability of being able to evacuate in the event of a fire.

The test setup for determining the residual strength is suitable for qualitative comparisons between the examined configurations for uniform flame treatments. It reveals significant improvements with only small global amounts of RP when concentrated at the fire loaded surface. However, the number of modified plies must be adjusted for specific applications to fulfil all requirements to pass demanded large-scale tests.

According to Cheng et al. [91], epoxy resins achieve UL94 ratings starting at 7 % RP. Own results (Table 5.1) show that UL94 V-0 rating is achieved with 10 % RP in the specific epoxy system 827/137H. A minimum amount of flame retardants is therefore necessary for effective operation. Even though it was not possible to test this conclusively due to the filtration effects that occur, for example with regard to the residual strengths after flame treatment, it can be assumed that, for example, modifying 1/8 of the layers with 12 % RP leads to better results than distributing the same amount of RP over the entire cross-section (1.5 % RP), as the proportion is considered locally too low to be effective.

3.5. Conclusions

In summary, this chapter provided a methodology for tailored modification of composites. It was possible to show that pre-curing ensures that the modification remains in the desired plies so that the FR content can be kept as low as necessary. In addition, the mechanical properties did not change beyond the standard deviation. The test scenarios developed from various existing flame tests provide a screening method for making qualitative comparisons between different flame retardants or flame retardant proportions and their distribution in the laminate. A modification of individual layers with a small amount of FR already shows significant improvements in fire behaviour compared to unmodified configurations. In a direct comparison of the partially modified, handlaminated configuration $[\mathrm{NW}^{12\%*}, 0^{12\%*}, 0_7, \mathrm{NW}]$ with the configuration $[\mathrm{NW}, 0_8, \mathrm{NW}]^{3\%}$, approximately one third of FR can already be saved and similar results can be achieved with respect to the after-flame times. According to optical analyses, the tailored modified specimen is even less affected. 82.5 wt. % RP can be saved compared to the configuration modified with 12 % RP throughout. Differences are recognisable only with increasing fire load (180 s flame exposure). In addition, the use of a NW is useful not only for uniform surface qualities but also for fire protection applications, as the high matrix content leads to a more pronounced char.

The combination of RTM and prepregs with FR particles enables an industrially feasible production method with a low total FR content (≈ 1.5 - 3 % RP) and improves flame retardancy and residual strength. The presented approach provides clear results for evaluating the flame retardancy and residual strength using minimal equipment. The developed screening method allows qualitative comparisons to be made between different laminates and acts as a complement to the more complex, standardised test methods. In industrial use, flame-retardant modified prepregs can be positioned in RTM moulds in an automated manner, allowing the manufacturing of large parts, e.g., train walls, in infusion processes. For certification in industrial applications, the number of modified plies must be adjusted to meet the respective standards.

However, the hypothesis below can be fully confirmed:

An efficient use of flame retardants in appropriate locations can save material, contribute to lightweight design and minimise the impact on mechanical properties at the same time.

4. Sustainable Matrix Materials

Using biomolecules instead of synthetic matrix components can significantly reduce the risks to health and the environment in composite manufacturing. As the properties of bio-based alternatives are currently still mostly below the requirements for their typical use in mobility applications or, e.g., in rotor blades of wind turbines for energy generation [121], the working hypothesis of this chapter is:

Matrix polymers derived from bio-based feedstocks can achieve competitive properties while minimising environmental and health risks during processing.

Numerous approaches are under investigation to enable the use of bio-based resources for matrix polymers (see Section 4.1). Among these broad possibilities, the main part of the following chapter deals with amino acid-cured epoxy resins (Section 4.2), in which the curing agent as the most harmful component of classic epoxies is replaced by biomolecules. In Section 4.3, fully biobased matrix materials based on epoxidised linseed oil are examined.

4.1. State of the Art

Current economic and social challenges such as climate change, as well as the dependencies and resulting scarcity of resources, lead to a variety of scientific tasks. In the field of polymers and composites, there is a growing demand for sustainable and environmentally friendly alternatives to petrochemical systems that are also safe for human health.

Due to their outstanding properties, epoxy resins are often used as matrix material in FRPs [122]. They consist of at least one resin component with epoxy groups and a minimum of one curing agent. The use of platform chemicals, i.e., basic chemicals produced from renewable raw materials that are suitable as precursors for numerous other chemicals, is the easiest way to achieve more

sustainable matrix materials. For instance, commercially available, partially biobased epoxy resins use epichlorohydrin from renewable feedstocks, which, for example, reacts with bisphenol A via condensation to DGEBA.

Nevertheless, bisphenol A is known to be an endocrine disruptor and has a harmful impact on human health [123]. For this reason, research is increasingly focusing on alternatives based on vegetable oils [124–127], lignin [128–132], vanillin [133, 134], rosin [135–138], tannin [139], sugar [140, 141], cardanol [142–144], eugenol [145, 146], itaconic acid [147, 148], resveratol [149, 150] and other bio-based resources for the A-component. Since this thesis will focus on vegetable oils as resource in Section 4.3, the following state of the art (Section 4.1.1) will also focus on this feedstock.

In their non-cured state, epoxy resins pose critical environmental and health risks. Epoxy allergies are quite common among workers [151–154]. In particular, conventional curing agents, mostly derived from petrochemical raw materials, pose high risks [122], some of them are classified as toxic or even carcinogenic. Therefore, recent developments in sustainable alternatives for curing agents are highlighted in Section 4.1.2.

In addition to their low environmental impact and easy access, biomolecules are often available at low-cost and have therefore potential to be used in industrial applications where, besides performance requirements, the economic efficiency is a major factor for choosing materials. Nevertheless, the sustainability of biobased resources must always be assessed individually. Cultivated land is also limited and competes with food supply. Therefore, the use of by-products, residues and waste streams from food production should be pursued [155]. In addition, efforts should be made to ensure that resources are extracted without negative side effects on global biodiversity [155]. Some biobased resources are also harmful to human health. One example is furfuryl alcohol, which is used in the production of furan resin and may also pose serious health risks [156, 157].

4.1.1. Epoxidised Vegetable Oils

The availability of large amounts of vegetable oils (VO) at a low cost, combined with their advantage of being renewable and low in toxicity, makes these biological raw materials attractive environmentally friendly substitutes for petrochemical platforms for polymerisation [158–161]. Vegetable oils consist of three

long-chain fatty acids chemically bound to a glycerol backbone. This forms a typical triglyceride structure [159]. According to Radojcic et al. [162], triglycerides are the only readily available biomass-based raw material with a carbon-hydrogen ratio similar to that of petroleum. Depending on the type of plant, the season, the growing conditions, and other factors that affect the crop itself, the composition of fatty acid chains can vary significantly [163, 164].

VOs such as linseed or soybean oil consist mainly of linolenic acid and linoleic acid [163, 164]. The unsaturated chains of linolenic acid (see Figure 4.1 (i)) have three double bonds between two carbon atoms. Linoleic acid contains two of these double bonds (Figure 4.1 (ii)), but oleic acids with a single double bond or stearic, respectively, palmitic acids without double bonds can also be found in VOs [158, 165].

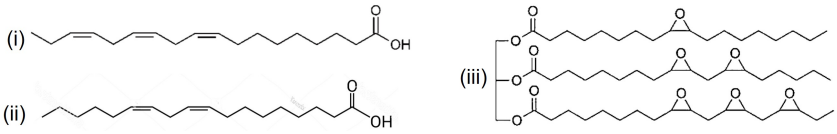

Figure 4.1.: Chemical structures of linolenic acid (according to [163]), linoleic acid and ELO (according to [162, 166]).

Table 4.1.: Composition of linseed and soybean oil in %. x is the number of carbon atoms, y the number of double bonds [167].

Fatty Acid (x:y)	Stearic (18:0)	Palmitic (14:0)	Oleic (18:1)	Linoleic (18:2)	Linolenic (18:3)
Soybean oil	4	11	23	53	8
Linseed oil	4	5	19	15	57

The unsaturation enables functionalisation with oxirane groups, with a conversion of more than 90 % usually being achieved [168]. Therefore, functionalised oil provides an excellent platform for a series of chemical reactions that can lead to polymeric materials [159, 162]. Epoxidation of these triglycerides can be achieved in a relatively simple and straightforward process by reaction with, for example, molecular oxygen or hydrogen peroxide [158, 163]. Table 4.1 compares the composition of linseed oil with soybean oil. Both vegetable oils differ in the proportion of linoleic and linolenic acid. Due to the larger number of double bonds, a higher functionalisation can be achieved with linseed oil. Figure 4.1 (iii)

shows an example structure of epoxidised linseed oil (ELO). Due to the influence of batch production, the number of oxirane groups can vary [162, 169, 170].

Conventional petrochemical epoxides have terminal epoxy groups. In contrast, epoxidised VOs have internal groups. This has a significant impact on the curing mechanisms and complicates thermal curing with amines, as is often used with fossil epoxides [171]. The literature reports successful curing with anhydride-based hardeners [172], with dicarboxylic acids [173], and with catalysts under radiation [159, 162]. However, even complete cross-linking of these monomers results in a flexible network with low cross-linking density due to long aliphatic chains, which is a challenge in the development of a composite material for structural applications with adequate mechanical properties [161, 174, 175].

In addition to linseed and soybean oil described in detail, canola [176], castor [177], karanja [178, 179], hemp [180], cottonseed [181], rapeseed [182, 183], and palm oil [184] have also been investigated as sustainable alternatives for epoxy resins.

4.1.2. Biobased Epoxy Curing Agents

For the production of bio-based curing agents, the literature often refers to bio-based feedstock for the synthesis of known, originally petroleum-based curing agents. For example, similar to the epoxy A component, curing agents can also be produced using cardanol. Cardanol is obtained from cashew nut shell liquid and enables the synthesis of phenalkamine via cardanol butyl ether using, among other substances, 1-chlorobutane and potassium carbonate [185]. Rosin-based [186, 187] or furan-based curing agents [188] have also been reported. However, bio-based feedstocks are very versatile and publications have also appeared on polyamine grape seed oil [189], gallic acid- [190] or isosorbide-based [191] curing agents.

Because these curing agents pose the same risks during synthesis and in their final state as the same chemicals from petrochemical sources, it may also be appropriate to use biomolecules as curing agents without additional synthesis if reactive functional groups are present.

For example, there are reports on the use of citric acid [192, 193] and itaconic acid [194] for the curing of epoxidised vegetable oils or the use of amino acids with accelerators [195, 196] for the curing of DGEBA.

4.2. Amino Acid-Cured Epoxy Resins

Amino acids are extracted and isolated from protein fermentation [197] or from protein hydrolysates through crystallisation and ion exchange chromatography. Gelatin, hair or feathers can be possible feedstocks. Amino acids are available at a low cost, permitted as food supplements, and are therefore harmless to the environment and health. In the literature, it has already been shown that amino acids are capable of curing epoxy resins using accelerators such as 2-Ethyl-4-methyl imidazole [195] or 1,1'-(4-methyl-1,3-phenylene)bis(3,3-dimethylurea) [196]. Nevertheless, there are open questions, for example in terms of their reaction mechanisms and curing kinetics with and without accelerators. Furthermore, the effects of variations in mixing ratios on the thermo-mechanical properties, their lifetime properties and durability, e.g., their stability towards environmental influences, or their use as matrix materials in FRPs have not yet been addressed.

Based on the functional groups they contain and preliminary tests, the amino acids L-arginine (L-Arg), L-tryptophan (L-Trp) and L-phenylalanine (L-Phe) were selected and tested as part of this dissertation. L-Arg is especially prevalent in seeds and nuts (e.g., pumpkin seeds and peanuts), as well as in meat, fish, and legumes. Relatively large amounts of L-Trp are found in grains (e.g., bran), while L-Phe is contained in eggs and dairy products (e.g., cheese) [198–200].

4.2.1. Methods

Where necessary, additional specifications are given to carry out the tests in this chapter, expanding on those already presented in Chapter 2.

Uncured Systems

In order to investigate not only the temperature-dependent viscosity of the resin/hardener dispersions, but also their shelf life under different storage conditions, rheological measurements were repeated after 1, 4, 8, 12, 16, 20 and 24 weeks with cooled storage (11.5 ± 0.6 °C) and storage at room temperature. The viscosity at 35 °C is evaluated. For selected systems, namely 827/L-Arg and 827/L-Arg/UR500, DSC measurements after 34 weeks of room temperature and cooled storage were conducted with 10 K/min and compared to the initial state. Thermokinetic methods were used as described (see Section 2.2.5) to determine

individual curing profiles for each system. For example, the system 827/L-Arg is cured in two steps, including 60 min at 167 °C followed by 70 min at 180 °C. Defined heating and cooling rates as well as all other curing profiles are listed in Table A.4.1 in the Appendix.

Cured Thermosets

To screen the mechanical properties of different resin/amino acid combinations, dogbone specimens of type 1BA according to DIN ISO 527 [26] are used in Section 4.2.3 (1 mm/min for the determination of Young's modulus, 5 mm/min afterward). For selected systems, the tensile strength was validated with specimens of type 1B. As specimens were partially tested using a modified setup (lower stiffness of the machine due to extended rods), the respective elongations at break were corrected according to Hook's law.

Since a qualitative comparison is made in Section 4.2.4 for varying mixing ratios and in Section 4.2.7 to analyse the impact of environmental and chemical influences on the mechanical properties, the geometry according to [201] was chosen due to their known accurate and reproducible performance in tensile testing. Furthermore, this geometry allows resource-saving manufacturing and the use of similar specimen design also for thermo-mechanical analysis (DMA-T_g measurements). Dogbone-shaped samples are milled and conditioned for 24 h at 40 °C under vacuum and tested on the introduced DMA-device in static tensile tests 1 mm/min (5 % strain/min) until failure. Dynamic tests were performed with 1 Hz, 2 K/min, 20 °C to 150 °C). Additionally, T_gs are determined by DSC by midpoint analysis. A heating rate of 10 K/min was defined for two heating runs (maximum temperatures: 1. 180 °C; 2. 200 °C).

Stoichiometric Variations

Section 4.2.4 investigates the effects of changes in the mixing ratio of the system 827/L-Arg. This serves, among other purposes, as a basis for establishing mixing tolerances in potential industrial applications. The theoretically calculated stoichiometric mixture (see Section 2.1 is referred to as R = 1.0). In this study, the amount of L-Arg is changed between 50 % and 150 % of the theoretically stoichiometric amount. Table 4.2 shows their weight-related mixing ratios.

Table 4.2.: Mixing ratios of all manufactured configurations.

Stoichiometric Ratio R	827 in g	:	L-Arg in g
0.5	100	:	6.87
0.6	100	:	8.24
0.7	100	:	9.62
0.8	100	:	10.99
0.9	100	:	12.36
1.0	100	:	13.74
1.1	100	:	15.11
1.2	100	:	16.49
1.3	100	:	17.86
1.4	100	:	19.24
1.5	100	:	20.61

Immersions

Immersions in demineralised water take place at 8 °C, 22 °C, 50 °C and 70 °C, while in isopropanol, acetone, and hydraulic oil, the immersion temperature is set to 22 °C. For faster saturation, small dogbone specimens as published by Gibhardt et al. [201] are used. In order to compensate for slight changes in the thickness of the specimen due to their different manufacturing methods, the immersion time is subsequently standardised to 1 mm. This standardisation was verified using specimens of different thicknesses. Closed vessels ensure that test specimens are exposed to the respective medium from all sides. Before immersion, specimens are dried in a vacuum chamber at 40 °C, unless mass consistency. Changes in mass and geometry are tracked with a precision scale (AT261DeltaRange®, Mettler Toledo, Columbus, Ohio, USA), an outside micrometre and a caliper gauge during immersions using at least three specimens. The immersed specimens were re-dried and weighted in a vacuum oven at 40 °C until mass consistency, followed by re-drying at 100 °C under vacuum to obtain additional information on degradation.

FTIR measurements in the MIR range are performed for dry and immersed specimens and for 48 h at 40 °C under vacuum re-dried specimens in ATR mode. Furthermore, FTIR analyses of the immersion media after immersions of specimens are conducted and compared to references stored in similar vessels without specimens.

Composites

The composites examined in Section 4.2.8, were manufactured using the Direct-Preg process. Before autoclave curing, impregnated fibres are used directly or stored for three months at –19 °C respectively 20 °C to investigate the feasibility of energy efficient prepreg storage. Mechanical testing was performed as described in Chapter 2.

4.2.2. Mixture and Shelf Life of Dispersions

Representative for all configurations, Figure 4.2 shows microscopy images of L-Arg as received (a) and the different dispersion methods in 827 (b-e). Of the methods described in Section 2.2.1, the three-roll mill (b) is the most suitable to break up agglomerates and is therefore used for this study. Due to the minimal gap of 5 µm, the particles are reduced in size and well dispersed. Although the other tested methods (c-e) lead to a reduction in particle size compared to the initial state (a), particles > 100 µm are still present in each case, causing sedimentation and also leaving less surface of the particles available for interaction with the epoxy resin.

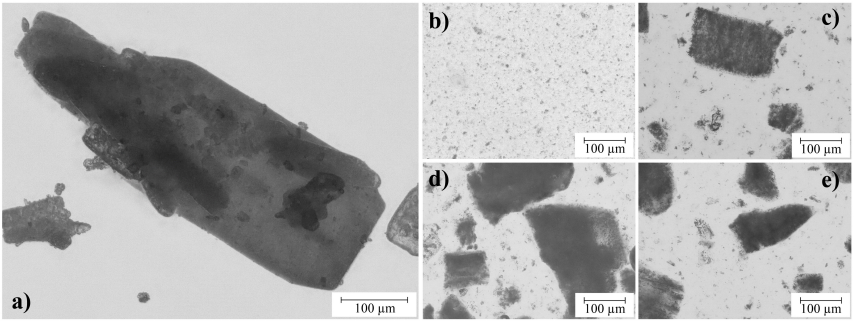

Figure 4.2.: Micoscopy images of L-Arg. a) Initial state as well as dispersed into 827 via b) three-roll mill, c) Thinky-Mixer, d) ultrasonic bath and e) ultrasonic homogeniser.

Rheological tests are conducted to determine the flow behaviour of the mixtures of resins and curing agents. In the case of the utilised plate-plate rotational rheometer, torsional shear is applied, and the correlation between shear stress and shear rate is determined. The viscosity of the thermosets increases with the degree of curing. Repeated measurements over a longer period can be used to

determine whether the material shows significant increases in viscosity over time due to curing reactions and is therefore not storable under the tested conditions. Figure 4.3 (left) displays that SR810/L-Arg has a viscosity lower than that of 827/L-Arg. 827 consists solely of DGEBA, while SR810 also consists partially of DGEBF and 1,4-Butanediol diglycidyl ether, which are less viscous components compared to DGEBA [202].

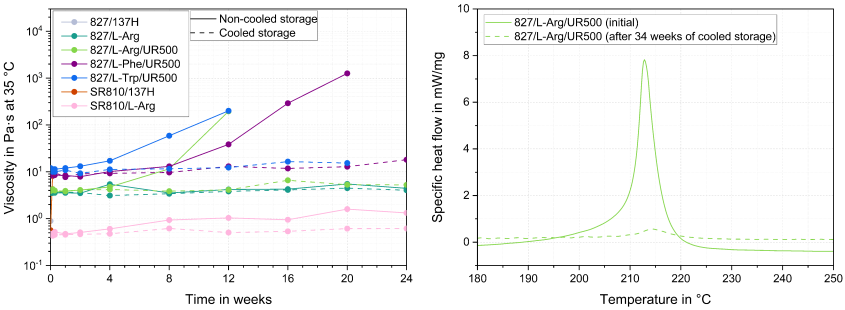

Figure 4.3.: Left: Viscosity at 35 °C within 24 weeks for cooled (≈ 11.5 °C) and room temperature storage. Right: Thermograms of 827/L-Arg/UR500, initial and after 34 weeks of cooled storage at ≈ 11.5 °C.

Evidently, the viscosities of all resin-hardener dispersions do not increase considerably within 24 weeks of cooled storage (≈ 11.5 °C). For 827/L-Arg and SR810/L-Arg, it also does not increase significantly under room temperature conditions. In contrast, the classical amine-curing agent 137H cures both epoxy resins within one day under both storage conditions.

DSC measurements conducted after 34 weeks confirm, that cooling generally extends the shelf-life, whereas the accelerator causes a decrease in latency. While for 827/L-Arg the enthalpy of reaction in cooled (406.2 J/g) and non-cooled storage (411.7 J/g) does not show any deviations beyond the measuring accuracy compared to the initial state (411.4 J/g), the same curing agent with accelerator shows a different behaviour (see Figure 4.3, right). The initial reaction enthalpy of 414.1 J/g reduces to 43.8 J/g (equivalent to 89.4 % curing) for cooled storage, although the viscosity shows no significant changes, at least for the first 24 weeks. For non-cooled storage, measurements are not feasible after 34 weeks due to its high viscosity.

Both the rheological measurements and the DSC results indicate possible applications as prepreg resin systems for dispersions without accelerator, whereby

energy can be saved by storing prepregs at room temperature or slightly cooled at approximately 11.5 °C compared to the common storage temperature of prepregs (- 18 °C). Besides energy savings, simplified production planning and lower investment costs are further advantages in this case.

4.2.3. Characterisation

Thermal Properties

The glass transition temperatures obtained from DSC and DMA are summarised in Table 4.3. The plates were manufactured with the same cooling rate so that the influence of the thermal history on T_g is minimised in the first heating run. The second heating run shows only small changes within tolerances, which, in addition to the absence of exothermic post-curing peaks in the first heating run, indicates complete curing for all configurations. The curing with L-Arg leads to a T_g-onset (DMA) of almost 130 °C and exceeds that of 827/137H by more than 10 K. 827/L-Trp/UR500 also shows a higher T_g than the reference system. The dependence of T_g on the resin component can also be shown, SR810 leads to lower T_gs. As mentioned in Section 3.1, SR810 consists in part of DGEBF and 1,4-Butanediol diglycidyl ether as a reactive diluent. In addition to lower viscosities [202], both also generally result in lower T_gs due to less dense network structures [203, 204].

Table 4.3.: Glass-transition temperatures of all configurations obtained from DSC and DMA.

	T_g (°C) DSC: Mid-point			T_g (°C) DMA: Onset		
827/137H	114.13	±	0.69	118.66	±	0.81
827/L-Arg	121.23	±	0.90	129.05	±	0.38
827/L-Arg/UR500	99.77	±	1.13	106.74	±	0.33
827/L-Phe/UR500	92.87	±	1.19	97.95	±	1.65
827/L-Trp/UR500	113.83	±	1.84	122.86	±	0.46
SR810/137H	90.37	±	0.45	94.56	±	0.77
SR810/L-Arg	84.93	±	3.02	94.55	±	0.33

TGA can be used to investigate the temperatures at which decomposition processes occur. The decomposition is expressed as a loss of mass. The mass loss curves obtained from the TGA under nitrogen as well as under synthetic air

atmosphere are shown in Figure 4.4. As expected, residues (8.42 ± 1.82 %) are retained under nitrogen atmosphere, while samples are completely decomposed under synthetic air [205]. Compared with the reference system, the mass loss with the biobased curing agents starts at lower temperatures and extends over a wider temperature range. Therefore, the decomposition temperatures T_d (see Table A.4.2 and A.4.3) are at comparable temperatures which are within the normal range of literature values for epoxies [206]. More relevant for practical use is the temperature at which mass loss begins. All configurations demonstrate no significant mass loss up to 200 °C. By comparing the mass loss curves of the configurations 827/L-Arg and 827/L-Arg/UR500, it is noticeable that the accelerator contributes to a premature onset of the mass loss. After evaluation of the T_gs and T_ds, it can be stated that the accelerator reduces the thermal properties.

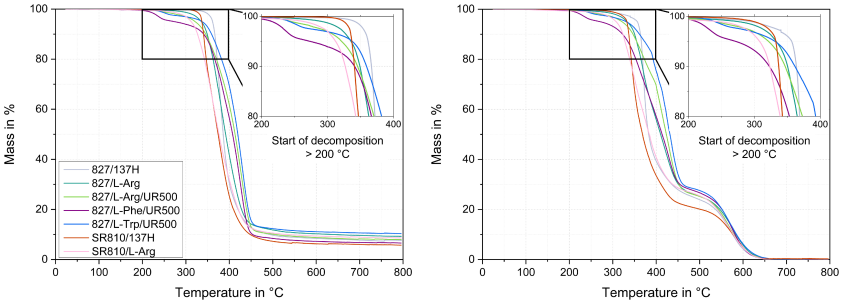

Figure 4.4.: Mass loss curves with detailed view on the onset of mass loss obtained from TGA. Under nitrogen atmosphere (left) and under synthetic air (right). One representative graph for each configuration.

Mechanical Properties

Table 4.4 summarises the mechanical properties determined for specimens with geometry 1BA. Especially 827/L-Arg achieves excellent tensile strengths and suitable tensile moduli. This can be explained by the fact that L-Arg has the comparatively highest number of reactive side. This results in a higher cross-linked polymer, which tends to improve tensile strength and modulus [207, 208]. The resulting network structures are discussed in detail in Section 4.2.6. In addition, compared to the other amino acids under investigation, less L-Arg particles are required for a theoretically stoichiometric mixing ratio. In contrast to nanoparticles, most microparticles reduce mechanical properties (see

Section 5.3.3), because larger particles may initiate failure [209, 210]. Therefore, a lower proportion of particles can be expected to have a less negative effect on the mechanical properties as the probability of non-reacted and agglomerated curing agents decreases. This is investigated in detail in Section 4.2.4. The negative influence of the accelerator on the mechanical properties is less than on the thermal properties but also significant. With the partially biobased resin SR810, slightly higher tensile moduli and lower strengths are achieved when cured with 137H, for which the existing DGEBF content can be mentioned as an explanation [203]. Cured with L-Arg, SR810 provides comparable tensile strengths, since the failure is defect-driven (see Section 4.2.4).

For the configuration 827/L-Arg/UR500, specimens of type 1BA (see Table 4.4) achieve tensile strengths of 73.66 ± 0.96 MPa, while 74.68 ± 1.18 are evaluated for specimens with geometry type B. Therefore, the differences between test geometries are not significant in terms of tensile strength. When tested on DMA (small dogbone geometry [201]), the Young's modulus does not show significant differences, which confirm comparable machine stiffnesses / results. Exemplary for the configuration 827/L-Arg, values of 2.90 ± 0.11 GPa are determined for the small dogbone geometry (vs. 2.91 ± 0.08 GPa for type 1BA as displayed in Table 4.4). Nevertheless, comparisons will only be made between identical geometries and machine configurations in the following chapters. In order to investigate the temperature dependency of the mechanical properties, tensile tests were also performed at various test temperatures for 827/L-Arg. The results can be found in Section 4.2.7.

Table 4.4.: Mechanical properties of the materials under investigation (specimen type: 1BA; test temperature: 22 °C).

	Tensile strength in MPa	Elongation at break in %	Young's Modulus in GPa
827/137H	76.61 ± 0.60	9.14 ± 0.73	2.63 ± 0.74
827/L-Arg	85.22 ± 0.40	4.57 ± 0.14	2.91 ± 0.08
827/L-Arg/UR500	73.66 ± 0.96	3.51 ± 0.07	3.13 ± 0.14
827/L-Trp/UR500	50.70 ± 2.51	2.15 ± 0.13	3.11 ± 0.08
SR810/137H	71.64 ± 0.29	7.76 ± 0.35	2.60 ± 0.07
SR810/L-Arg	86.31 ± 4.04	3.40 ± 0.28	3.29 ± 0.07

The results of the SENB tests conducted that analyse the fracture toughness of several investigated systems are listed in Table 4.5.

Table 4.5.: Critical-stress-intensity factor ($K_{I,C}$) and the energy per unit area of crack surface ($G_{I,C}$) at fracture initiation obtained from SENB tests of several configurations. Test temperature: 22 °C.

	$K_{I,C}$ in $MPa \cdot \sqrt{m}$	$G_{I,C}$ in kJ/m^2
827/137H	0.824 ± 0.272	0.260 ± 0.180
827/L-Arg	0.723 ± 0.052	0.164 ± 0.024
827/L-Arg/UR500	1.191 ± 0.197	0.424 ± 0.146
827/L-Trp/UR500	1.574 ± 0.078	0.726 ± 0.073
SR810/L-Arg	0.838 ± 0.108	0.196 ± 0.056

The critical-stress-intensity factor at fracture initiation ($K_{I,C}$) of 827/L-Arg is comparable to what was calculated for 827/137H, but 827/137H is more ductile and more energy is dissipated at fracture initiation (increasing $G_{I,C}$). SR810/L-Arg and 827/L-Arg are in a comparable range with an overlapped standard deviation. The DGEBF content leads to a minimal increase in fracture toughness, as it results in slightly more flexible network structures. However, the calculated values are in the range of literature values for epoxies [211].

Figure 4.5 displays differences in the fracture surface, also providing information on crack propagation. Stable crack propagation can be seen for 827/137H, where clear concentric curved lines emanate from the crack tip, as bending results in non-uniform stresses across the thickness. In contrast, 827/L-Arg exhibits a fracture pattern that is much rougher in appearance. The 3D profile of the fracture surface in Figure 4.5 (right) shows significant height differences. This may be the case because the crack propagates in an energetically favourable manner and can evade possible agglomerates, which may act as crack suppressors.

UR500 as additional implemented particles significantly increases $K_{I,C}$ and $G_{I,C}$ of arginine-cured epoxies. This might be due not only to the added particles as additional crack suppressors but also to differences in the occuring curing reactions and the resulting network structures. Figure 4.5 displays significant differences and shows the occurrence of cristal structures on the fracture surfaces for 827/L-Arg/UR500 and 827/L-Trp/UR500. 827/L-Trp/UR500 showed the highest fracture toughness of the investigated configurations, most likely because of the highest particle loading. Figure 4.5 shows the occurrence of agglomerates/cristals throughout the cross-section. The rough appearance of the fracture surface is also conceivable developing, because the crack reaches the

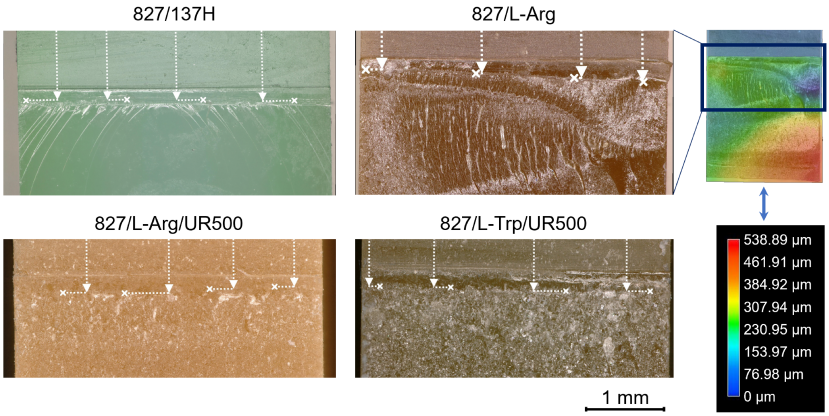

Figure 4.5.: Representative fracture surfaces after SENB testing and 3D roughness evaluation of 827/L-Arg. Arrows indicate the respective initial crack length.

sonic velocity of the material. More energy within the specimen cannot be dissipated by further accelerating the crack, resulting in the creation of multiple and bifurcate cracks and greater energy dissipation [211].

Taking into account its overall thermal and mechanical properties, L-Arg offers the highest potential of the investigated configurations (see Figure 4.6).

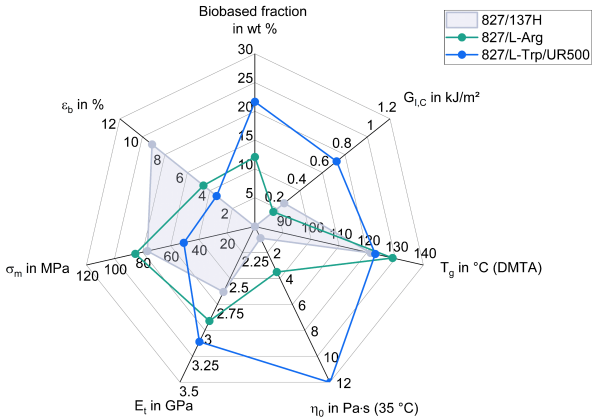

Figure 4.6.: Comparative overview of the analysed material properties for selected matrix systems.

In addition, plate production was successfully carried out without an accelerator. This simplifies the investigation of the reaction mechanism (Section 4.2.5), which is expected to provide insight into the efficient use of catalysts/accelerators. Despite the high potential, limitations and special requirements have to be explored. For the reasons mentioned above, this is done in the following sections using 827/L-Arg as an example.

4.2.4. Stoichiometric Variations

So far, the stoichiometric mixing ratio was calculated via the number of active hydrogen atoms per amino acid molecule. This assumes that all reactive groups react. Since it is not yet clear whether, which and when specific reactions take place, it is important to conduct more in-depth experimental investigations in this regard. With respect to the desired application as matrix resin in FRPs, the analysis of different mixing ratios offers the possibility to find a performance-optimised mixing ratio allowing to exploit the full potential and the limits of amino acid-cured epoxy resin. From this, it may be possible to determine how deviations in the mixing ratio affect the reactions that take place, influencing the resulting network structures and consequently the thermo-mechanical properties. Because of its highest potential, this analysis is conducted with the system 827/L-Arg.

According to previous reports, the stoichiometric ratio of epoxy A components and their curing agents has a significant effect on the chemical and physical properties of epoxy resins [212–214]. While anhydrides are normally used with stoichiometric ratios of 0.5 to 0.85 [215] due to significant epoxy homopolymerisation, amine curing agents are used in near stoichiometric ratios to obtain performance-optimised polymers [215]. The use of excess amine will result in unreacted amine-terminated dangling chain ends and reduced cross-linking, resulting in tougher but less moisture- and chemical-resistant polymers. Morsch et al. [213] reported that systems with a volume of over-stoichiometric curing agents resulted in an increase in tensile strengths and moduli and a decrease in the thermal expansion coefficient. Furthermore, Li et al. [216] found that over-stoichiometric mixtures can improve cryogenic properties. While amine-rich mixtures showed a greater deformation capacity, D'Almeida et al. [217] and Tavares et al. [218] reported the formation of tight macromolecular structures in epoxy-rich mixtures that result in brittle behaviour. Besides, the stoichiomet-

ric ratio had a great influence on the room-temperature aging process of epoxy resins. Among other reasons, D'Almeida et al. [217, 219] identified the recrystallisation of unreacted epoxy monomers for increased brittleness of epoxy-rich systems with aging treatment, while amine-rich configurations had more stable mechanical properties.

In a nutshell, off-stoichiometric mixing ratios are known to affect the resulting network structures, because functional groups cannot find a suitable reaction partner and remain unreacted or react via otherwise not favoured paths. Depending on the specific system, epoxy-rich mixtures tend to embrittlement while curing agents in excess lead to tougher polymers.

Most studies are conducted with liquid curing agents. However, especially particulate curing agents such as amino acids might show differences. Some studies investigated changes in the mixing ratio for amino acid-cured epoxies: With an increasing amount of L-Tyrosine as a curing agent, Rothenhäusler et al. [220] found improved fracture toughness due to crystal formation, while, e.g., the glass transition temperature only changed slightly. Li et al. [221] investigated L-Tryptophan-cured DGEBA with three different mixing ratios and found differences in reaction enthalpies and glass-transition temperatures with maximum values for theoretically sub-stoichiometric ratios.

Optical Examination

Arginine-cured epoxies become increasingly opaque with an increasing number of L-Arg particles (see Figure 4.7).

Figure 4.7.: Photographs of test specimens with different mixing ratios. Labelling x-y with x: L-Arg content in wt % of the theoretical stoichiometric amount and y: Numbering for traceability. Stoichiometric configuration from plate D.

This is caused by increased light diffraction in the agglomerates of particles. For up to 80 % of the theoretically stoichiometric amount of L-Arg, the specimens are

still yellow-transparent, for 90 % and 100 % becoming increasingly brownish. In over-stoichiometric mixtures, the background is no longer recognisable. Within the over-stoichiometric mixtures, no significant differences with further increases in arginine quantity are observable.

Rheological Characterisation

Temperature-dependent viscosities for selected mixing ratios are shown in Figure A.4.1 in the Appendix. Because of the higher amount of the solid component, an increase of the stoichiometric ratio results in higher viscosities at room temperature, whereas the differences decrease with higher temperatures. In detail, the complex viscosities are between 9 Pas (R = 0.5) and 16 Pas (R = 1.5) at 25 °C and approximately 1 Pas for all configurations at 50 °C onwards.

Fourier Transform Infrared Spectroscopy

The thermograms of the DSC measurements carried out for all mixing ratios do not show any exothermic peaks after curing. This indicates that in each case all possible exothermic reactions occured during the defined curing process. However, this neither means that the occuring reactions must be similar, nor that no unreacted resin or curing agent is left. If one component is missing, the other cannot react completely and is present partially reacted or unreacted. FTIR measurements are performed to gain deeper knowledge of the reactions that occur in the different configurations.

Figure 4.8 (left) displays the absorbance data of the cured systems in the range of the epoxy peak ($\approx 910 - 915$ cm^{-1}) [222, 223]. The severely sub-stoichiometric ratios with 50 % and 60 % of the theoretically stoichiometric amount of L-Arg show a significant epoxy peak. For the other sub-stoichiometric ratios, the left-over epoxy is still visible in the form of a shoulder in this wavenumber range. All other configurations do not show specific epoxy peaks. The shape and heights of the peak correspond to expectations: For R = 0.5 the peak is larger as the epoxy groups remain. This observation is in line with the outstandingly different results of the thermo-mechanical characterisations for R = 0.5 and R = 0.6 compared to the other theoretically sub-stoichiometric ratios discussed later.

Figure 4.8 (right) shows the spectra between 1720 cm^{-1} and 1600 cm^{-1}. In this range there are various vibrations of C=N groups, which can be present in argi-

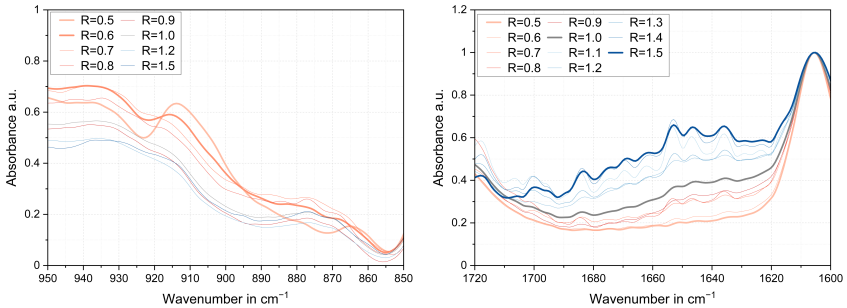

Figure 4.8.: Normalized FTIR Spectra of all stoichiometric ratios between 950 – 850 cm^{-1} (left) and 1720 – 1600 cm^{-1}(right).

nine acyclic (1690 – 1640 cm^{-1}), conjugated (1660 – 1630 cm^{-1}) and as imines (1640 – 1633 cm^{-1}). The vibrations of primary amides (1650 – 1620 cm^{-1}) are also present. These can be formed during the reaction of two arginine molecules through the formation of peptide bonds. According to Li et al. [221], a peak at 1665 cm^{-1} corresponds to asymmetric deformations in NH_3 $^+$. Primary and secondary amines (1650 – 1590 cm^{-1}) are also reported in this wavenumber range. These cannot be detected for the configurations R = 0.5 and R = 0.6, which is consistent with the still present epoxy groups discussed above. From R = 0.7 onwards, an increase in the spectrum in this wavenumber range is recognisable as a superposition of the oscillations mentioned. This increase rises with an increase in the arginine content, whereby a disproportionately high enhancement is visible for over-stoichiometric mixtures (R $\geq$ 1.1). This supports the forthcoming discussion that a significant drop in many of the thermo-mechanical properties analysed is observed from R = 1.1 upwards.

A significant change for over-stoichiometric configurations is also visible in the peak position between 3600 and 3100 cm^{-1} (Figure 4.9). Both a clear peak shift and a change in peak height with an increase in the arginine content are recognisable. In this range, the peaks of several oscillations overlap, the exact naming and position of which sometimes shows slight deviations in the literature. According to Mora et al. [224], there are peaks in this region that can be assigned to different types of hydrogen bonds. The wavenumber of hydrogen bonds, e.g. (-OH — HO-) or (-OH — HN-),would shift to lower wavenumbers in molecules and prepolymers than in networks, which matches the peak shift shown in Figure 4.9,

as more molecules are present unreacted when more arginine is present in the system.

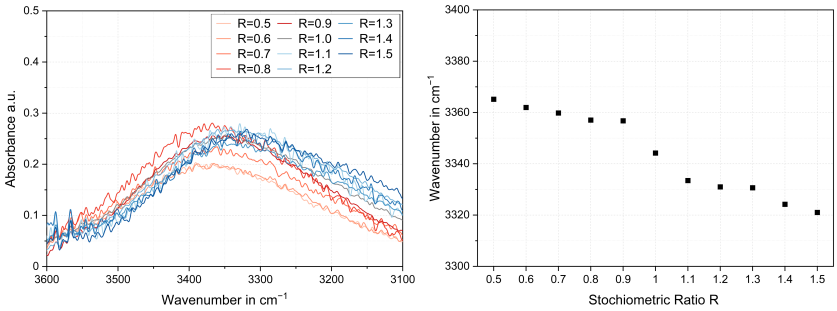

Figure 4.9.: Peak shift between 3600 cm^{-1} and 3100 cm^{-1} with stoichiometric variation.

Furthermore, according to Kolev [225], a peak at 3288 cm^{-1} is characteristic of amides. As described above, these are likely to form more when more L-Arg is present in the system. This may be another reason for the shift of the superimposed peak to lower wavenumbers for over-stoichiometric configurations. Li et al. [221] reported a broad peak between 3200 cm^{-1} and 2700 cm^{-1} corresponding to $NH_3{}^+$.

The peak shift is shown in Figure 4.9 (right) over the stoichiometric ratio R. The theoretical stoichiometric ratio R = 1.0 represents a turning point in this curve. The position of the peaks is determined using Gaussian fitting as shown in Figure A.4.2. It is noticeable that the peaks for low L-Arg ratios are symmetric, so that the Gaussian fit fits over a wide range of the peak. This is no longer the case for higher stoichiometric ratios; a strong asymmetry can be observed, which can be explained by a significant increase in an additional peak at lower wavenumbers (e.g., remaining $NH_3{}^+$, amide formation, intermolecular hydrogen bonds). For this reason, the limits were adjusted for the comparison of the peak maximum so that the maximum of the peak could be visualised with the Gaussian fit.

An increase in peak height has also been reported to be an indicator of an increase in the number of hydrogen bonds [226]. A quantification evaluation is omitted, as the signal strength of the ATR measurements should be treated with caution. However, qualitatively, the peak height is the lowest for R = 0.5 and

R = 0.6, which is consistent with Figure 4.8 (left), indicating that there is no significant amount of amide and -NH bonds for the formation of hydrogen bonds for these configurations. Furthermore, it is conceivable that the different L-Arg proportions in the configurations could also lead to differences in water absorption (see Section 4.2.7), which would also influence the formation of hydrogen bonds and thus the IR peak in this wave number range.

Mechanical Characterisation

Figure 4.10 displays the tensile strength, the elongation at break, and the complex modulus for all stoichiometric ratios tested determined at room temperature. Furthermore, the corresponding stress-strain diagrams are given in Figure A.4.1 (Appendix). The achievable tensile strengths cover a range from about 70 MPa to 95 MPa and follow a clear dependence on stoichiometry. Consequently, the range that can be set encompasses an order of magnitude of 25 %. While the stiffness remains largely unaffected, the maximum elongation at break is most sensitive to changes in the stoichiometry of the L-Arg-cured epoxy. Differences of more than 50 % occur, whereby the most brittle configurations are found for both extremes, significantly over- and sub-stoichiometric mixtures. Young's moduli were also determined in quasi-static tensile tests and, for clarity, the corresponding results are not shown in Figure 4.10, but in the Appendix (Table A.4.4).

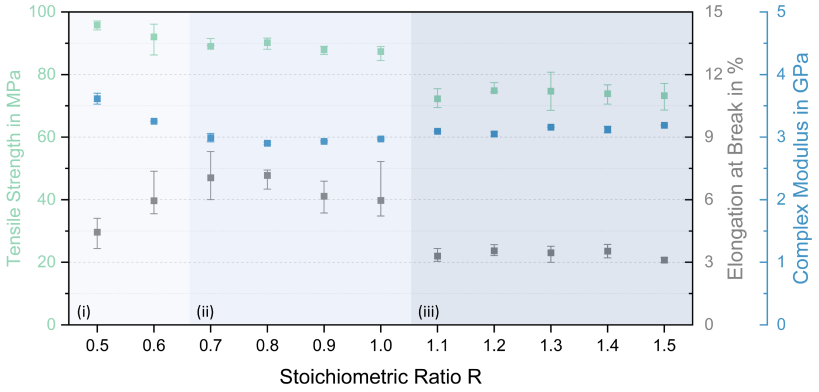

Figure 4.10.: Tensile strength, elongation at break and complex modulus for all investigated mixing ratios and categorisation into three zones (i-iii).

From the results obtained, it is evident that the investigated stoichiometry range can be divided into three areas (i-iii). The highest mechanical properties in the combination can be observed very consistently for a large range of R = 0.7 – 1.0. (ii). If the proportion of the particulate curing agent is further increased (iii), the stiffness remains, while the elongation at break drops dramatically. This also leads to a significant reduction in tensile strength, as the specimens break before reaching a yield plateau. Taking into account the propensity for agglomeration of the arginine particles, it can be assumed that an increasingly defect-driven failure occurs for over-stoichiometric mixtures. Here, the non-reacted L-Arg particles serve as imperfections in the network and favour crack initiation. In the investigated range of over-stoichiometric mixing ratios, the L-Arg content only differs by approximately 5 g per 100 g of DGEBA (see Table 4.2). For occurring failure-initiation, it seems that conceivable differences in agglomerate size or distribution have no measurable influence in these relatively small quantities, which might be one reason why no significant decrease in properties is recognisable.

For the considerably sub-stoichiometric configurations R = 0.5 and R = 0.6 (i), the failure behaviour also tends to be more brittle. Although stiffness and strength are increasingly high and the highest in comparison with all investigated ratios, the elongation at break is progressively decreasing. From a purely mechanical point of view, the configurations with the greatest epoxy excess (i) would even be favoured. An explanation for this unintuitive behaviour can be found by taking into account the thermo-mechanical response as shown in Figure 4.11.

Here, an analogy to incompletely but stoichiometric cured thermosets can be drawn. In detail, mechanical properties at room temperature have been reported regularly as not simply following a monotonous trend with an increasing conversion rate. Even though one would expect a higher cross-linking in a stoichiometrically cured thermoset should lead to higher mechanical properties, most properties such as stiffness, strength, fracture toughness, creep resistance, etc., show their maximum values at conversion rates of ≈ 75 - 90 % [227, 228]. Further and closer cross-linking then merely raises the glass-transition temperature and the properties at higher temperatures, while the mechanical properties at room temperature are significantly lowered. The reason for these effects are the differences in the free volume of the corresponding networks at room temperature. In fact, a thermoset with a high cross-linking density has a more restricted molecular mobility on cooling and is therefore less able to densely pack in the

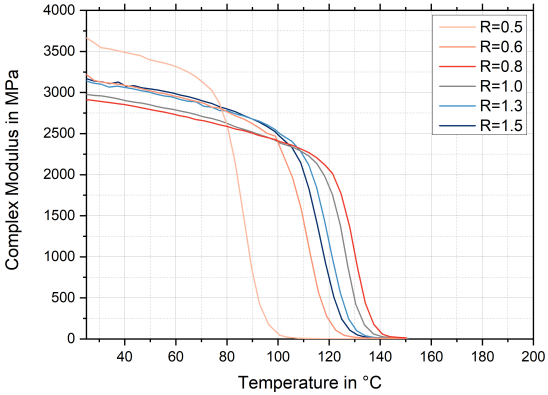

Figure 4.11.: Temperature-dependent complex modulus of the mixing ratios investigated. For better visibility, not all configurations are plotted.

amorphous glassy state [229, 230]. This also means that a matrix with a higher degree of cross-linking will have a larger free volume and consequently lower mechanical properties [229, 230]. In other words, a favourable minimum of the reachable free volume will be passed during the conversion process. Besides, a contribution of the 'rigid filler' effect is conceivable. In addition to improving the stiffness and general mechanical properties of a material according to the rule of mixture through the use of rigid additives, this effect can reduce the free volume [231, 232]. The extent depends on the size of the embedded fillers, their properties, and the interphase interactions with the matrix [233].

Applied to the present situation of different mixing ratios, conclusions can also be drawn here about the resulting network structure and the free volume. Starting with region (i), it can be assumed that a wider network will form if a relatively large amount of epoxy is present during the reaction. Accordingly, the fewer available arginine molecules lead to longitudinal and lateral cross-linking. Furthermore, relatively mobile unreacted or only partially reacted DGEBA molecules are present. These can act as plasticisers on the one hand and increase the mobility of the network on the other, so that a very dense packing with minimal free volume can form during cooling. For the second region (ii), the cross-linking density increases as the ratio approaches the stoichiometric ratio. Consistently with the increase in steric hindrance during cooling and the resulting higher free volume, the mechanical properties decrease, while the T_g increases significantly, as shown later in Figure 4.14. The third region (iii) then shows the most

significant changes from the point where the ratio becomes over-stoichiometric onwards. Here, the formation of a wider network is assumed again as there is not enough epoxy available for the reaction. Especially the T_g decrease discussed in section 4.2.4 and the modulus increase strengthen this hypothesis. However, improvements of the other mechanical properties cannot be observed as in the first region (i). In contrast, the tensile strength and elongation at break significantly decrease. In addition to the likely absence of a crucial cross-linking reaction with missing epoxy (see Section 4.2.5), this is mainly a result of the agglomeration of non-reacted arginine particles acting as defects in the structure.

To support the findings, digital microscopy and SEM images of fracture surfaces of various configurations are shown in Figure 4.12 and Figure 4.13.

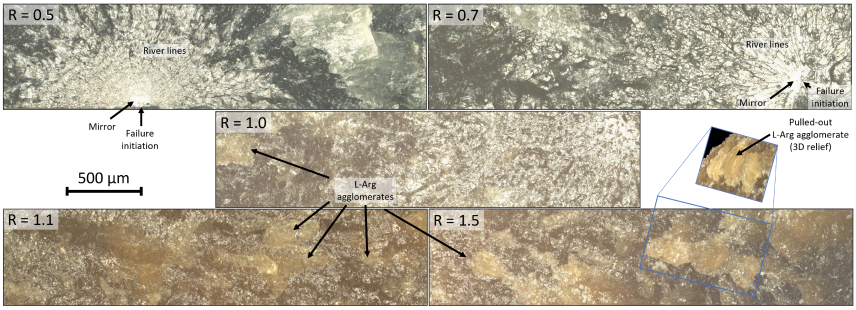

Figure 4.12.: Digital microscopy images of fracture surfaces.

Firstly, they confirm the observation from the optical examination of increasing light diffraction as a result of increasingly remaining particles or agglomerates occurring with increasing L-Arg content. Together with the findings from the FTIR investigations, the agglomerated L-Arg particles seem to form strong secondary valence forces (hydrogen bonds) between the unreacted functional -NH and -OH groups of the amino acid molecules, or they might also form peptide bonds. The 3D image and the SEM image show for R = 1.5 that agglomerate pull-outs occur in the fracture surface and that the fracture mechanism differs strongly from the configurations R $\leq$ 1.0. According to Cantwell et al. [211], these show typical fracture surfaces for brittle materials under tensile loading. After failure initiation (e.g., caused by a defect), a smooth area (mirror) occurs, where crack propagation takes place slowly. Attributed to the generation of secondary cracks in the region of high stress, parabolic profiles (river lines) arise afterwards. Depending on the ratio of crack propagation rates of primary and

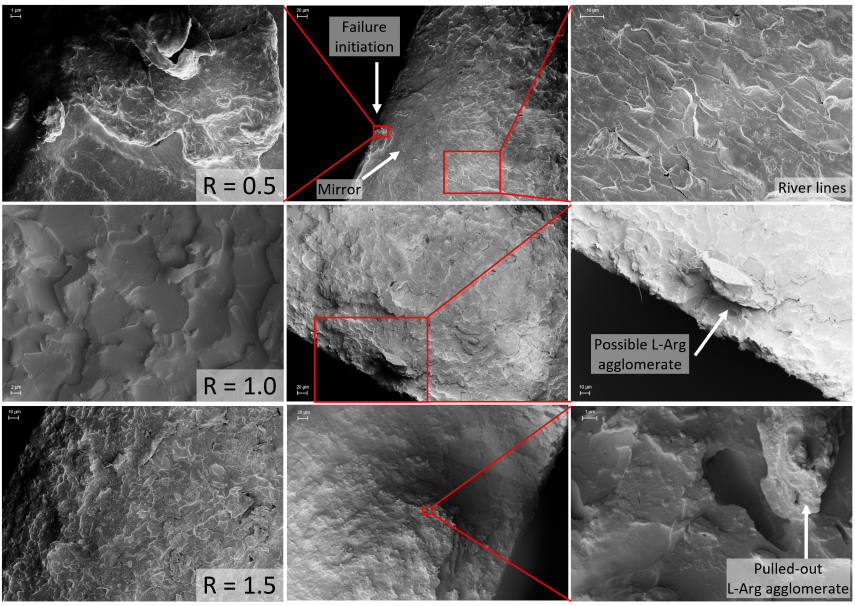

Figure 4.13.: SEM images of fracture surfaces for R = 0.5, R = 1.0 and R = 1.5.

secondary cracks, their appearance range from parabolic to elliptical. In later stages, a rougher pattern develops, due to interactions of the parabolas [234]. In the theoretical stoichiometric configuration R = 1.0, the formation of agglomerates is already visible but appears to be less critical, since the mechanical properties still remain at a high level.

Glass-Transition Temperatures

The T_g is one of the most relevant thermo-mechanical material parameters of amorphous polymers because it is associated with significant changes in the viscoelastic properties. It provides a description of the transition from the glassy state to the rubbery state and is typically correlated with the degree of cure, network formation, and mobility, as well as with structural transformations. For example, it gives information on changes in the segmental mobility of polymers [235]. Consequently, T_g is relevant for determining possible service conditions of polymeric or composite parts. According to the literature, different measurement methods yield slightly different values for T_g, because different processes are analysed: The authors of the works [228, 236] argue that the val-

ues for T_g differ when the mobility of the molecular chains (DMA), the free volume (TMA) or the thermal effects (DSC) are tested. However, Startsev et al. [235] found that parameters (such as the heating rate) also influence the determined T_gs. However, the equivalence of T_gs determined with different methods is shown to be achievable.

Since the determination parameters in this study were chosen uniformly for all mixing ratios, the determined T_gs of the analysed configurations are comparable within each analysis method. Figure 4.14 shows the T_gs for all investigated mixing ratios, and the exact values are listed in Table A.4.5 in the Appendix. Generally, values determined using DMA (DMA curves, see Figure 4.11) and DSC show the same trend.

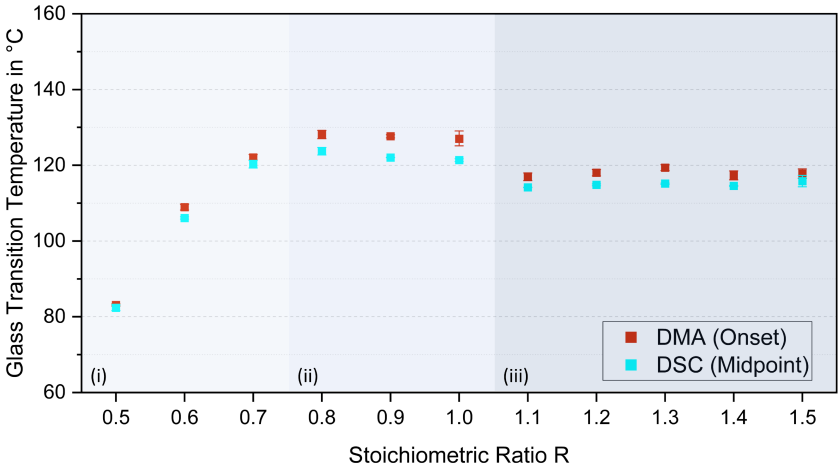

Figure 4.14.: Glass-transition-temperatures for all investigated mixing ratios analysed via DMA-Onset (red) resp. DSC-Midpoint (turquoise) and categorisation into three zones (i-iii).

Importantly, the T_gs are with approximately 127 °C (DMA onset) the highest for the also mechanically preferred ratios between R = 0.8 and R = 1.0 (ii). Here, only marginal changes ($\Delta T_g < 2$ °C) can be found (ii). In contrast, significantly reduced T_gs with a clear decreasing trend are observed with lower curing agent contents. This observation indicates insufficient network formation due to incomplete curing as a result of the lack of the required proportion of hardener. Significant reductions of more than 30 °C can be measured for the configurations R = 0.5 and R = 0.6 (i). For these ratios, much unreacted epoxy

remains , as shown in the previous section of the FTIR analysis. A slightly reduced T_g is also evident for R = 0.7, where the epoxy band is already significantly reduced but still observable. All over-stoichiometric configurations (iii) show constant T_gs of about 118 °C (DMA onset). No decreasing or increasing trend appears with more L-Arg content. Therefore, it can be assumed that the network structure remains basically similar but is hindered by agglomerates of the particulate curing agent added in excess. The formation of agglomerates or peptides is detectable with the results of the FTIR analyses carried out and the optical impressions of the fracture images. Because of the different reactivity of the functional groups, it can be assumed that the network density is reduced, as with an increasing amount of hardener, predominantly the most reactive groups of the L-Arg molecules react.

4.2.5. Postulation of Occuring Reactions

The chemical structure of L-Arg indicates that the mechanism of occurrence of reactions is more complex than that for curing agents with fewer functionalites, such as diamines. The results of the simple thermokinetic method show slight deviations with the experimental validation for 827/L-Arg (see Figure 4.15), as restrictions might not adequately capture concurrent reactions.

Nevertheless, both validation methods show complete conversion of the detectable reactions at the end of the curing cycle. A comparison of the two validation methods shows that the oxirane groups initially react faster than the reaction enthalpy decreases. This is a first indication that different reactions with different activation energies take place at elevated temperatures. The differences in stoichiometric variation between the investigated stoichiometric variations are additionally used in the following to derive insights into the occurring reactions.

Based on FTIR-measurements, Li et al. [221] postulated a reaction mechanism for epoxies cured with L-Tryptophan containing an imidazole as catalyst. The findings discussed in the previous sections enable a transfer and postulation of a conceivable extension to the reactions taking place in L-Arg-cured epoxies without catalysts. As described in Section 4.2.2, rheological measurements and determination of the reaction enthalpy were used to show that the system 827/L-Arg can be stored for a relatively long time at room temperature. Since L-Arg is in the solid state at room temperature and is therefore predominantly / almost

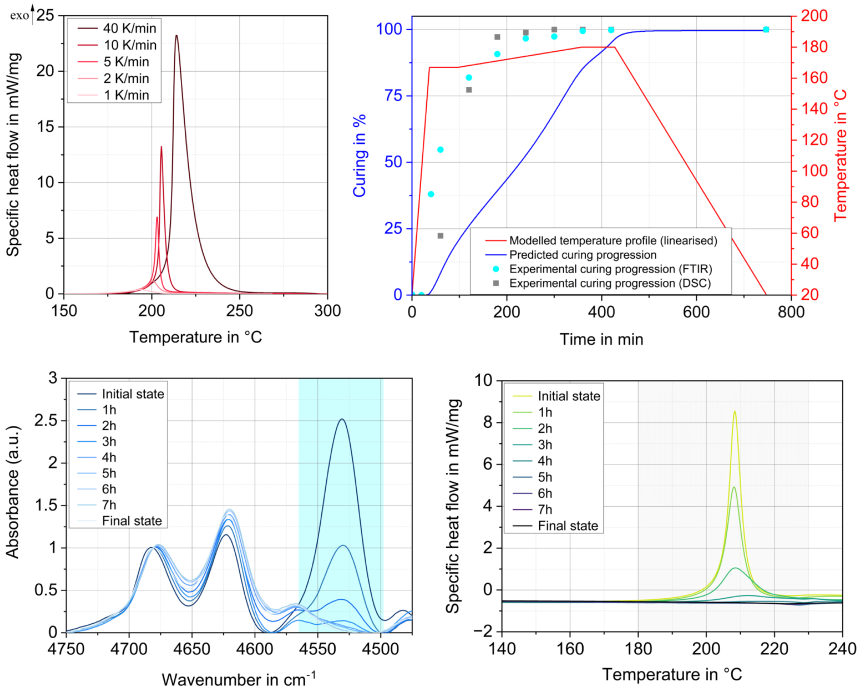

Figure 4.15.: Thermokinetic prediction for the configuration 827/L-Arg. DSC thermograms with different heating rates (top left). Linearised, modelled temperature profile, related prediction for curing progression and validation with ex-situ measurements: FTIR, DSC (top right). Decrease of epoxy peak area over time in FTIR spectra during curing (bottom left) and decrease of reaction enthalpy over time in DSC thermograms during curing (bottom right).

exclusively ionised as described in the introduction [237], it can be assumed that arginine molecules assemble into crystal lattices via these ions [238]. Common amine-epoxy reactions, as shown in Figure 4.16b, cannot occur in this state because there are no pairs of free electrons available for nucleophilic attack.

It is now assumed that analogue to catalyst-initiated deprotonation postulated in [221], the α-NH_3^+ groups deprotonate when the temperature increases during the curing process (Figure 4.16a) and that the reactions mentioned in Figure 4.16b can consequently take place. At elevated temperatures, the molecules in the ion lattice tend to vibrate more, presumably allowing deprotonation to occur. It is possible that the carboxylates are consequently deionised or that water in the resin (e.g., due to humidity or peptide formation) accepts the proton.

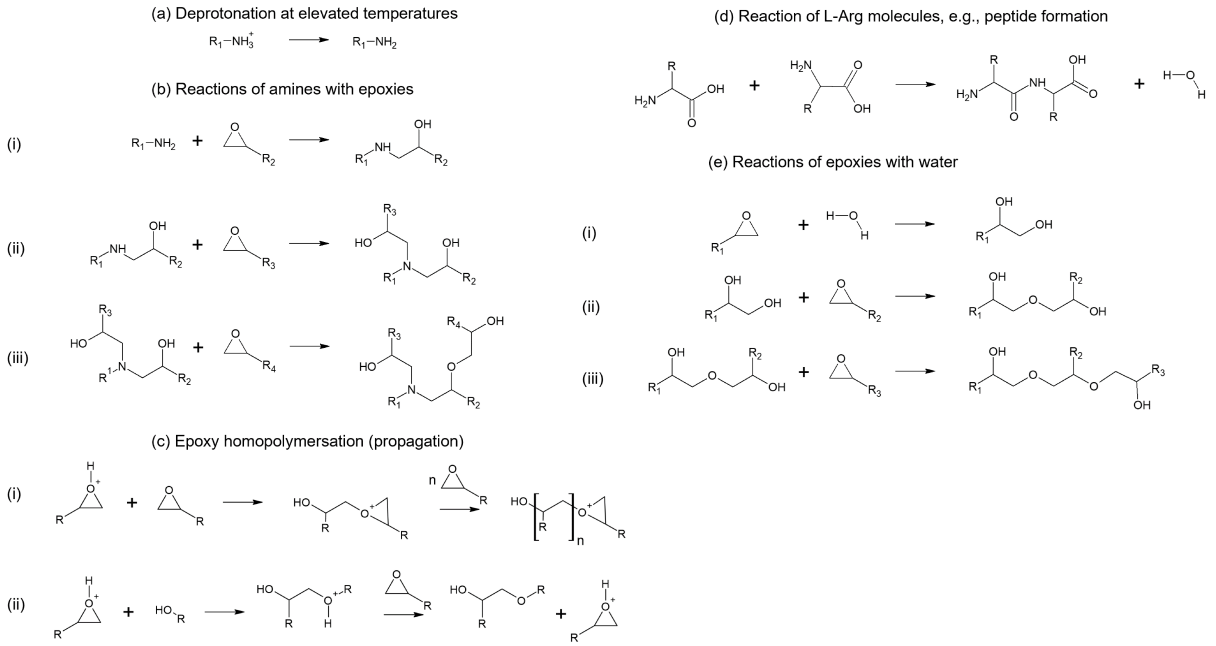

Figure 4.16.: Postulated possible reactions in amino-acid cured epoxies. (a) Deprotonation of α-$NH_3{}^+$ at elevated temperatures allows (b) common amine-epoxy reactions: (i) Reaction of primary amines; (ii) reaction at secondary amine and (iii) etherification. (c) Catalytic epoxy homopolymerisation is also conceivable at high curing temperatures: (i) ACE mechanism and (ii) AM mechanism. (d) Amino-acids can react to amides (e.g. peptides) and water. (e) Water-initiated reactions with epoxies (i) hydrolysis; (ii) initiation and (iii) propagation of cross-linking.

As proposed in [221], the formation of primary amines may significantly increase the reactivity of COO^- leading to esterification, resulting in the extraction of more hydrogen atoms from the NH_3^+ groups. The postulated deprotonation is supported by own preliminary studies showing that amino acids stabilised with counter-ions, e.g., from hydrochloride (HCl) [239] do not cure epoxides, as the deprotonation of the α-NH_3^+ is significantly more difficult here.

However, Section 4.2.4 demonstrates that the stoichiometric ratio calculated by the number of active hydrogen atoms does not lead to performance-optimised polymers. Instead, this is the case for slightly sub-stoichiometric mixtures. Taking into account the common epoxy-amine reactions shown in Figure 4.16b, primary amino groups might react first, as this is energetically favourable in (i), before forming secondary amino groups and hydroxyl groups. The secondary amino groups then react further to form the tertiary (ii) and generate additional -OH groups at the opening of the ring, which can etherify (iii) by opening other oxirane groups [240]. In principle, therefore, an active hydrogen atom can open up more than one oxirane group.

Since the guanidium group is considered very stable in almost all environments [237] due to its mesomeric stabilisation, deprotonation is less likely compared to the α-NH_3^+ group. This is comparable to the suggestions of Li et al. [221], because L-Trp includes a nitrogen atom in its indole group delocalised in an aromatic system and was postulated to have a lower reactivity. Therefore, the number of active hydrogens is drastically reduced with a limited number of epoxide groups, which theoretically would lead to a higher necessary proportion of L-Arg. However, because the results of the thermo-mechanical characterisation tend to indicate a reduced amount of the amino acid as positive, cross-linking via etherification is likely, if sufficient epoxy groups are present. Because of the high temperatures in the curing process, there tends to be enough energy available for these reactions to take place. For the same reason, homopolymerisation of epoxy groups (c) and amide/peptide formation (d) are also conceivable but not preferred in terms of energy.

The mechanism of possible homopolymerisation is conceivable and is catalysed by tertiary amines without an additional catalyst due to the high curing temperatures [241]. However, a cationic mechanism of homopolymerisation is also plausible due to proton shifts (e.g., due to the proton released by deprotonation of the α-NH_3^+ group of L-Arg). In this case, the epoxide oxygen is protonated

and becomes more susceptible to nucleophilic attack as a more electrophilic ring. In principle, the propagation of cationic curing, shown in Figure 4.16c, can take place via the (i) active chain end (ACE) or (ii) activated monomer (AM) mechanism. [242, 243]. Compared to amino curing, cationic curing typically produces more linear epoxy chains. Alternatively, the opening of an anionic ring by carboxylate groups (COO^-) is also theoretically possible. Additional investigations are required to clarify the details.

There are some indications of the formation of the amide / peptide mentioned (d) in the FTIR results presented. Amide formation releases water, which in turn enables the water-induced reactions with epoxides shown in (e) or may accept the protons of the deprotonations.

As no significant epoxy peak is visible above R = 0.7 using FTIR, the epoxy resin still reacts almost completely above this curing agent content, which speaks in favour of the postulated reaction diversity. The non-conclusive list of possible reactions described above explains why the calculation of the stoichiometric ratio is only a guide to find a suitable mixing ratio. However, as mentioned for anhydride-cured epoxies, for some standard systems, a sub-stoichiometric mixture is also recommended for optimised performance, e.g., due to occuring epoxy homopolymersiation [215].

The postulated mechanisms are also conceivable for other amino acids in solid form. The respective side chains may be relevant for:

- The temperatures at which α-NH_3^+ is deprotonated: Compared to other amino acids, L-Arg probably requires more energy to deprotonate α-NH_3^+ due to the effects of the stable guanidium ion.
- The density of the network, for example, due to steric hinderance.
- Secondary / valence forces: It is conceivable that, e.g., the ionic bonds of the guaninium ions in L-Arg may improve thermo-mechanical properties.
- Additional reactions of the side chains.

Nevertheless, it can be assumed that accelerators or catalysts may change the mechanisms and network structures differently than just lowering the needed energy for deprotonation. Furthermore, other phenomena, such as crystal formation, can occur as reported in [220], which may change mechanisms and the resulting properties.

4.2.6. Postulation of Network Structures

These considerations support the origin of different network structures with different mixing ratios, which change the properties examined in Section 4.2.4. Figure 4.17 shows schematic visualisations of postulated network structures for three groups of mixing ratios, explaining the measured thermo-mechanical differences. The configuration R = 0.7 represents a transitional case between (a) and (b) and is therefore not listed below.

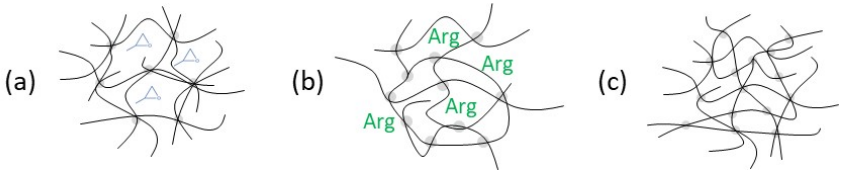

Figure 4.17.: Schematic visualisation of postulated network structures. (a) Severely sub-stoichiometric configurations, (b) over-stoichiometric configurations and (c) slightly sub-stoichiometric to stoichiometric configurations (with designation of the theoretical stoichiometric ratio).

Severely Sub-Stoichiometric Configurations

In severely sub-stoichiometric mixtures (R = 0.5 and R = 0.6), a sufficient number of epoxy rings are available to allow all reactions presented in Figure 4.16b, including cross-linking through ether bonds (iii), to take place [244]. The significant excess of epoxy probably even deprotonates guanidium ions, since no more peaks are recognisable in the FTIR in the 1600 – 1720 cm^{-1} range. This leads to further cross-linking points. In contrast, homopolymerisation is also possible because of the availability of many epoxy rings, which leads to chain extension between the cross-linking points. There is also the probability that not both epoxy rings of the DGEBA molecules react because of the lack of curing agent molecules. Consequently, the cross-linking density is reduced at these points. The reaction of L-Arg molecules with each other is unlikely to be favoured due to a lack of availability. Despite all possible reactions, unreacted epoxy groups (detected by FTIR) are still present, which are deposited between crosslinked polymer chains and increase their distance and for this reason have a plasticising effect and, for example, reduce the T_g. For the cross-linking density of the configuration R = 0.5, a comparatively low value of $\nu_C = 0.59 \cdot 10^{-3}$ mol/cm^{-3} was determined, which supports the postulated network structure. To further

support the assumption that energetically non-preferred reactions also occur, Figure A.4.3 shows the DSC thermogram during curing. For the configuration R = 0.5, the exothermic peak is significantly shifted to higher temperatures compared to mixtures with more L-Arg. Additionally, the evaluated reaction enthalpy is 205.3 J/g, which is approximately half of the enthalpy of the stoichiometric ratio (411.4 J/g).

Over-Stoichiometric Configurations

In over-stoichiometric mixtures (R > 1.0), more linear polymer chains are expected, since reaction Figure 4.16b (i) is energetically the most favourable and the reactions from Figure 4.16b (ii) and (iii) and other reactions that require epoxy rings are unlikely due to the lack of epoxy groups, so fewer cross-links occur. This is in line with the shift of the exothermic peak to lower temperatures in Figure A.4.3. Moreover, L-Arg-terminated dangling chain ends can be expected [215].

The surplus of L-Arg molecules may tend to agglomerate (FTIR, microscopy), i.e., because of its ionisation. These agglomerates accumulate between chains and cause defect-driven failure and a less dense network (decreasing T_g). The cross-linking density for R = 1.5 ($\nu_C \approx 1.54 \cdot 10^{-3}$ mol/cm^{-3}) is approximately three times higher than for R = 0.5, which speaks in favour of the discussed structure. Additionally, the evaluated reaction enthalpy (348.5 J/g) is significantly higher. It could not be conclusively clarified whether the additional L-Arg molecules react with each other and form peptide bonds with water cleavage.

Slightly Sub-Stoichiometric to Stoichiometric Configurations

The DGEBA:L-Arg ratios between R = 0.8 and R = 1.0 tend to lead to a complete reaction of the deprotonated amino acid (including cross-linking but without reaction of the guanidium groups) without unreacted molecules reducing the network density. Accordingly, the thermo-mechanical properties are highest in this range. The highest reaction enthalpy (411.4 J/g) and the estimated cross-linking density for R = 0.9 ($\nu_C \approx 3.0 \cdot 10^{-3}$ mol/cm^{-3}) underline this outcome.

4.2.7. Aging in Various Environments

The adequate initial property profile overcomes the first barrier to more sustainable matrix materials for composites. However, sustainability should not be compromised by a quicker need to replace components if the long-term properties would be impaired by the use of biomolecules.

When in use, composites are exposed to many environmental influences that cause the material to age with time. In composites, this is, of course, a multi-scale problem influenced by fibres, matrix, and the interphase [245]. Nevertheless, this section focuses on the long-term thermo-mechanical properties of L-Arg-cured epoxy compared to standard epoxides.

Thermal Aging

Starting with the short-term behaviour at elevated temperatures, specimens were tested at different temperatures. As is common for thermoset materials, the tensile strength decreases linearly until about 30 Kelvin below T_g (see Figure 4.18, left). The slope of the linear fit is compared to several other thermoset materials [246] in Figure 4.18, right). Because the slope is above the linear fit of the other materials, the tensile strength of the amino-acid cured epoxy is less sensitive to temperature changes than other thermosets. This behaviour is positive for applications under elevated temperatures.

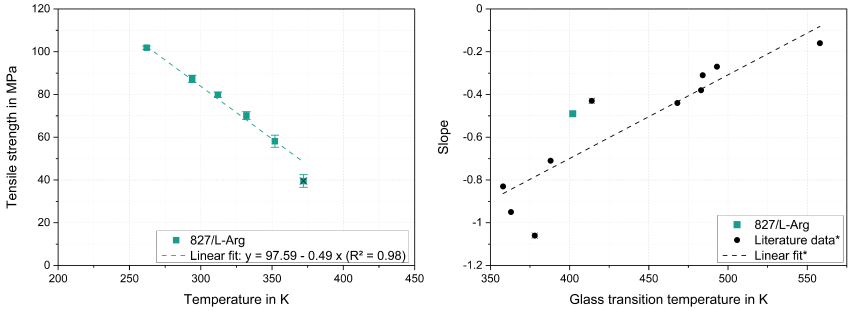

Figure 4.18.: Temperature-dependent tensile strength of 827/L-Arg and evaluation of linear fit before disproportional decrease below T_g (left). Comparison of slope related to respective T_g with other thermosets *[246].

Standardised to the glass-transition temperature, the amino acid-cured epoxy also shows comparatively high strengths (see Figure 4.19). Therefore, the short-

term temperature-dependent tensile strength is positively assessed for the investigated L-Arg-cured epoxy.

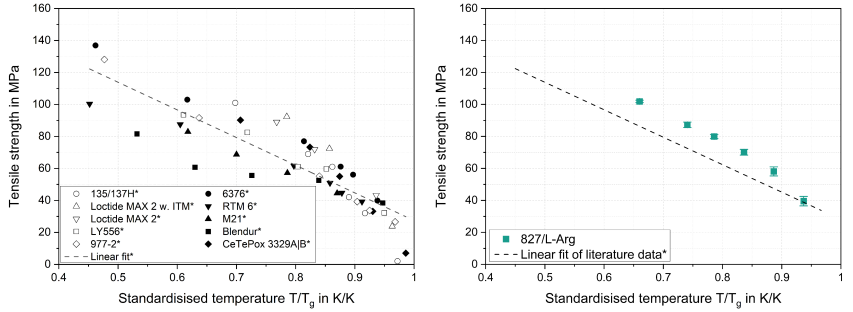

Figure 4.19.: Tensile strength of literature data *[246] (left) and 827/L-Arg (right) displayed over T_g-standardised temperature.

After exposure to elevated temperatures over a longer period of time, an increase in strength, as well as embrittlement of epoxies is observed [247]. This mechanism is called physical aging. Thereby, the free volume is a very important factor. It affects the chain mobility [247] and therefore also the thermo-mechanical response of the thermoset. The free volume is, for example, influenced by the cooling rate during manufacturing (see Figure 4.20).

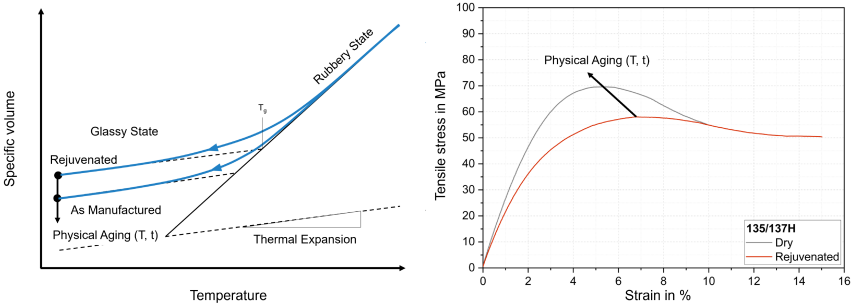

Figure 4.20.: Schematic explanation of physical aging caused by changes in specific (free) volume, adjusted from [247] (left). Impact of physical aging on stress-strain curves of 135/137H (right) [245]. Rejuvenation process for 135/137H: 5 min in 100°C oil bath followed by 1 min rejuvenation in ice bath.

The highest possible free volume can be achieved with rejuvenation, which involves heating the thermoset above T_g and then quenching it [248]. This process maintains the molecular state [249], where lower tensile strengths but higher

elongations at break are observed, because the chains are more mobile due to the larger free volume. After a while, the free volume decreases again, caused by relaxation processes [247]. As long as the temperatures are below T_g, higher temperatures accelerate these relaxation processes. Physical aging is a reversible effect, as the rejuvenation process reverses the effects of physical aging.

The amino acid-cured epoxy also shows this behaviour. Elevated temperatures lead to higher tensile strengths and embrittlement while after rejuvenation the elongation at break is increased. In Figure 4.21 (left) it is shown that the manufacturing process leads to a good balance between tensile strength and elongation at break. With physical aging the elongation at break does not decrease significantly. This allows the conclusion that the biomolecule-cured epoxy investigated is also well suited for long-term exposure at higher temperatures, as long as they are sufficiently below T_g.

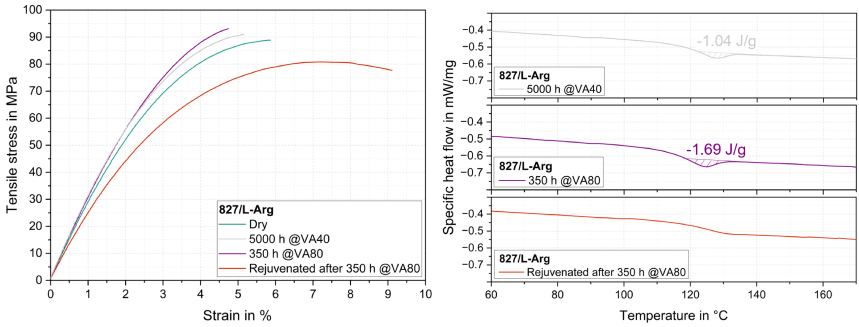

Figure 4.21.: Effects of physical aging in the stress-strain-diagram (left) and DSC-thermograms (right). Rejuvenation process for 827/L-Arg: 5 min in 150 °C oil bath followed by 1 min rejuvenation in ice bath.

On the other hand, this observation also offers the potential to achieve higher elongation at break with only a slight loss of strength for the same network formation by cooling more quickly at the end of the curing process. Due to the relatively high T_g, physical ageing is likely to proceed very slowly, at least at room temperature, and the high elongation at break is expected to remain for a long period of time.

In addition, the state of physical aging can also be seen in DSC thermograms at the endothermic peak after T_g. With increased physical aging, the peak area increases (-1.04 J/g after 5000 h at 40 °C vs. -1.69 J/g after 350 h at 80 °C). As a

result of the rejuvenation process, this peak disappears completely (Figure 4.21, right).

Hygrothermal Aging

The durability of epoxies in the presence of water absorption has already been investigated in numerous studies in the past [250, 251]. Most of them use accelerated aging processes at elevated temperatures to predict the evolution of properties due to slow diffusion rates at moderate ambient temperatures [252–254]. Therefore, we know that absorbed water can cause significant changes in thermomechanical properties through simultaneous plasticisation and relaxation (physical aging) [248, 255]. Because the plasticising effect of water is understood as a reduction in intramolecular forces by increasing chain spacing, it is often compared to an increase in ambient temperature. In contrast, Gibhardt et al. [201] revealed significant differences between aging conditions, e.g., that physical aging could be easily overseen or misinterpreted by accelerated aging alone.

In general, tensile strength and glass transition temperature were shown to be the properties most affected by water absorption. They can be reduced by a factor of two or even more [256, 257]. The amount of water absorbed at equilibrium in polymers or epoxies in this case depends mainly on the structure of the polymer [258]. In the past, a distinction was often made between 'volumetrically' and 'interactively' determined explanations. In this case, volumetric approaches mainly consider absorption in the free volume, which can vary depending on the degree of cure and temperature, and in space, which is a consequence of unwanted defects such as micropores or cracks [259]. According to this approach, the interactions between water and the polar sites of the polymer network are largely neglected. However, these interactions between water and the polymer network are often considered dominant for water absorption [260]. It has been shown that water molecules are attracted to the polarity of the chemical structure of polymers and that water is also bound to these molecular segments by hydrogen bonds [261, 262]. Furthermore, spectroscopy and absorption-desorption experiments have shown that there are at least three states in which water interacts with the molecular network. These are defined as free or unbound water, weakly bound water (type I) that forms one hydrogen bond with the network, and strongly bound water that forms two hydrogen bonds (type II) [257, 261] found that type II water bonding increases the T_g of wet epoxy.

Figure 4.22 displays the weight changes in 22 °C water. 827/L-Arg absorbs higher amounts of water than 827/135H, which can be explained by the higher polarity and the high number of possibilities for hydrogen bonds in the arginine-cured epoxy (see Section 4.2.4). Maximum values were obtained with weight change ≈ 4.8 wt. % for 827/L-Arg vs. ≈ 2.8 wt. % for 827/137H. Both values are in the range of values reported in the literature of 1.0 to 5.0 wt.% [201, 251, 263, 264].

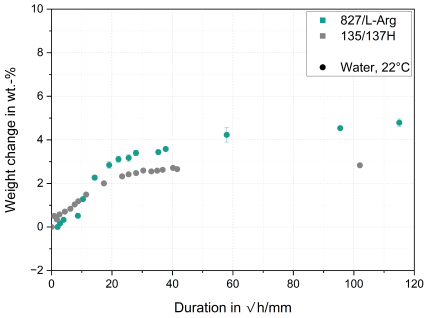

Figure 4.22.: Weight change over time for investigated epoxy resins during immersion in water (22 °C). Data for 135/137H obtained from [245].

As reported in [245], deviations from Fickian absorption can be found in the transition from linear to asymptotic range. A continuous increase of weight changes, typical for two-stage or non-Fickian sorption behaviour, is observed in both cases. Such deviations from Fickian sorption are typically related to water-induced relaxation phenomena in epoxy [265–268].

As observed in the literature, the absorption of water initially shows a reduction in strength due to plastification for both epoxies (Figure 4.23, left). The strength decreases linearly with an increase in the amount of water absorbed (Figure 4.23, right). In relative terms, a decrease of ≈ 10 % per wt.-% absorbed water can be observed for both systems. Due to slightly increased water absorption, the strength decreases to approximately 60 % of the initial value for 827/L-Arg, but due to the higher initial strength, this corresponds to the absolute value of the minimum observed in the reference system. Subsequently, there is an increase in strength as a result of physical aging without further water absorption. Compared to standard epoxy resin, DGEBA cured with arginine shows no significant changes in long-term behaviour when immersed in water at 22 °C. Nevertheless, the increase in strength caused by physical ageing appears to be slightly lower

in epoxy resin cured with L-Arg. This could be caused by the existing network structure (more steric hindrance), which has already shown less physical ageing in the dry state (see section 4.2.7). Another reason may be that a higher amount of water molecules prevents the polymer chains from packing densely, resulting in lower strength values for 827/L-Arg. Looking ahead, additional measurements after longer immersion times could provide further insight in this regard.

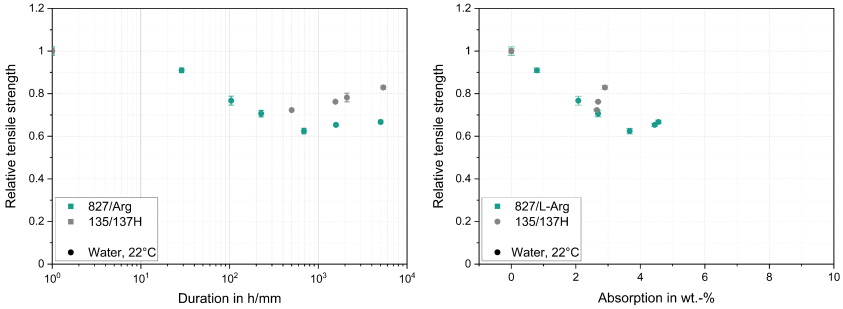

Figure 4.23.: Changes in relative tensile strength with immersion time (left) and absorbed mass (right) in water (22 °C). Data for 135/137H obtained from [245].

Figure 4.24 shows the changes in the glass transition temperatures with time and water absorption. At full saturation, T_g decreases for both systems to approximately 70 % of the respective initial value.

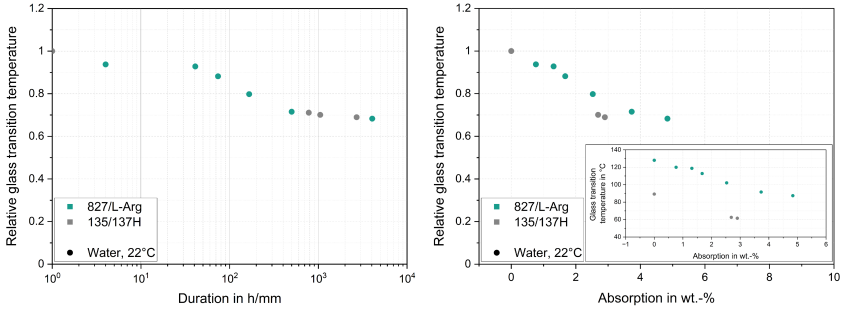

Figure 4.24.: Changes in (relative) glass transition temperature with immersion time (left) and absorbed mass (right) in water (22 °C). Data for 135/137H obtained from [245].

The data set indicates that the reduction in T_g correlates linearly with the amount of absorbed water and falls by 8.9 K for 827/L-Arg and by 9.7 K for

135/137H per percentage of absorbed mass. Figure A.4.4 (Appendix) displays that there are no detectable (IR-active) changes in the recorded spectra for 22 °C water. For specimens, re-dried at 40 °C in a vacuum oven after 3000 h of immersion in water, 0.8 wt. % of the nearly 5 wt. % absorbed water remained, indicating type 2 bound water.

As introduced, the combination of temperature and water exposure is important not only for applications at higher temperatures in humid environments but also for the accuracy of predictions, when long-term properties are determined on the basis of the time-temperature superposition principle using accelerated tests at elevated water temperatures. Therefore, the weight gain curves for 827/L-Arg are shown in Figure 4.25 in addition for immersion in water of 8, 50 and 70 °C.

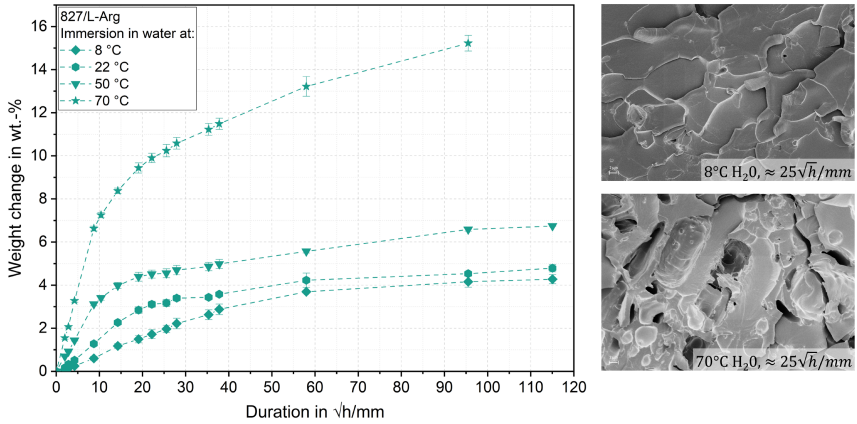

Figure 4.25.: Weight change of 827/L-Arg over time for investigated epoxy resins during immersion in water of different temperatures (left). SEM images of specimens after ≈ 25 $\sqrt{\text{h}}$/mm immersion in 8 °C and 70 °C warm water.

For the system 135/137H, ≈ 0.5 % difference in absorbed mass between 8 °C and 50 °C water is reported [245]. In contrast, for 827/L-Arg, a delta of 2.5 % is measured between water at 8 and 50 °C. Due to the higher T_g, storage at 70°C is possible, leading to weight gains of more than 15 %. This is only feasible to this extent if water clusters are present in the material due to defects or degradation processes. Therefore, fracture surfaces were examined by SEM (Figure 4.25, right). After ≈ 25 $\sqrt{\text{h}}$/mm in water at 8 °C, no significant changes compared to the initial fracture pattern are visible, but at 70 °C, it can be clearly observed,

how parts of the polymer have dissolved or degraded, creating space for water clusters.

However, the tensile strength decreases by much less than 10 % per wt % absorbed water as analysed for water immersions at 22 °C. After $\approx 25\ \sqrt{\text{h}}/\text{mm}$ in 70 °C water, still 52.19 ± 1.66 MPa (vs. 54.49 ± 1.16 MPa in 22 °C water) are measured. Thus, it can be suggested that either the physical aging at this point in time at 70 °C already counteracts degradation processes, or that these areas are not significantly load-bearing if they are initially present.

This raises the question whether accelerated aging in fact demonstrates that degradation occurs over time even at low water temperatures. As the occurring differences in weight gain are that significant and the weight yields saturation for lower temperatures, it is conceivable that degradation in the 827/L-Arg system only occurs at higher temperatures as a third aging process, e.g., by exceeding the necessary activation energy. Specimens immersed in 22 °C water exhibit even higher tensile strengths after $85\ \sqrt{\text{h}}/\text{mm}$, than after $\approx 25\ \sqrt{\text{h}}/\text{mm}$ caused by physical aging (58.25 ± 0.79 MPa), and fractography does not show any degraded parts after this time. In addition, test specimens were re-dried under vacuum at 100 °C after 3000 h of water exposure at various water temperatures. For water temperatures of 8, 22 and 50 °C, mass losses of approximately –0.25 % were determined compared to the initial mass, which had only been vacuum dried at 40 °C. The decrease can be explained by the additional mass loss assigned to bound water between the two drying temperatures. Since a greater mass loss of –0.77 % compared to the initial mass was determined for 70 °C warm water, this comparison underlines the assessment that degradation/dissolution processes only take place at severly elevated water temperature. To ensure that this represents the real scenario, measurements should be repeated after even longer immersion times.

In conclusion and as expected, these results emphasise that accelerated aging at elevated temperatures cannot necessarily be used to make predictions at ambient temperatures, especially if processes do not occur in all temperature ranges. For the 827/L-Arg system, it is recommended to avoid hot-wet applications to avoid a negative impact on service life.

Aging in Chemical Environments

Components made of continuous fibre-reinforced polymers are occasionally exposed to specific media over long periods of time during use. Oil-conveying pipes are one example. However, contamination with media can also occur in other applications, for example, in hydraulic oil in wind power plants. It is also relevant to know which solvents can be used, e.g., for surface cleaning without causing lasting damage to the polymer even after brief exposure.

Because particle modifications are often performed using solvents, many studies deal with the addition of solvents in the uncured state and the influence of their incomplete evaporation on the curing process [269–271]. With regard to the durability of epoxies against chemicals, there is considerably less literature on cured epoxy resins.

Kaplan et al. [272] immersed different epoxy resins in several chemicals at different temperatures to investigate solvent uptake and diffusion. The authors measured the sorption kinetics finding diffusion into the epoxy network, with the rate and extent of diffusion depending on both the epoxy formulation and the solvent properties. The diffusion process generally followed Fickian or anomalous diffusion behaviour, and the diffusion coefficients for solvents were in the range of 10^{-9} to 10^{-11} cm^2/s.

However, more studies are conducted in industrial research and are occasionally published [273]. According to Zheng et al. (Evonik Corporation) and Aziz et al. [274], the curing agent and the formed network have significant influences on the chemical resistance of epoxy resins. The denser the network (high network density), the better the resistance to swelling and diffusion [273]. According to the authors, a chemical attack of a thermoset can be divided into three processes: swelling of the polymer network, chemical diffusion into the network, and chemical reaction and degradation of the network. Standard epoxies show good chemical resistance to alcohols (e.g., isopropanol) and paraffinic or naphthic hydrocarbons (e.g., hydraulic oil). However, resistance to ketones such as acetone is poor and can lead to swelling and irreversible damage due to micro-cracking or network destruction.

Figure 4.26 (left) displays that immersion in hydraulic oil did not show a weight change, while the specimens immersed in isopropanol first lose small amounts of mass. This phenomenon is in line with the investigations of Kaplan et al. [272]

and is explained by the removal of soluble components and the relatively high viscosity of isopropanol (1.77 cP at 30°C, compared, e.g., to methanol with 0.51 cP).

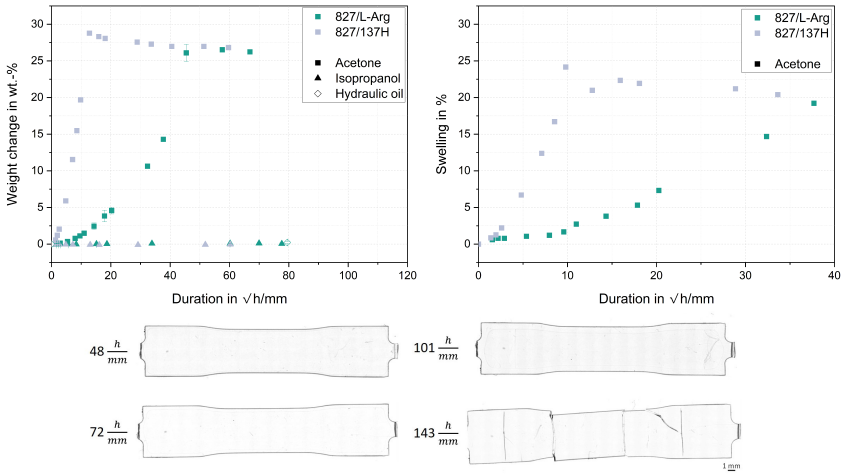

Figure 4.26.: Weight change over time for investigated epoxy resins during immersion in acetone, isopropanol and hydraulic oil (top left). Swelling of 827/L-Arg and 827/137H with elapsed immersion time in acetone (top right) and transmitted light microscopy images of an 827/137H specimen after immersion in acetone with formation of a diffusion front and stress cracks (bottom).

The highest increase in mass is observed for immersion in acetone with a mass increase of almost 30 % for the petrochemical reference system 827/137H. For this system, the progression of acetone diffusion could be tracked by digital microscopy with transmitted light, shown in Figure 4.26 (bottom). The time of complete saturation (143 h/mm $\approx$ 12 $\sqrt{\text{h}}$/mm) corresponds to the maximum increase in mass. This is followed by a decrease in mass, indicating degradation, which is further analysed later on. An overshoot was also reported by Kaplan et. al [272].

A diffusion coefficient of D = $5.29 \cdot 10^{-8}$ cm/s can be calculated from microscopy images using the progression of the diffusion lines. This value is slightly lower than the diffusion coefficients reported by Kaplan et al. [272]. Due to the two-dimensional evaluation of a three-dimensional process, a more detailed evaluation is omitted in this study. Stress cracking was observed for 827/137H specimens already after short times ($\approx$ 100 h/mm). After the formation of stress cracks,

the characteristic mechanical properties cannot be determined. It is remarkable that 827/L-Arg specimens show the first stress cracks after ≈ 1800 h/mm. Stress cracks occur when approximately the same weight gain of ≈ 15 wt. % is observed. Due to the non-transparent appearance, no diffusion lines can be traced. The change in geometry is shown in Figure 4.26 (right) for acetone through the change in cross-section of the free test length of the dogbones and is analogous to the change in mass (left). Consequently, swelling of almost 25 % can be observed for the petrochemical reference system. Swelling of this magnitude explains the formation of the stress cracks and the time delay in their formation in the test specimens cured with L-Arg.

A comparison of both resin systems shows that 827/137H has approximately twice the cross-link density of 827/L-Arg. Contrary to the literature, which states that a higher network density leads to better chemical resistance, the results of this study show that 827/L-Arg has better resistance, e.g., to acetone uptake. This may be due to the higher polarity of arginine as well as ionic components in the arginine molecule. Because ketones, such as acetone, can form hydrogen bonds, it is conceivable that diffusion is initially inhibited, and thus delayed by the formation of hydrogen bonds. The change in crosslink density with the absorption of different media is not analysed in this study but is interesting as an explanation for this deviation.

Analogue as discussed in section 4.2.7 for water absorption, the immersion in the tested chemicals (Figure 4.27) also shows a linear behaviour of the decrease in strength with the amount absorbed and thus the delayed decrease for the amino acid-cured epoxy.

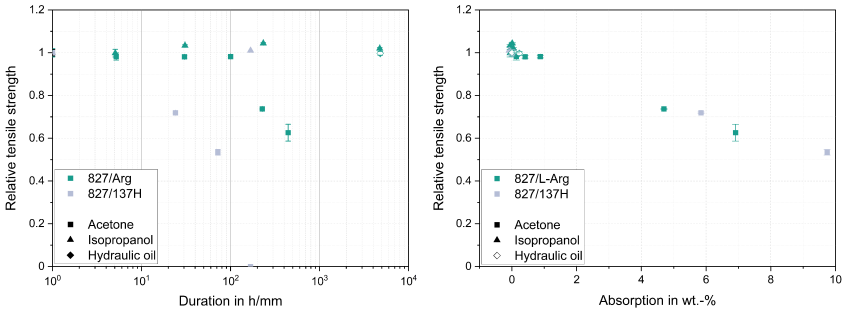

Figure 4.27.: Changes in relative tensile strength with immersion time (left) and absorbed mass (right) in acetone, isopropanol and hydraulic oil.

Due to the stress cracks that occur in acetone, no subsequent increase in strength can be observed. A small part of the loss in strength can be explained by the swelling and the increase in the effective cross-section of the test specimens. With isopropanol, increased strength can be observed due to reductions in the effective cross-section. Hydraulic oil does not have a significant absorption behaviour and therefore does not lead to any changes in strength.

Absorption of the same amount of acetone has less influence on the glass transition temperature (Figure 4.28) than the absorption of water (see Section 4.2.7). It is conceivable that acetone is predominantly present in the free volume and less between the molecular chains of the polymers due to the larger molecules compared to water. Therefore, inter- and intramolecular forces are less influenced. For hydraulic oil and isopropanol, neglectable decreases of the T_g are measured.

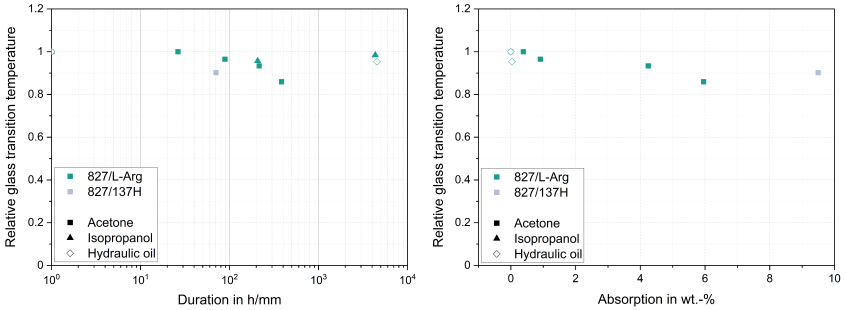

Figure 4.28.: Changes in relative glass transition temperature with immersion time (left) and absorbed mass (right) in acetone, isopropanol and hydraulic oil.

The thermo-mechanical properties indicate that arginine-cured epoxy resin has no disadvantages compared to standard epoxy regarding long-term exposure in the tested media. The delayed acetone absorption is even favourable.

Figure 4.29 shows SEM images of fracture surfaces of dry and acetone-immersed 827/L-Arg specimens after 100 h/mm and 450 h/mm immersion. After 100 h/mm the specimen absorbed less than 1 wt.% resulting in no significant influences in the tensile strength and fracture surfaces compared to not-immersed specimens. In contrast, the specimen after 450 h/mm immersion with $\approx$ 7 wt % absorbed acetone and $\approx$ 60 % of the initial tensile strength indicating plastification.

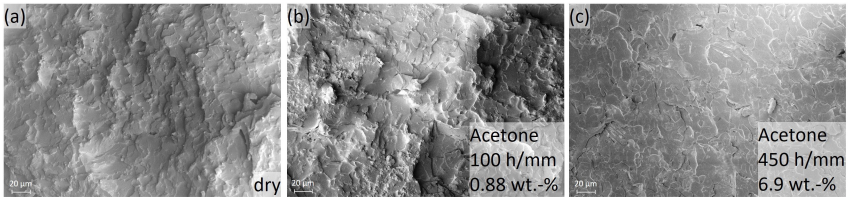

Figure 4.29.: SEM pictures of fracture surfaces after tensile test of 827/L-Arg specimens (a) dry and after immersion in acetone (b) after 100 h/mm immersion (0.88 wt. % mass increase) and (c) after 450 h/mm immersion (6.9 wt. % mass increase).

To analyse, if immersion in the investigated media leads to chemical degradation, FTIR-measurements have been conducted. Figure A.4.4 (Appendix) displays, that there are no detectable (IR-active) changes in the recorded spectra for isopropanol, indicating no chemical degradation within the analysed time. Furthermore, the re-dried specimens show no mass loss compared to the initial dry condition. Re-drying of 3700 h isopropanol immersed specimens at 40 °C under vacuum shows a reduction of 0.02 $\pm$ 0.02 wt. % for 827/L-Arg resp. 0.16 $\pm$ 0.02 wt. % for 827/137H of the initial mass, which supports the position that isopropanol removes soluble components.

In contrast, 8.01 $\pm$ 0.22 wt. % of $\approx$ 26 wt. % absorbed acetone for 827/L-Arg and 8.18 $\pm$ 0.12 wt. % of $\approx$ 29 wt. % for 827/137H remain after drying at 40 °C (vacuum). This also supports the formation of hydrogen bonds, which, analogous to type 2 bonded water, require more energy to be broken. The swelling decreased on a similar scale. Subsequent drying at 100 °C under vacuum showed a further reduction in mass. However, a weight gain of 2.67 $\pm$ 0.29 wt. % for 827/L-Arg resp. 3.04 $\pm$ 0.23 wt. % for 827/137H remains compared to the initial mass. Therefore, no reliable statements can be made about actual degradation processes from re-dried weights.

Figure 4.30 displays the FTIR-spectra related to acetone immersion. The additional FTIR-peak at $\approx$ 1738 cm^{-1} in the acetone spectra after immersion (left) and the resp. specimens after immersion and re-drying (right) may be assigned to phenyl formate, which is likely to form via beta scissioning [275]. Krauklis et al. [276] obtained spectra for hygrothermal aged epoxy indicating that there was no significant difference observed in the chemical structure of the initial and dried samples, except for the peak at 1736 cm^{-1}, corresponding to carbonyl

groups ($\nu_{C=O}$) [277–279] which is part of phenyl formate. It can therefore be expected that chemical degradation occurs for both epoxy resin systems during long-term exposure to acetone. For the standard epoxy 827/137H, a slightly increased peak can already be seen for 820 h of immersion, which is in line with the faster absorption. The test specimens were dried briefly before the FTIR spectra were recorded, but acetone is still present in the test specimens, as indicated by the peak at 1710 cm^{-1}, although this has no influence on the peak at 1738 cm^{-1}.

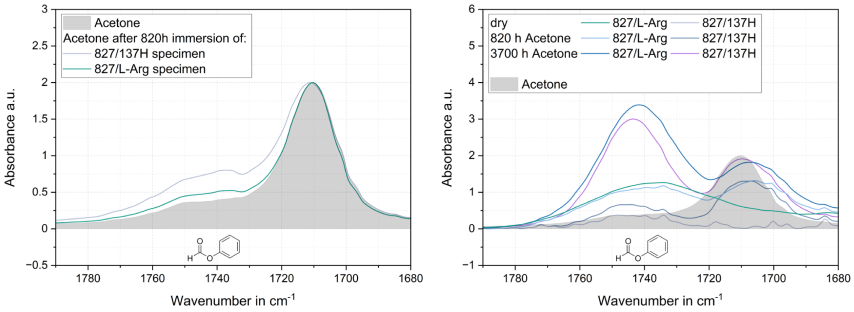

Figure 4.30.: FTIR-spectra of acetone without and after immersion of 827/L-Arg resp. 827/137H specimens (left), as well as dry and immersed specimens after 820 h and 3700 h acetone immersion (right).

Under the investigated aspects, arginine-cured epoxy is not lacking in long-term use when exposed at 22 °C to isopropanol or hydraulic oil, which would reduce its value regarding sustainability. Additionally, the amino acid-cured epoxy shows advantages in short-term exposure to acetone compared to the reference, which is, e.g., positive for cleaning purposes.

4.2.8. Transfer to Fibre-Reinforced Amino-Acid-Cured Epoxies

After extensive demonstrations that amino acid-cured epoxies can be a valuable alternatives to petro-cured epoxy resins, a successful transfer to FPRs must be ensured for use in composite applications. To the best of the author's knowledge, this is not yet described in the literature. In the following, manufacturing and testing of FRPs is exemplary explored for the system 827/L-Arg.

Caused by the L-Arg particles, manufacturing via RTM-process leads to filtration effects (see Section 3.1.2) and is not applicable for this reason. Therefore, manu-

facturing is conducted with the DirectPreg / autoclave process as described in Section 2.2.1. The results of quasi-static tensile tests of uni-directional composites in longitudinal and transversal direction are displayed in Figure 4.31 in comparison to the system 827/137H. Small deviations ($\Delta V_f \leq 3$ %) from the targeted fibre-volume fraction $V_f = 50$ % were equalised by normalisation to $V_f = 50$ %.

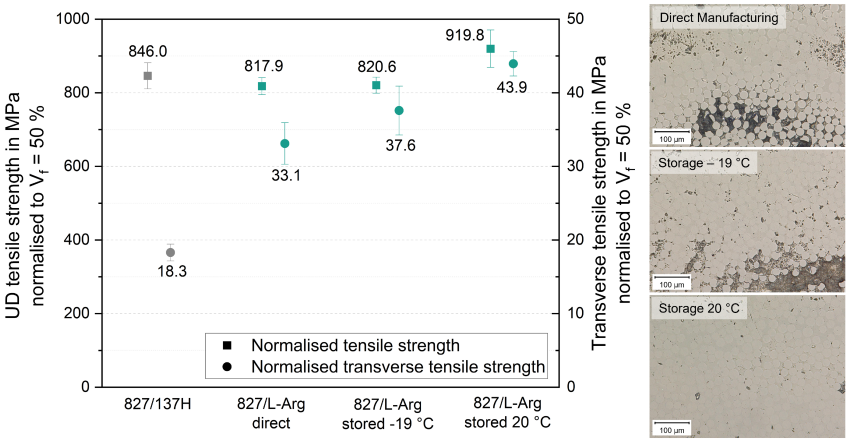

Figure 4.31.: Left: Unidirectional, longitudinal tensile and transverse tensile strength of 827/137H and 827/L-Arg specimens normalised to $V_f = 50$ %. 827/L-Arg specimens were manufactured directly, respectively after three months storage at 20 °C or -19 °C. Right: Cross-sections of 827/L-Arg after different storage conditions before DirectPreg/autoclave process.

From rheological and DSC measurements over several months (Figure 4.3), the question arised, whether prepregs containing amino acid-cured epoxy can also be stored at room temperature without negative effects on the performance. Compared to deep-frozen prepreg storage, as usual for prepregs, this would not only be energy efficient but would also simplify manufacturing, because defrosting of prepregs has to be planned before lamination. To evaluate this, prepregs manufactured via DirectPreg process were cured directly after fibre-impregnation, as well as after three months of storage at -19 °C and 20 °C.

As the uni-directional tensile strength is mainly influenced by the used fibres, no significant differences can be identified in Figure 4.31. However, it becomes apparent that the directly cured and deep-frozen stored samples exhibit sligthly lower strengths. The reason for this can be seen by microscopic analysis of

the plate quality (see Figure 4.31, right). For both configurations, the selected process results in insufficient infiltration of the matrix into the fibre bundles, which hinders load transfer over the fibre-matrix interphase. One possible reason for this is the comparatively high viscosity of the resin-hardener mixture. When the prepregs were stored at 20 °C, adequate infiltration into the fibre bundles was achieved over time, resulting in higher tensile and transverse tensile strengths. Under deep-frozen conditions, this cannot be achieved to the same extent, so that storage at room temperature is not only more energy-efficient but also results in improved manufacturing quality.

The range of the analysed transverse tensile strengths is in line with the values from Gibhardt et al. [280]. In the aforementioned study, transverse tensile strengths were evaluated for laminates manufactured with three different unidirectional glass fibre fabrics and 135/137H, using the same evaluation method as in this thesis but manufacturing via RTM. In Figure 4.31, it becomes apparent, that 827/L-Arg shows significant higher transverse tensile strengths regardless of the prepreg-storage conditions. However, in all cases, the transverse strength is far below the matrix strength, and therefore the 11 % higher matrix strength of 827/L-Arg compared to 827/137H is not the reason for the measured differences. The significant discrepancies between 827/L-Arg and 827/137H cannot be explained solely by the DirectPreg process, as 827/137H achieved a comparable level of manufacturing quality and fibre infiltration to that achieved with 827/L-Arg composites stored at 20 °C. A corresponding microscopy image can be found in Figure A.4.5 (Appendix). As the transverse strength is known to depend on the compatibility of sizing and matrix [280], the results indicate differences between the utilised curing agents regarding the fibre-matrix interphase or the fracture behaviour.

To ensure comparable high manufacturing quality for the subsequent tests, the prepregs were not cured immediately after impregnation, but after at least three days of storage at room temperature. Cross-ply (CP) and QI-laminates were investigated regarding their fatigue properties (R = 0.1). The Wöhler curves are shown in Figure 4.32. During the manufacture of CP-laminates, the backing fibres of the fabric were removed by hand for half of the laminates. These laminates achieve better fatigue properties than those with backing fibres, as the backing fibres (90° to the load direction) can additionally initiate transverse cracks and also may cause fibre misalignments due to ondulations.

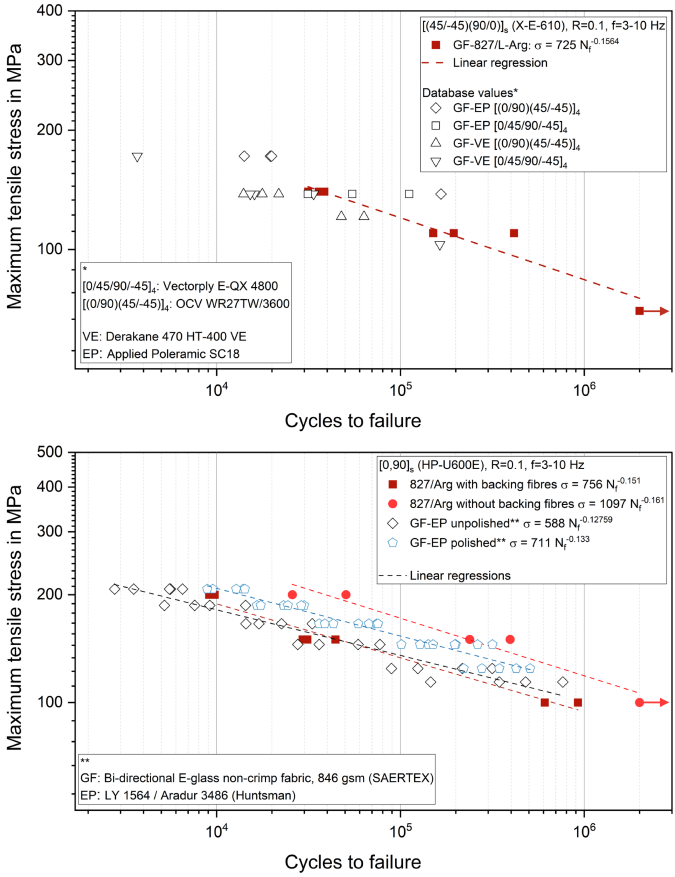

Figure 4.32.: Wöhler curves for QI- (top) and CP-laminates (bottom) with additional literature data: *[281], **[282].

The mathematical representations of the Wöhler curves can be found in Figure 4.32 in the form of Equation (4.1), where $\sigma_{\max}$ is the maximum stress of the cycle to which the component was subjected.

$$\sigma_{max} = A \cdot N_f^{-\frac{1}{k}} \tag{4.1}$$

A is the y-axis intercept used to determine the load level at which the laminate fails in the first cycle from cyclic tests. While this corresponds well with the quasi-static tensile strengths for UD laminates [245], the A values for CP and QI

laminates are higher than the determined quasi-static strength ($\sigma_{QI} \approx 350$ MPa; $\sigma_{CP} \approx 500$ MPa). This can be explained by the occurring damages. In UD-laminates, fibre breakage dominates in both quasi-static and cyclic tests due to higher load levels, while for QI and CP laminates, matrix cracking dominates at the beginning (especially in layers that are oriented off-axis, such as 90° layers). In contrast to quasi-static tests, delamination and fibre debonding follow after crack saturation during cyclic loading.

Therefore, A for QI and CP laminates is in a similar range, although QI has a lower quasi-static strength due to the lower 0° fibre content, but the 0° fibres are not 'decisive' at low load levels. With similar slopes, high values of A indicate that the component has a better fatigue life. k represents the inverse slope of the curve, with a higher k value indicating that the number of cycles to failure increases rapidly with a decrease in the maximum cycle stress.

Based on a comparison with literature values [281, 282], it can be concluded that the fatigue life properties of AS-cured epoxies do not present any disadvantages compared to standard epoxies. The literature values are shown as unfilled dots in Figure 4.32. It is even likely that the micrometre-sized particles can stop cracks, thereby achieving better fatigue properties than with standard epoxy resins. The first indicator of this is the comparatively high A value.

For this reason, the influence of L-Arg particles on the fracture toughness was also investigated using DCB and ENF tests. These tests are highly dependent on several factors as investigated in [283, 284]. Among other facts, the distance between the layers is crucial, especially in the layer with the crack. Figure 4.33 therefore compares the systems 827/137H and 827/L-Arg with the same GF-fabric (HP-U600E) and comparable $V_f \approx 40$ % as well as matrix layer thickness in the crack initiation.

While $G_{I,C}$ is very similar for both systems, as the notch was implemented in the same way, the propagation value with L-Arg is significantly higher (+73 %). In contrast to the SENB test, where the crack can find the most energy-efficient path. In the composite, however, the crack must pass through the particles due to the confinement by the fibres, and the particles can positively influence the fracture toughness [120].

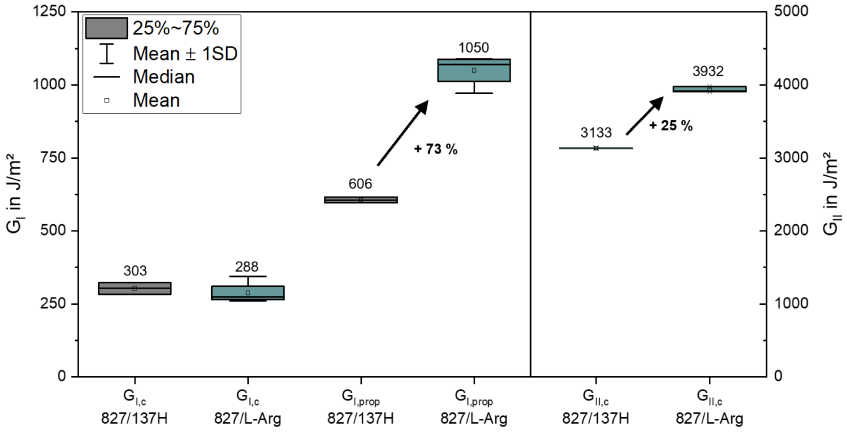

Figure 4.33.: Comparison of DCB and ENF results for 827/137H and 827/L-Arg.

DCB specimens manufactured with 827/137H (Figure 4.34, bottom) show alternating / adhesive crack propagation along the backing fibres and the interphase, as well as exposed fibres.

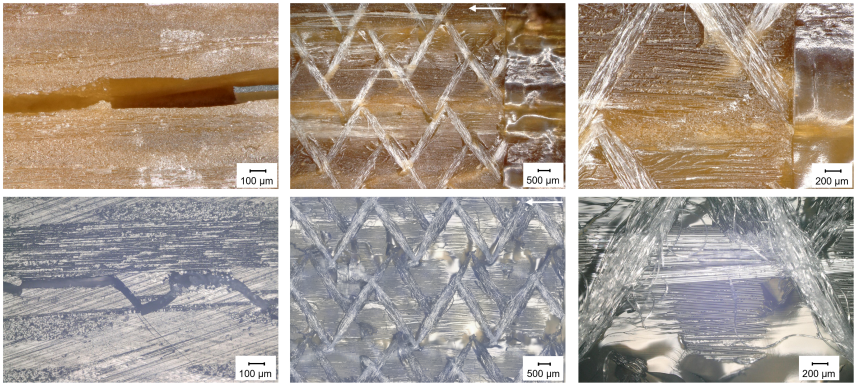

Figure 4.34.: Microscopy of DCB-specimen: 827/L-Arg (top) vs. 827/137H (bottom). Left: side view, centre and right: top view of separated samples.

In contrast, with 827/L-Arg, the crack in the DCB test progresses cohesively through the matrix (Figure 4.34, top), with evenly embedded fibres. Hence, the fibre-matrix interphase with the investigated GF-sizing can be considered com-

paratively positive with 827/L-Arg. Thereby, the high temperature difference during curing of 827/L-Arg may positively influence the fibre-matrix bonding through shrinkage and thus much higher compressive stresses of the matrix on the fibres. The fracture toughness in mode II (ENF test) has also increased by +25 % compared to the reference.

Concluding, the transfer to fibre-reinforced, amino acid-cured epoxies has been successful. Composites manufactured via DirectPreg/autoclave process achieve high thermo-mechanical properties, comparative to standard prepreg systems. Simultaneously, the feasibility of energy-efficient prepreg storage has been demonstrated as positive impact on the energy balance.

4.3. Fully Biobased Matrix Materials

As introduced in Section 4.1, epoxidised vegetable oils (VO) have the potential to be used as an epoxy A-component and further increase sustainability of matrix materials. In the literature, VOs are used, e.g., as reactive diluents to increase the fracture toughness of epoxies [175]. However, Park et al. [285] and Chen et al. [286] report the deterioration of other properties. Epoxidised soybean oil (ESBO) is generally used to increase toughness, as a reduction in network density is helpful for this purpose. However, ELO is used in the following section because of its higher linolenic acid share for superior functionalisability to completely replace the A-component.

So far, reported thermal and mechanical properties are not adequate for load-bearing applications in the field of composites using a full replacement of the epoxy A component through ELO [175, 287]. The following sections will therefore focus on the investigation of different curing conditions and explore optimisation potentials in terms of thermal and mechanical properties. Besides recent studies of UV-curable systems [288], carboxylic acids and anhydrides are reported to cure VOs [175, 287, 289], which is why biomolecules with these functionalities are chosen to investigate fully biobased epoxy alternatives.

4.3.1. Methods

For the investigation of different temperature profiles for curing with citric acid (ELO/CA), the maximum temperatures serving as boundary conditions for utilised thermokinetic methods are changed compared to the previous systems

(100, 120, 140, 160, 180 °C) in Section 4.3.2, while in Section 4.3.3, predictions are made for maximum curing temperatures of 140 °C comparing the use of ELO directly after production and after 1 month of storage. The experimental verification measurements were only carried out after one month of storage.

4.3.2. Curing with Biobased Carboxylic Acids

Typical reactions of carboxylic acids with epoxies are shown in Figure 4.35 [215]. Shimbo et al. [290] have shown that the distribution of the proportions of occuring ester and ether bonds influence the properties of the cured material. Besides the stoichiometric ratio, the curing conditions also influence, which reactions are favoured.

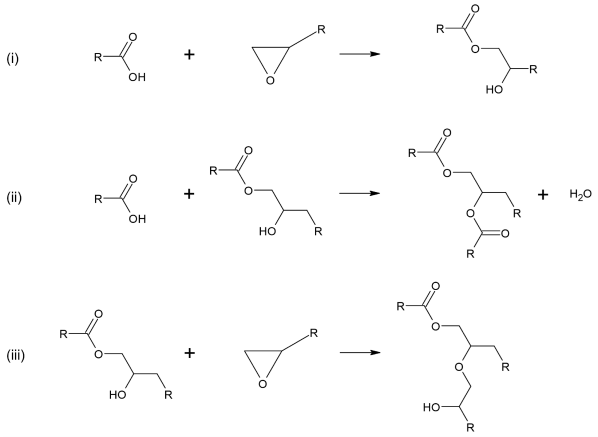

Figure 4.35.: Reactions of carboxylic acids with epoxies. (i) Half-ester formation through reaction with oxiran group. (ii) Subsequent reaction with carboxylic acids leads to diester and water. (iii) Ether formation via reaction with oxiran.

Carboxylic acids can be obtained from petrochemical resources as well as from natural sources [205, 291]. For example, sebacic acid can be produced from castor oil. Janesch et al. [287] cured flexible ELO/sebacic acid polymers with a stoichiometry-optimised T_g of 34°C (DMA tan δ) and tensile strength at room temperature of 2 to 3 MPa after curing for 24h at 140 °C.

With citric acid, higher T_gs are reported, e.g., by Sahoo et al. [175], where sample preparation contained Tetrahydrofuran (THF) and curing at 90 °C (6 h) followed by post-curing at 110°C (2h), leading to a T_g (DMA tan δ) of 43 °C

and a tensile strength of 5.25 MPa when tested at room temperature. As citric acid is frequently occurring in nature, available as a mass-produced and low-cost product, this acid is used in the following.

As introduced, curing conditions for several maximum temperatures are modelled using thermokinetic methods. The temperature profiles are listed in the Appendix (Table A.4.6) in detail. All generated temperature profiles were successfully used to produce plates. As the maximum temperature increases, yellowing of the specimen can be observed (see Figure 4.36), which is likely due to increased physical aging at elevated temperatures. In addition, it is noticeable that the plates appear opaque up to maximum temperatures of 140 °C, which is related to the fact that citric acid melts at 153 °C [292], thus preventing light refraction on crystals that appear to still be present at lower temperatures.

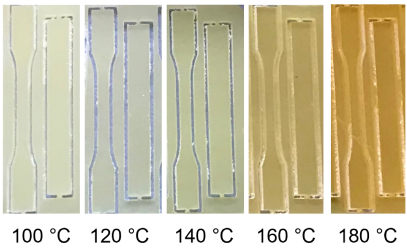

Figure 4.36.: Colour changes of ELO/CA with increasing maximum curing temperature.

Figure 4.37 displays the results of tensile tests and Figure 4.38 the T_gs of specimens cured with the different curing profiles. The optimum of stiffness, strength and elongation at break is obtained for maximum curing temperatures of 160 °C, where citric acid crystals have melted during curing.

A significant decrease in thermal and mechanical properties is evaluated for maximum curing temperatures of 180 °C, most likely due to degradation processes of citric acid [292]. For specimens with curing temperatures below 153 °C, the results of tensile tests are very similarly. As described in Section 4.2.7, determined tensile strengths of polymers decrease overproportional starting at test temperatures approximately 30 °C below T_g. Especially for these ELO-based polymers with low T_gs, the strength values obtained from room temperature tests are very dependent on slight differences in T_g. Since the utilised manufacturing process

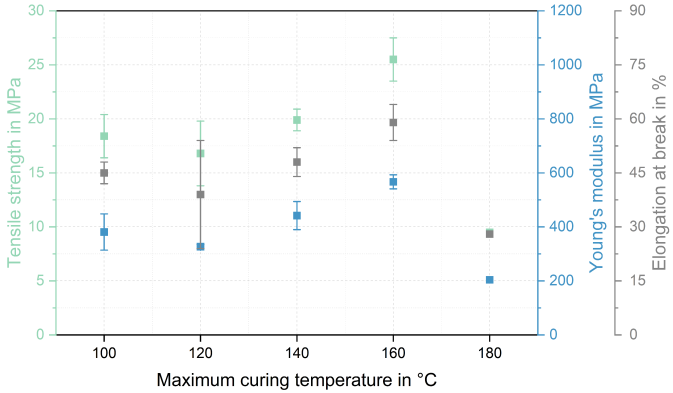

Figure 4.37.: Mechanical properties of ELO/CA cured with different temperature profiles (specimen type: 1BA; test temperature: 22 °C).

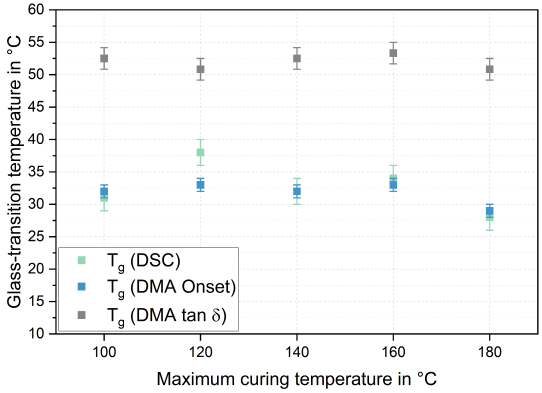

Figure 4.38.: Glass-transition temperatures of ELO/CA cured with different temperature profiles determined using various methods.

caused higher T_gs than those reported in the introduced literature, this explains the higher strength values.

Since the thermal and mechanical properties of all ELO/CA polymers at room temperature are not sufficient for load-bearing composite applications, this system will not be further investigated in this thesis.

4.3.3. Curing with Biobased Anhydrids

There are various possibilities for the ring opening of anhydrides that is required for the reaction with epoxies. For example, -OH groups can be used to form hemiacetals (Figure 4.39 i). This also makes esterification (ii) and etherification reactions possible during anhydride curing, e.g., by reaction of epoxy groups with the resulting -OH groups (iii) [293]. However, according to Ullmann's Encyclopedia [215], the mechanism is controversial because several competing reactions may occur.

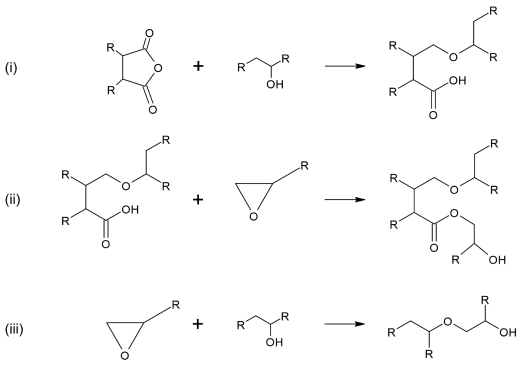

Figure 4.39.: Ring opening of anhydrides (i), subsequent esterification (ii) and etherification (iii).

In the case of the investigated itaconic anhydride (IAH), a conversion from IAH to itaconic acid takes place at higher temperatures (≈ 69 °C [294]). It is conceivable that this conversion initiates the ring opening of the anhydride. It has not been conclusively investigated whether this leads mainly to reactions of carboxylic acids. In this case, the associated initiation at elevated temperatures offers the advantage of potentially allowing storage of unreacted mixtures, as investigated for partially bio-based systems. The influence of air humidity on this conversion process offers further opportunities for investigation.

After 1 month of storage (Model 2, Appendix Figure A.4.6), a slightly lower reactivity can be observed, suggesting a temperature profile with initially slightly higher temperatures Figure 4.40 (left). Nevertheless, the thermokinetic methods lead to results that match the experimental validation well (see Figure 4.40, right). For better comparison, verification measurements were carried out isothermally at 110 °C.

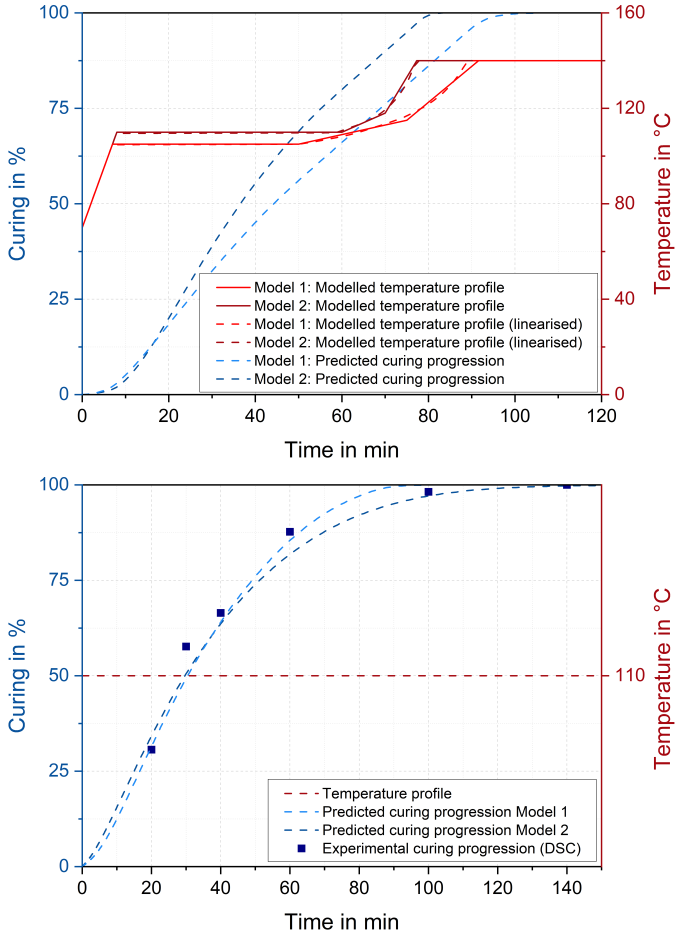

Figure 4.40.: Modelled temperature profiles and predicted curing profiles for ELO/IAH before and after on month of storage of ELO (top). Isothermal validation at 110 °C via DSC (bottom).

A plate manufactured using model 1 already behaves rubber-like at room temperature (T_g = -25 ± 2 °C (DMA onset) resp. 27 ± 2 °C (DMA tan δ), meaning that its use as a matrix material in FRPs is not meaningful for most applications. For this reason, no further investigations (e.g., stoichiometric variations) were carried out, even though Todorovic et al. [289] found for the conversion of ELO with methyltetrahydrophthalic anhydride that the epoxide groups near

the triglyceride centre remained unreacted and understoichiometric ratios lead to optimised conversion.

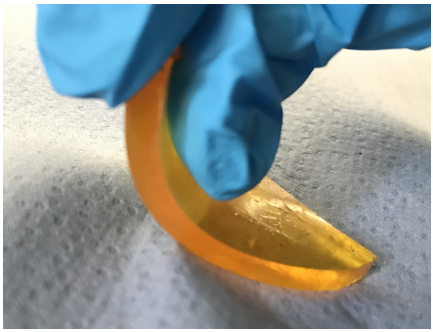

Figure 4.41.: Rubber-like behaviour of ELO/ITA.

In preliminary tests, succinic anhydride (Merck KGaA, Darmstadt, Germany) was tested, but the thermokinetic methods based on DSC measurements did not lead to any meaningful curing conditions in a meaningful temperature range. The method of using thermokinetic methods as described is therefore useful for performing an initial screening of different material combinations with little material input, selecting catalysts and accelerators, and subsequently selecting suitable systems.

4.4. Conclusions

The findings presented in this chapter demonstrate that the use of biomolecules in epoxy systems can lead to successfully cured polymers. By generating suitable curing profiles, amino acid-cured epoxies proved competitive property profiles compared to commercial, petrobased epoxy systems. Simultaneously, they offer major advantages in terms of environmental and health risks due to their food approval, and their ease of availability. Therefore, the hypothesis

Matrix polymers derived from bio-based feedstocks can achieve competitive properties while minimising environmental and health risks during processing.

can be entirely confirmed. The investigation of effects of environmental and chemical influences on the partially bio-based system 827/L-Arg also showed no

significant deterioration in long-term properties, which would reduce sustainability. However, hot-wet properties still need to be investigated over a longer period of time. The reaction mechanism for 827/L-Arg was identified through investigations of stoichiometric variations and shelf life. The use of amino acid-cured epoxies as matrix in composites has also been shown. Based on these findings, these systems will be examined in the next chapter for their flame retardant properties.

The fully bio-based systems based on epoxidised vegetable oils that were investigated are not suitable for fibre-reinforced use in load-bearing applications at room temperature and elevated temperatures due to their low T_gS. Nevertheless, high thermo-mechanical properties were achieved in comparison to the literature. The curing predictions of the thermokinetic methods correspond very well with the experiment. In preliminary tests, this made it possible to exclude systems that did not show curing in useful temperature ranges, thus saving material and time.

Thermokinetic methods are therefore a simple and efficient way of determining curing conditions. Due to their introduced limitations, suitable experimental validation is relevant. The selected methods using DSC and FTIR have proven to be suitable for this purpose. Fine dispersing using a three-roll mill appears to be a very important but also time-consuming step for all examined systems with solid curing agents, reducing inhomogenities and defect driven failures. In the framework of this thesis, the investigation of alternative solvent-based processes was omitted, as this, contrary to the motivation for this work, generally entails risks for humans and the environment.

5. Flame-Retardancy of Biomolecules

In addition to the increasingly restrictive regulatory requirements for flame retardants, the environmental and health aspects of the resources used and their sustainable and independent availability motivate the investigation of biomolecules as flame retardants. Nature offers a variety of biomolecules with chemical structures similar to those of industrially used flame retardants. For example, phosphorus-containing molecules occur naturally. Consequently, the working hypothesis of this chapter is:

Biomolecules can improve flame retardancy in an environmentally friendly manner.

After demonstrating that biomolecules can be successfully used to produce environmentally friendly and health-friendly polymers, the question arises whether these biomolecules can also be successfully used as flame retardant modifications. Therefore, the flame behaviour of amino acid-cured epoxies is examined in the first section (Chapter 5.2), while the second section (Chapter 5.3) investigates the fire behaviour of additivated biomolecules.

5.1. Methods

In addition to UL94 V and LOI tests, TGA measurements were performed on the TGA/DSC 1 device under nitrogen and synthetic air atmosphere between 30 and 850 °C (10 K/min). As suggested by van Krevelen [295], the char residue (CR) from TGA measurements in a nitrogen atmosphere was evaluated at 850 °C to calculate the oxygen index (OI) using Equation (5.1). For better distinguishability, the abbreviation LOI is used for the values determined in the flame tests and OI for the values calculated according to Equation (5.1).

$$\mathrm{OI} \cdot 100 = 17.5 + 0.4 \cdot \mathrm{CR} \tag{5.1}$$

Mechanical testing is conducted on DMA using the same specimen geometry and parameters as in Section 4.2.7.

5.2. Flame Retardancy of Amino Acid-Cured Epoxies

In this section, the promising amino acid-cured epoxies 827/L-Arg and 827/L-Trp/UR500 are analysed regarding their flame retardancy and compared with the reference system 827/137H. Furthermore, the phosphorous-containing flame retardants RP and APP are added in different amounts to investigate if synergistic effects become apparent when they are used together with the amino acids.

5.2.1. Flame Tests

Figure 5.1 shows the results of the LOI tests conducted, while the respective values are listed in Table 5.1. Starting with the comparison of the neat polymers without additional flame retardants, it becomes apparent that 827/L-Trp/UR500 exhibits an exorbitant higher LOI compared to the reference. This is most likely due to the aromatic groups contained, which can act as precursors for char building [296–298].

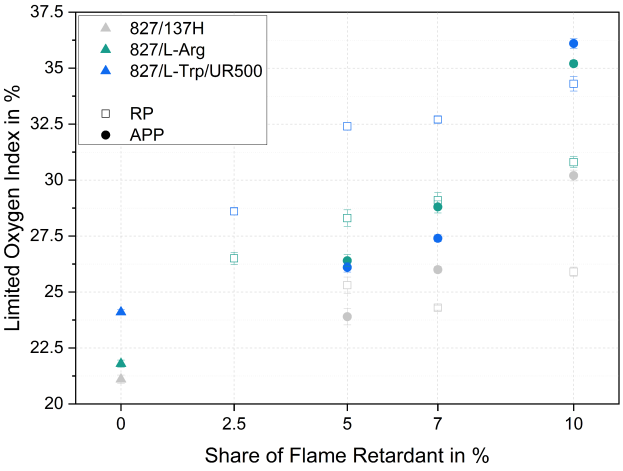

Figure 5.1.: LOI results for 827/137H, 827/L-Arg, and 827/L-Trp/UR500 specimens with and without APP and RP modifications in various compositions.

For L-Arg-cured epoxy, an increased LOI is also measurable, but without the presence of aromatic groups and the relatively lower added proportion of L-Arg compared to L-Trp, the LOI value is much closer to the reference system 827/137H. Nevertheless, it is reported, that imine groups show "blowing-out" effects in burning processes [296], positively influencing the flame retardancy. However, the measured value for 827/137H is in the range of literature values [299–301].

When APP and RP are added, improved LOI values can be seen for all systems. RP offers significantly increased LOI values even when added in small proportions, but compared to APP, the increase is smaller as the proportion increases. This trend is consistent with the commonly used proportions of RP and APP in polymers to achieve, for example, UL94 V0 classifications, which are generally lower for RP due to its higher phosphorus content.

The extent of the increase in LOI varies with each resin. The improvement is smallest with 827/137H, providing initial indications of a synergistic effect with amino acid-cured epoxies. It is conceivable that the relatively higher nitrogen content in the amino acids can serve to dilute combustible gases in the gas phase and as a blowing agent in the solid phase. In this context, synergistic effects of imine bonds and phosphorus-containing compounds are also stated by Zhou et al. [296]. However, based on the limited data available, it is not possible to make a clear prediction of the required flame retardant content in similar systems or for higher flame retardant contents, especially since stagnating LOI values are to be expected above a certain additive content. For the RP-modified resins, a saturation value is already apparent in the additive content range investigated, with the lowest value for the 827/137H system and the highest for 827/L-Trp. Further measurements with higher additive contents may confirm this observation that supports the indications of a occuring synergistic effect.

In general, the standard deviations determined in the LOI tests are low, so the influence of any heterogeneous FR distribution across the plate, such as that which can occur due to sedimentation when particles are added, can be considered insignificant.

Figure 5.2 displays specimens modified with 7 % APP as well as 7 % RP after LOI tests. Regardless of the curing agents used, the burnt specimens demonstrate differences between both flame retardants. For APP the condensed phase mechanism leads to itumescent char building. The visual comparison supports

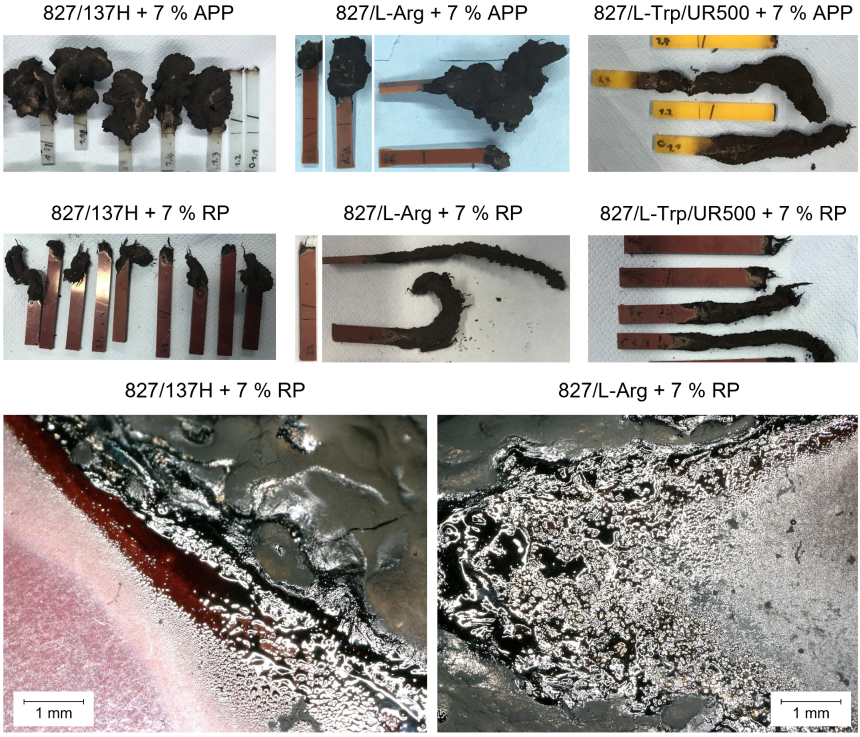

Figure 5.2.: Specimens of 7 wt % APP and RP modified epoxies after LOI tests (top). Digital microscopy image of glassy char developing with RP (bottom).

the assumption that the amino acids serve as an additional blowing agent, as the flamed test specimens show expanded char formation far beyond their original geometry. In contrast, the char with RP looks denser. By taking a closer look via digital microscopy, the developed condensed phosphoric acid is visible shiny, as already observed in Chapter 3 (Figure 3.14).

Zhi et al. [87] evaluated different studies and found that LOI values of approximately 26 % have to be achieved for UL 94 V0 classification, but depending on the system, the respective LOI might be shifted to higher values. Figure 5.3 displays that this is also the case for the configurations studied in this thesis. The higher the share of FR, the lower the LOI value must be for the classification UL 94 V0, which could be caused by increased gas phase mechanisms and char building abilities. Since flame tests are naturally subjected to many influencing factors, individual configurations show unexpected UL 94 results, which could be

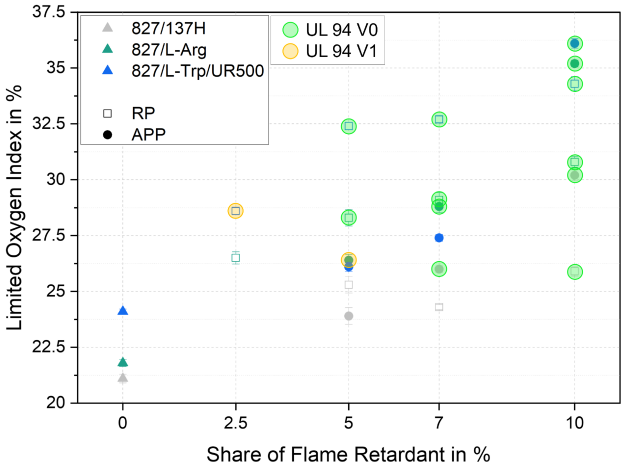

Figure 5.3.: Combined LOI and UL 94 results for all investigated configurations. Configurations marked with green colour achieved UL 94 V0 rating, while orange colour displays configurations with UL 94 V1 classification. Otherwise, the configurations do not achieve any UL 94 rating.

prospectively checked with repeated measurements. In detail, the configuration 827/L-Trp/UR500 + 7 % APP achieved no classification although the LOI of $\approx$ 27.5 % indicates otherwise.

Furthermore, Figure 5.4 shows selected specimens after UL94 V tests. Without FR-modification, 827/L-Trp/UR500 performs best and remains its initial geometry, most likely caused by the aromatic structure of L-Trp. Nevertheless, no UL 94 rating is achieved in the neat configuration. When examining APP-modified test specimens, it is noticeable that intumescent behaviour occurs, especially with amino acid-cured epoxies. The geometry of the specimen expands fan-like. An improvement over the petrochemical reference system 827/137H is clearly visible in the specimens modified with 5 % APP.

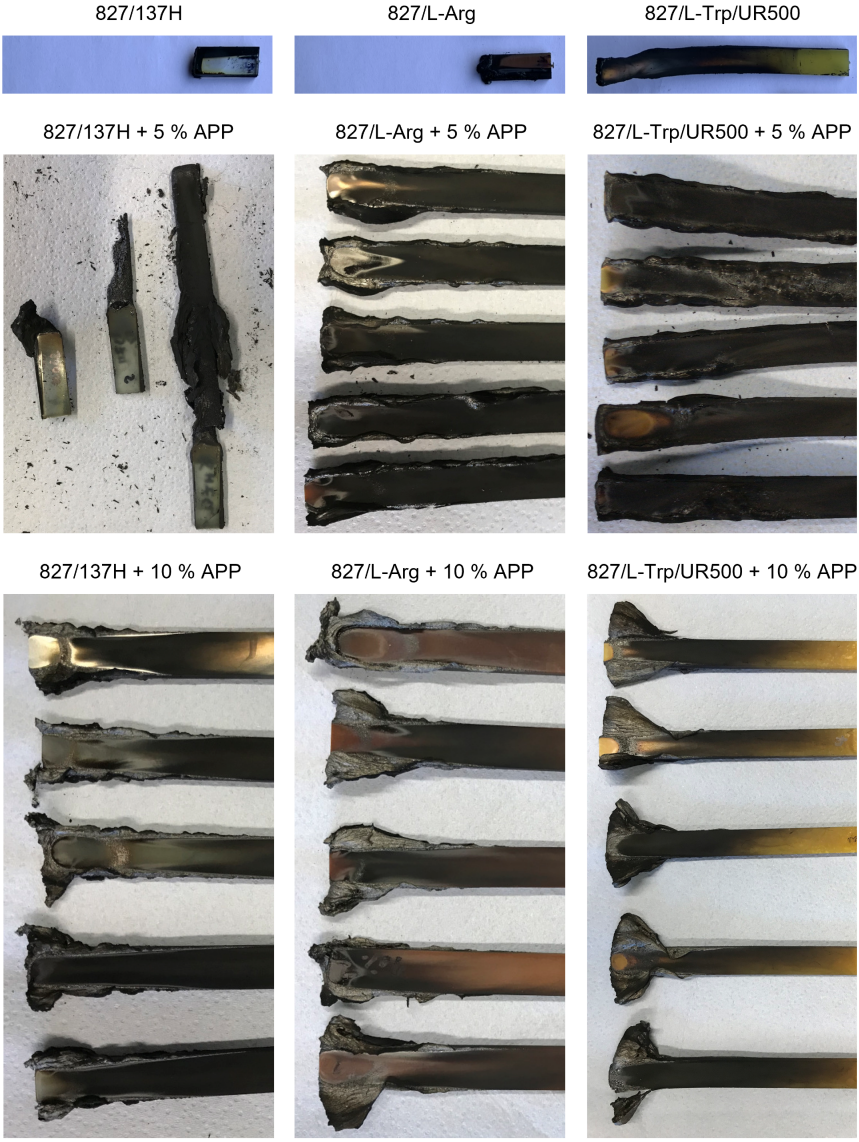

Figure 5.4.: Unmodified and APP-modified specimens of several epoxies after UL 94 V tests.

5.2.2. Thermogravimetric Analysis

Because flame tests are costly to perform, it is meaningful to figure out whether less time- and material-consuming test methods can also provide insight into the flame retardant properties of polymers. As suggested by van Krevelen [295], TGA measurements were performed in a nitrogen atmosphere. The corresponding mass loss curves are shown in Figure 5.5 and Figure 5.6. The OI values calculated using Equation (5.1) are listed in Table 5.1 together with the results of the LOI and UL 94 flame tests. The respective rates of mass change from derivative thermogravimetry (DTG) are displayed in the Appendix (Figure A.5.1).

It is noticeable that the amino acid-cured epoxies without additional FR (Figure 5.5, left) show a higher residue than 827/137H. According to van Krevelen,

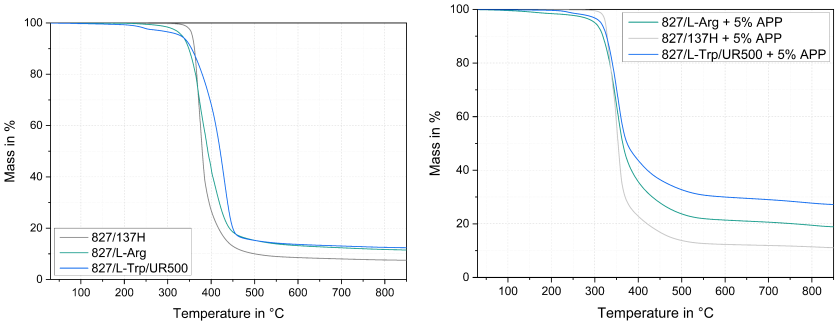

Figure 5.5.: Temperature-dependent mass loss of neat polymers (left) and modified with 5 wt % APP (right), determined via TGA under nitrogen atmosphere.

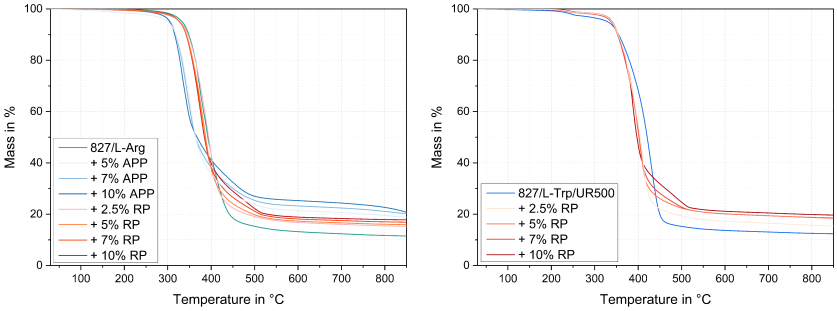

Figure 5.6.: Temperature-dependent mass loss of 827/L-Arg with and without APP and RP modifications (left) and 827/L-Trp/UR500 with and without RP modifications (right), determined via TGA under nitrogen atmosphere.

Table 5.1.: Results of LOI and UL 94 flame tests of all investigated configurations, as well as TGA residuum at 850 °C under nitrogen atmosphere and thereof calculated OI value according to van Krevelen [295].

	LOI in %	**UL94**	**TGA (N_2) residue**	**OI [295] in %**
827/137H	21.08 ± 0.19	None	7.53	20.54
+5 % APP	23.89 ± 0.37	None	11.09	21.94
+7 % APP	25.95 ± 0.15	V-0		
+10 % APP	30.21 ± 0.24	V-0		
+5 % RP	25.29 ± 0.37	None		
+7 % RP	24.31 ± 0.11	None		
+10 % RP	26.00 ± 0.24	V-0		
827/L-Arg	21.81 ± 0.16	None	11.57	22.13
+5 % APP	26.37 ± 0.26	V-1	18.88	25.05
+7 % APP	28.75 ± 0.27	V-0	20.26	25.60
+10 % APP	35.21 ± 0.15	V-0	20.75	25.80
+2.5 % RP	26.45 ± 0.27	None	15.30	23.62
+5 % RP	28.29 ± 0.37	V-0	15.93	23.87
+7 % RP	29.09 ± 0.33	V-0	16.88	24.25
+10 % RP	30.79 ± 0.24	V-0	17.78	24.61
827/L-Trp	24.11 ± 0.11	None	12.37	22.45
+5 % APP	26.12 ± 0.20	None	27.27	28.39
+7 % APP	27.37 ± 0.15	None	28.77	29.01
+10 % APP	36.06 ± 0.21	V-0	28.53	28.91
+2.5 % RP	28.59 ± 0.15	V-1	15.38	23.65
+5 % RP	32.41 ± 0.16	V-0	18.39	24.86
+7 % RP	32.65 ± 0.15	V-0	18.52	24.91
+10 % RP	34.28 ± 0.32	V-0	19.64	25.35

this is a sign of an enhanced flame resistance of the polymer, which is consistent with the LOI flame tests. Although 827/L-Trp leads to the highest residue and thus the highest calculated OI value, this is significantly lower than the LOI value determined in the flame test. However, for the other two neat epoxies, the OI values correspond well with the LOI values. Analysis of the rate of mass change (see Appendix, Figure A.5.1), supports these findings, as the decomposition peak is significant broader and lower for amino acid-cured epoxies compared to 827/137H. In the literature, this trend is positively reported for the respective flame resistance, as slower degradation can improve char building [302].

In contrast, when 5 % APP is added to all three epoxies, a significantly higher residue is measurable with L-Trp compared to L-Arg, although the LOI values do not differ considerably from each other. As suspected by the LOI flame tests, the lowest residue is measurable here with 137H. The reason for the deviations may be the small amount of material ($\approx$ 15 mg) in the TGA, which can lead to a reduction in representativeness in the event of inhomogeneities. In addition, a slight decrease in mass at elevated temperatures can be seen in the mass loss curves. The complete hermeticity of the device cannot be guaranteed as the mass loss is most likely due to oxidation processes, but these deviations do not exceed differences of different configurations.

Investigating various modified amino acid-cured epoxies in Figure 5.6 clearly shows a gradual increase in residue with FR content. Contrary to the results of the LOI flame tests, in which RP leads to greater improvements than APP, higher residues can be determined for APP in Figure 5.6 (left). The related DTG plot (see Appendix, Figure A.5.1) displays a shift of the respective peak temperatures to lower temperatures with higher amounts of FR. This trend is also in line with reports in the literature [303], as, for example, phosphorus-containing FRs have a catalytic effect on ongoing reactions. In the event of a fire, char building at lower temperatures is beneficial for an early barrier effect against heat and mass transfer.

The reason for this behaviour stems from differences in the mechanisms that occur. For APP, all mechanisms take place even without oxygen. The (poly)phosphoric acids are formed, for example, by intramolecular dehydration, and carbonisation does not require oxygen. The formation of diluting NH_3 from NH_4^+ also takes place without oxygen, but cannot be explicitly investigated using TGA. In the event of fire, oxygen only acts to solidify the char through surface oxidation. In contrast, the mechanism involving RP requires oxygen because the phosphoric acids used for char formation are achieved by phosphorus oxides (e.g., P_2O_5). Radical scavenging is another mechanism for the effect of RP. Although this takes place without oxygen, it cannot be investigated using TGA [304, 305]. Consequently, the occurring mechanisms need to be considered before transferring data of non-flame test data (e.g., TGA) to estimate flame behaviour. Nevertheless, additional tests conducted alongside flame tests can provide valuable information.

Figure 5.7 (left) shows the TGA curves of 827/L-Arg with and without modification of 10 % APP in nitrogen and synthetic air, while on the right-hand side, the modification with and without 10 % RP for both atmospheres is shown using the example of 827/L-Trp/UR500.

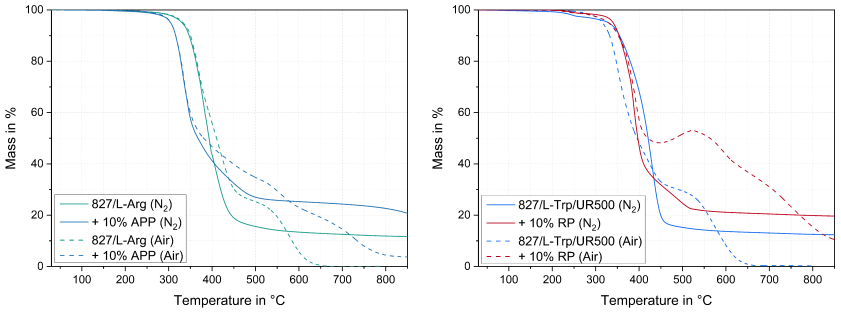

Figure 5.7.: Temperature-dependent mass loss of 827/L-Arg with and without 10 % APP (left) and 827/L-Trp/UR500 with and without 10 % RP (left) (right), determined via TGA under nitrogen and synthetic air atmosphere.

With oxygen in the atmosphere, the components of neat epoxies oxidise completely (oxidation/formation of CO_2, H_2O, N_2), while with flame retardants, a residue remains (phosphorus-containing char). Here, it is striking that RP shows an increase in mass between $\approx$ 440 °C and 600 °C, while the mass of APP-modified epoxy in synthetic air falls monotonically. This is closely related to the fact that self-sustaining gas phase combustion of RP is possible at 416 °C [305]. The exothermic reaction accelerates the oxidation to P_2O_5 in this range, thus intensifying char formation. This results in a temperature window where oxygen uptake and char building outpaces matrix degradation and volatilisation of RP.

In short, amino acid-cured epoxies show favourable flame behaviour. Without additional FRs, 827/L-Trp/UR500 already demonstrates a 3 % higher LOI than 827/137H , and both L-Arg and L-Trp can significantly enhance the effect of phosphorus-containing FRs through synergistic effects, enabling classification with much less FR use. Beyond the aforementioned results, the influence of FRs on the glass transition temperature (DSC, midpoint) for 827/L-Trp/UR500 was analysed. With 10 % APP, a reduction of 6 % to 106.9 °C was observed. Modification with 10 % RP even reduces T_g by 7.5 % to 105.2 °C, which underlines the positive influence of a lower required additive content. Nevertheless, there

are differences in the mode of action, so that, in the case of 7 % APP-modified L-Trp, a high LOI is achieved, but it is still not classified according to UL 94. Consequently, the necessary tests must be carried out to meet the respective requirements, depending on the application. However, TGA measurements cannot fully replace flame tests, as they only analyse small parts of the complex mechanisms of flame retardancy, but they can help to understand ongoing processes.

5.3. Biobased Flame Retardants

Attempting increasingly sustainable flame retardants and avoiding the potentially critical working conditions associated with the extraction of raw materials such as phosphate ore [306, 307], industry and academic institutions are currently working on the development of new bio-based flame retardants based on renewable resources [87].

In the literature, lignin, a by-product of the pulp and paper industry, is often used because of its highly aromatic, ring-rich structure, which facilitates char formation. In addition, lignin contains many phenolic groups that slow the propagation of flames by forming phenoxyl radicals, which scavenge combustion radicals ($H^\bullet$, $OH^\bullet$) [308, 309].

Besides, the use of chitosan (CS) is reported in this context. Thereby, CS is a natural polysaccharide obtained by alkaline deacetylation of chitin, which is extracted from the exoskeletons of arthropods and shellfish. CS consists of amino-containing 2-deoxyglucan units and is well known for its non-toxicity, biodegradability, and biocompatibility. Due to its low cost and wide availability, CS has been used in various industrial and environmental applications, including biotechnology and wastewater treatment [310]. It has potential as a flame retardant because it contains nitrogen, which dilutes combustible gases, e.g., through the formation of ammonia. The linked glucosamines (see Chapter 2, Figure 2.2) form an efficient char, as their thermal decomposition produces a large amount of aromatic carbon. Furthermore, synergies with phosphorus-containing systems (e.g., APP, DOPO) are reported in the literature [311, 312], as N-P-C combinations are typical for flame retardant systems.

Phytic acid (inositol hexakisphosphate, IP_6) is found, for example, in corn bran (e.g., rice, corn or wheat bran) and legumes. After aqueous extraction, the minerals are precipitated and filtered in an acidic environment. Alternatively,

phytic acid is extracted from food industry waste using phytase enzymes [313]. In the combustion process, PA can be used as an acid source in intumescent flame retardant systems. Its thermal decomposition produces metaphosphoric acid that promotes carbonisation processes. In addition, PA produces noncombustible gases and free P-radicals (radical scavenger). At the same time, its large share of phosphorus can be used as a charring agent, promoting the formation of stable carbon residues [9]. Some studies on its effects as flame retardants are reported, for example, using complexes with metal ions (e.g., with Zn^{2+} [314] or Mg^{2+} [315]). The high number of reactive -OH functionalities of PA has led to excessive pore formation by reacting with the epoxy component in preliminary tests. In order to obtain an N-P-C system, the following investigations examine the combination of CS and NaPh compared to the separate modification with one of the biomolecules in the 827/137H system.

NaPh results from the neutralisation of phytic acid (e.g., with NaOH or Na_2CO_3). NaPh has been reported in combination with CS as a surface-functionalisation of microcrystalline cellulose in epoxy resin [316] but no studies have been found in which epoxy resin is modified solely with CS and NaPh.

5.3.1. Thermogravimetric Analysis

To obtain initial indications of possible solid-phase mechanisms and the necessary additive quantities to influence these, the TGA results of the biomolecule-modified epoxy resin are presented below. However, based on the results in Section 5.2, it is not expected that the flame retardant behaviour of the polymers can be meaningfully predicted from TGA residues.

Figure 5.8 (left) displays changes in the mass loss curves of NaPh modified 827/137H under a nitrogen atmosphere. The char residuum is significantly higher when 20 wt % NaPh is added. However, a further increase of NaPh has no considerable influence on the residuum. CS also increases the char residuum (Figure 5.8, right). In combined additivation, the char residuum has been further increased. Table 5.2 lists the OI according to van Krevelen [295] calculated from the residuum, among other experimental results. The resulting OI of 29.7 % for the configuration containing 30 % NaPh and 10 % CS indicates a successful FR effect, further examined in Section 5.3.2.

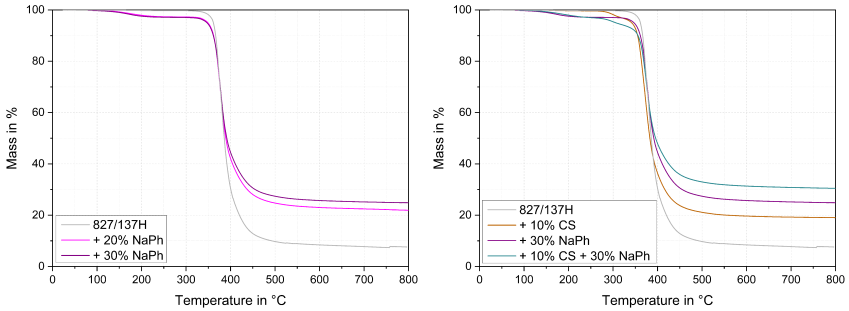

Figure 5.8.: Temperature-dependent mass loss of 827/137H with and without NaPh modifications (left) and NaPh + CS modifications (right), determined via TGA under nitrogen atmosphere.

The first mass loss can be observed at lower temperatures. According to Dowbysz et al. [317], removal of bound water (dehydration), deacetylation and depolymerisation of CS take place between 250 and 360 °C. For NaPh, the initial mass loss is shifted to temperatures between 120 and 220 °C, mainly attributed to dehydration and starting carbonisation, as described by Daneluti et al. [318] for PA. The corresponding DTG plots are shown in Figure A.5.2 (Appendix). As previously described in Section 5.2 as a positive indicator of the resulting flame retardant effects, reduced peak heights are also observed by adding the investigated biomolecules.

In an oxidising atmosphere (synthetic air, Figure 5.9), carbon dioxide (CO_2) and water (H_2O) are the main gaseous products of combustion. In the case of NaPh, inorganic sodium phosphate salts (e.g., sodium pyrophosphate ($Na_4P_2O_7$) and/or sodium metaphosphate ($NaPO_3$) are formed. Consequently, approximately the same amount of residue remains with and without CS, as CS does not contribute significantly to the residue in synthetic air atmosphere.

5.3.2. Flame Tests

LOI tests were performed to assess the flame retardant effect of different combinations. The results are listed in Table 5.2 together with the calculated OI according to van Krevelen [295].

When comparing the OI values calculated according to van Krevelen [295] with the LOI values determined by flame tests, it can be seen that there is adequate

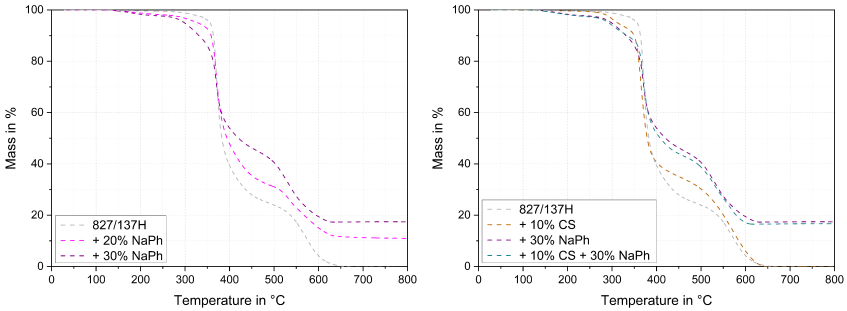

Figure 5.9.: Temperature-dependent mass loss of 827/137H with and without NaPh modifications (left) and NaPh + CS modifications (right), determined via TGA under synthetic air atmosphere.

Table 5.2.: Results of LOI flame tests of all investigated configurations, as well as TGA residuum at 850 °C under nitrogen atmosphere and the calculated OI value according to van Krevelen [295].

	LOI in %	**TGA (N_2) residue**	**OI [295] in %**
827/137H	21.08 ± 0.19	7.53	20.54
+10 % CS	20.05 ± 0.95	19.00	25.10
+15 % CS	20.83 ± 0.28	13.96	23.09
+10 % NaPh	**22.82** ± 0.61	11.72	**22.19**
+15 % NaPh	**24.05** ± 0.36	16.31	**24.02**
+20 % NaPh	**25.10** ± 0.33	21.55	**26.12**
+30 % NaPh	24.19 ± 0.17	24.83	27.43
+10 % NaPh + 5 % CS	21.94 ± 0.20		
+15 % NaPh + 10 % CS	22.25 ± 0.84	21.08	25.93
+20 % NaPh + 10 % CS	20.91 ± 0.86	21.90	26.26
+30 % NaPh + 10 % CS	23.06 ± 0.30	30.50	29.70

agreement (formatted **bold** in Table 5.2) for the configurations modified only with NaPh, except for the configuration modified the highest. With 30 % NaPh, no improvement in flame retardancy is apparent compared to the 20 % modification in the LOI test. Possible reasons for this are, on the one hand, that the flame retardant effect has reached saturation and no additional active species are formed, and, on the other hand, that the high filler content significantly hinders network formation during the curing process. Furthermore, it is possible that the fillers increasingly agglomerate and/or sediment. At higher FR quantities,

the resulting char can also become porous and flake off, which actually reduces its ability to reduce heat flow. The formation of excessively large macropores instead of a desired fine-pored structure can be caused by the release of too much expanding gas and over-rapid foaming. The ratio between acid generator, carbon source and blowing agent is also important, otherwise the char may collapse or rupture [296, 319, 320].

CS consistently led to a deterioration in the LOI value in the flame test. Figure 5.10 and Figure 5.11 show specimens after flame tests, demonstrating that CS leads to foam-like chars with large pores, which means that the barrier effect is not achieved optimally. It is striking in the middle image of Figure 5.11 that NaPh alone forms a noticeable, separated, and shiny char on the flamed surface, which likely consists of condensed phosphoric acid and sodium phosphates. The formed char is uniform and intact.

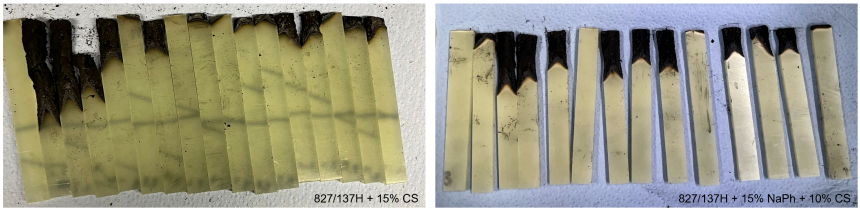

Figure 5.10.: LOI specimens of the configuration 827/137H + 15 % CS (left) and 827/137H + 15 % NaPh + 10 % CS (right) after testing.

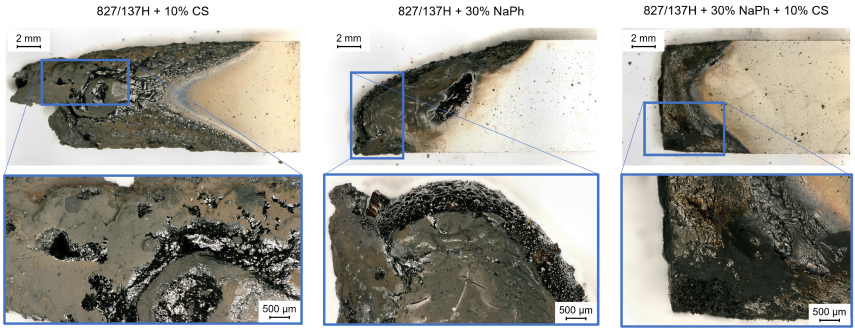

Figure 5.11.: Differences in char building of configurations modified with CS and/or NaPH.

The combination of both biomolecules forms a denser char compared to the pure CS modification. It cannot be excluded in Figure 5.11 (right) that part of the char has broken off for the reasons described previously. The flame test revealed comparatively slower burning behaviour, which can also be attributed, for example, to the dilution of combustible gases. However, an increase in volume as an indication of successful intumescence is not visible for any of the configurations shown. This may be due to differences in the temperature requirements for the formation of different mechanisms, which means that they may not occur simultaneously and cannot interact synergistically.

For a selection of configurations with the most promising LOI values, additional UL 94 tests were carried out. No classification could be achieved here, which is consistent with the LOI results, as no configuration exceeds the literature value of 26 %. In short, it can be concluded that the investigated configurations do not achieve an efficient flame-retardant effect. An additional increase in the quantities is not expected to result in a significant improvement in terms of classifiability.

5.3.3. Impact on Mechanical Properties

Because high amounts of biomolecules have to be used to increase the LOI, the mechanical properties are significantly impaired. As shown in Figure 5.12, the tensile strength decreases by more than 35 % for the configuration with 30 % NaPh, compared to the neat resin. A modification with 15 % NaPh + 10 % CS also decreases the tensile strength by more than 25 %.

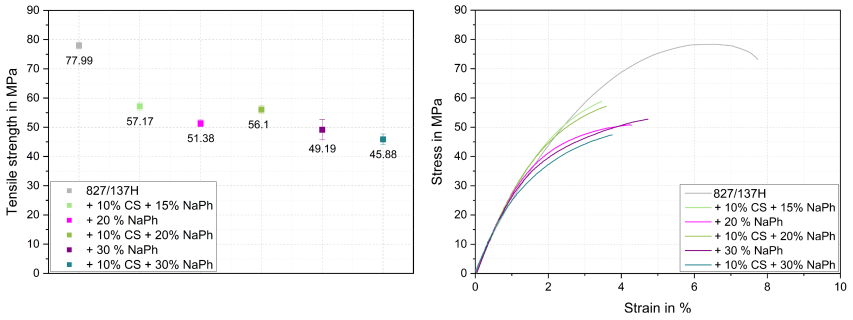

Figure 5.12.: Mechanical properties of selected configurations. Tensile strength (left) and representative stress-strain curves (right).

Due to its hydroxy- and amine-functionalities, CS can also react with the epoxy component, leading to an off-stoichiometric mixing ratio. As already seen in Chapter 4.2.4, Figure 4.10, varying networks are resulting in these cases, leading to differences in mechanical properties. Outlooking, the consideration of all reactive components in the stoichiometric ratio may offer potential for optimisation with regard to achievable mechanical properties. However, it is essential to examine the curing behaviour of each configuration, for example using thermokinetic analyses, in order to obtain a performance-optimised curing cycle due to competing curing reactions. Additionally, the high amount of particles might impair the network density during curing.

Higher additive shares lead to higher standard deviations, which is most likely caused by agglomerates acting as stress-concentrating defects and leading to failure at different stress levels. In this context, Selvam et al. [321] reported that CS is thermodynamically immiscible with epoxy and has a tendency to form moisture-rich aggregates, which create weak interfacial regions and reduce the load-bearing capability of the matrix. They investigated 8 % CS modified epoxy and also found an approximately 17 % decrease in strength compared to the unmodified epoxy, when CS particles are dispersed via a sonication method. However, NaPh impairs the tensile strength more than CS, because a total amount of 30 % additives leads to a greater decrease in strength for the 30 % NaPh configuration than for the mixture of 10 % CS and 20 % NaPh. Using these large amounts of additives, it becomes apparent that strategies for efficient flame retardancy are needed, e.g., as proposed in Chapter 3.

5.4. Conclusions

Amino acids can act as curing agents and improve flame-retardancy simultaneously. Especially L-Trp performed well in flame-tests, most likely due to its aromatic structure. The combination with commercially available FRs indicated synergistic effects, leading to an efficient and therefore sustainable use of FRs for UL 94 V0 classifications.

Biobased NaPh improves the LOI values of 827/137H, when added in large shares, showing its potential as a fully biobased FR. Nevertheless, the mechanical properties decreased significantly due to the high amounts (> 20 %) that must be added to achieve a slight increase in LOI. However, the improvement is still insufficient for classification according to UL 94. Synergistic effects with

CS could not be verified via LOI flame tests. The mechanisms of the various constituents occur within different temperature ranges and do not interact effectively. Consequently, no evidence of the desired intumescent effect could be detected. A chemical analysis of the char and the developing gas phase might provide interesting insights into the ongoing mechanisms, allowing further investigation of synergistic effects to enhance flame retardancy.

Therefore, the hypothesis

Biomolecules can improve flame retardancy in an environmentally friendly manner.

cannot be fully confirmed. Nevertheless, the investigations presented demonstrate that biomolecules have the potential to improve flame resistance.

Furthermore, TGA data indicate trends in flame retardancy, but quantified predictions of LOI values were not possible. Larger datasets may allow predictions, but the data measured in this chapter are not sufficient for a prognosis of the LOI through TGA measurements. This is particularly the case if the flame retardants require oxygen to achieve their effect.

6. Summary and Outlook

The preceding chapters have demonstrated the possibility of manufacturing environmentally friendly flame retardant composites in various ways. The overarching research hypothesis

High-performance composites can be designed flame-retardant and eco-friendly with compatible thermo-mechanical properties.

was investigated using several approaches. In summary, the hypothesis can be confirmed by the efficient use of flame retardants, resulting in a reduction in the amount required in FRP, and by the development of partially bio-based epoxy resins.

Within the scope of this dissertation, a method was developed to simultaneously avoid filtration effects in infusion processes and achieve significantly improved flame retardancy with a very low FR content. This was accomplished through the development of a CPI process whereby individual FR-modified plies are B-staged and subsequently infused together with dry fibre plies using unmodified resin. Thermokinetic methods were employed to successfully determine the process window, with the achieved objective of adequate ply adhesion and retention of the FR particles at the desired location.

As part of the research, it was therefore possible to produce different layups of partially FR-modified composites that demonstrate flame retardancy with significantly reduced amount of FRs. Since the effectiveness of individual layer modification cannot be meaningfully tested in standard tests (such as UL 94) without the use of special fire testing devices, new screening methods were successfully developed and applied. The chosen type of FR modification can therefore be considered a success in terms of environmental impact, achievable mechanical properties and the attained flame retardancy.

In order to develop novel bio-based matrix systems, a fast and simple procedure was developed for selecting material combinations using DSC analyses. These measurements can subsequently be used to create curing profiles using thermokinetic methods. The procedure was successfully applied to various conventional and bio-based systems. However, it has been found that simplified assumptions can lead to deviations for more complex reaction mechanisms, which can be detected using FTIR and DSC. As part of this thesis, both partly and fully bio-based systems were investigated. However, the studied fully bio-based polymers did not show sufficient properties for composite applications, which is why the focus was consequently placed on partly bio-based systems and, in particular, on avoiding critical curing agents.

Thereby, amino acid-cured epoxies as curing agents have proven convincing in many aspects. In addition to their cost-effective availability and environmental and human safety, they not only demonstrated favourable short-term thermo-mechanical properties, but also proved suitable for long-term use. Fatigue and ageing tests have not revealed any adverse effects. Only hot-wet environments with temperatures above 50 °C are leading to partial degradation. This has been evidenced, for example, by increased water absorption. Additionally, it has been shown that the thermo-mechanical properties of amino acid-cured epoxies remain consistently high over a wide range of stoichiometric ratios, allowing for certain tolerances in the mixing ratio, which is particularly relevant for industrial applications.

The production of FRPs with these systems has been proven to be feasible using the DirectPreg/autoclave process. A particularly appealing benefit is that the dispersed resin-hardener mixtures are latent at room temperature because the reaction initially requires a deprotonation step that occurs only at elevated temperatures. When using prepregs, this offers the advantage of eliminating the need for deep-freezing, enabling energy-efficient storage at room temperature and avoiding condensation issues. The manufactured composites exhibited comparably high fracture toughness and good compatibility with the chosen glass fibre sizing.

Within the scope of this dissertation, it must be emphasised that these partially bio-based epoxy systems also offer favourable flame-retardant properties. It could be demonstrated that even unmodified specimens achieve improved LOI values. Due to identified synergistic effects with phosphorus-based FRs, very

small amounts are sufficient to achieve an additional improvement in flame retardant properties and classifications such as UL 94 V0. Like the heterogeneous distribution of FRs (Chapter 4), this not only helps to save resources, but also simplifies processing and reduces the impairment of thermo-mechanical properties, which is a crucial aspect of the overarching research hypothesis. However, synergistic effects could only be proven with the use of RP- or APP-based FRs. The use of biomelcules, such as sodium phytate and chitosan show some improvement of the LOI without classification but lead to drastic loss in mechanical performance. This is because of the high amount needed for flame retardancy (> 30 %). Therefore, their use in combination with the resins examined is not advisable.

Based on these individual approaches, a combination of the strategies discussed in the chapters 3, 4 and 5 is a meaningful way to produce even more environmentally friendly flame-retardant composites covering various aspects. As proof of concept, partially RP-modified GFRPs with L-Arg-cured DGEBA were successfully manufactured.

Outlooking, the concepts presented in this dissertation can be regarded as tools in a toolbox to develop customised sustainable thermoset systems and solutions depending on specific applications. Going further, the toolbox can be extended by all known tools to further individualise systems.

In this context, it has already been demonstrated, that functionalisation with carbon nanotubes (CNTs) also works with amino acid-cured epoxies such as with commercially available resins. This enables sensing of damage, for example as published in [322]. In addition, it was shown that curing of the bio-based resin component ELO (Section 4.3) with amino acids could not be carried out within a suitable temperature range due to the lower reactivity of the non-terminal oxirane groups. Nevertheless, incorporation of epoxidised vegetable oils as an additional component in amino acid-cured epoxies can also increase the bio-based content and is known to act as a toughening agent in thermosets. This ability to adjust polymer properties could be used in the future as an additional tool for tailoring the examined thermoset systems.

As curing with amino acids is energy-intensive and requires high process temperatures, it is also desirable to find and use effective catalysts in order to improve the energy balance of curing. Since the deprotonation of $-NH_3^+$ was postulated

as the first essential step, accelerating this deprotonation is a reasonable approach. Non-nucleophilic bases such as 1,8-diazabicycloundec-7-ene (DBU) or N,N-diisopropylethylamine (DIPEA, Hünig base) could be used, as these bases do not react favourably with epoxy rings at the same time. However, although this may save energy and time, handling the chemicals mentioned also poses risks to humans and the environment, and the sustainability of their use must be evaluated from various perspectives. Since this work has shown that amino acid-cured epoxies can be considered promising for the development of prepreg resins, the use of catalysts requires further consideration of their influence on latency and the associated energy-saving storage of respective prepregs.

It is also conceivable that a suitable selection of dispersing agents could facilitate the production of the resin/biomolecule dispersions and thus improve the manufacturing quality. In order to also be able to use infusion processes for the production of respective FRPs, the development of dissolved biomolecule curing agents appears necessary in the future. Following the demonstration that amino acid-cured epoxies enable competitive property profiles, the toolbox presented in this dissertation can also be used in the future to achieve recyclability, which benefits environmental friendliness and sustainability. A suitable approach would be to use a vitrimeric epoxy component. There is also great potential in the research of effective, bio-based flame retardants, which could meaningfully expand the toolbox.

Bibliography

[1] G. W. Ehrenstein. *Faserverbund-Kunststoffe: Werkstoffe - Verarbeitung - Eigenschaften*. 2. Auflage. München and Wien: Hanser, 2006. ISBN: 978-3-446-22716-3.

[2] A. Puck. *Festigkeitsanalyse von Faser-Matrix-Laminaten: Modelle für die Praxis*. München and Wien: Hanser, 1996. ISBN: 3-446-18194-6.

[3] B. Fiedler. *Hochleistungs-Faserverbundwerkstoffe mit Duroplastmatrix: Werkstoffe, Struktur, Eigenschaften, Modellierung. Technische Universität Hamburg-Harburg, Arbeitsbereich Abwasserwirtschaft, Diss., 1999*. Vol. 7. Technisch wissenschaftliche Schriftenreihe / TUHH Polymer Composites. Hamburg: TuTech Innovation GmbH, 2009. ISBN: 978-3-93040-026-3.

[4] K. K. Chawla. *Composite Materials: Science and Engineering*. 4th ed. 2019. Springer eBook Collection. Cham: Springer International Publishing and Imprint Springer, 2019. ISBN: 978-3-030-28982-9. DOI: 10.1007/978-3-030-28983-6.

[5] J. J. Carruthers, M. Calomfirescu, P. Ghys, and J. Prockat. *The application of a systematic approach to material selection for the lightweighting of metro vehicles*. Vol. 223. Springer Fachmedien Wiesbaden, 2009. DOI: 10.1243/09544097JRRT279.

[6] J. Ihme. *Schienenfahrzeugtechnik*. 3. Auflage. Lehrbuch. Wiesbaden: Springer Fachmedien Wiesbaden, 2024. ISBN: 978-3-658-42977-5. DOI: 10.1007/978-3-658-42977-5.

[7] T.-C. D. GmbH. *GRP-based design solutions for commercial and railway vehicles*. 2025 [Accessed on January 28, 2026]. URL: https://www.tc-domine.de/en/solutions/traffic-and-transport.

[8] P. G. Ltd. *Growing use of composite materials in the rail industry*. 2025 [Accessed on January 28, 2026]. URL: https://www.permali.co.uk/rail-composites/.

[9] M. Wang, G.-Z. Yin, Y. Yang, W. Fu, J. L. Díaz Palencia, J. Zhao, N. Wang, Y. Jiang, and D.-Y. Wang. "Bio-based flame retardants to polymers: A review". In: *Advanced Industrial and Engineering Polymer Research* 6.2 (2023), pp. 132–155. ISSN: 2542-5048. DOI: 10.1016/j.aiepr.2022.07.003.

[10] T. Mariappan and C. A. Wilkie. "Flame retardant epoxy resin for electrical and electronic applications". In: *Fire and Materials* 38.5 (2014), pp. 588–598. ISSN: 0308-0501. DOI: 10.1002/fam.2199.

[11] M. Tshilidzi. *Integrating Sustainability into Material Selection Is an Ethical and Strategic Obligation*. 2024, [Accessed on January 28, 2026]. URL: https://unu.edu/article/integrating-sustainability-material-selection-ethical-and-strategic-obligation.

[12] M. Shekarchi, E. M. Farahani, M. Yekrangnia, and T. Ozbakkaloglu. "Mechanical strength of CFRP and GFRP composites filled with APP fire retardant powder exposed to elevated temperature". In: *Fire Safety Journal* 115 (2020), p. 103178. ISSN: 0379-7112. DOI: 10.1016/j.firesaf.2020.103178.

[13] M. Bar, R. Alagirusamy, and A. Das. "Flame retardant polymer composites". In: *Fibers and Polymers* 16.4 (2015), pp. 705–717. ISSN: 1229-9197. DOI: 10.1007/s12221-015-0705-6.

[14] M. Walter, A. Jarchow, and B. Fiedler. "Heterogeneously Distributed Flame Retardants in Fibre-Reinforced Epoxies: Novel Manufacturing Process and Tailored Flame Tests". In: *Proceedings of the 21st European Conference on Composite Materials: Nantes Université*. Ed. by Christophe Binetruy and F. Jacquemin. Vol. 3. 2024, pp. 93–100.

[15] M. Walter, A. Jarchow, and B. Fiedler. "Flame-retardant composites and analysis of their residual strengths after tailored flame tests". In: *Composites Part A: Applied Science and Manufacturing* 200 (2026), p. 109339. ISSN: 1359-835X. DOI: 10.1016/j.compositesa.2025.109339.

[16] M. Walter, M. Neubacher, and B. Fiedler. "Using thermokinetic methods to enhance properties of epoxy resins with amino acids as biobased curing agents by achieving full crosslinking". In: *Scientific reports* 14.1 (2024), p. 4367. DOI: 10.1038/s41598-024-54484-0.

[17] M. Walter, D. Gibhardt, and B. Fiedler. “Effects of Stoichiometric Variations in L-Arginine-Cured Epoxy Resins”. In: *Polymers* 17.22 (2025), p. 3089. DOI: 10.3390/polym17223089.

[18] M. Walter, D. Gibhardt, and B. Fiedler. “Environmental and chemical ageing of epoxy resins cured with bio-based amino acids”. In: *IOP Conference Series: Materials Science and Engineering* 1338.1 (2025), p. 012014. ISSN: 1757-8981. DOI: 10.1088/1757-899X/1338/1/012014.

[19] Deutsches Institut für Normung. *DIN EN ISO 3001:1999-11: Kunststoffe - Epoxid-Verbindungen - Bestimmungen des Epoxid-Äquivalents*. Berlin. DOI: 10.31030/8034848.

[20] H. Meeuw, V. K. Wisniewski, U. Köpke, A. S. Nia, A. R. Vázquez, M. R. Lohe, X. Feng, and B. Fiedler. “In-line monitoring of carbon nanoparticle epoxy dispersion processes”. In: *Production Engineering* 13.3-4 (2019), pp. 373–390. DOI: 10.1007/s11740-019-00884-5.

[21] Deutsches Institut für Normung. *DIN EN ISO 3219:1994-10: Kunststoffe - Polymere/Harze in flüssigem, emulgiertem oder dispergiertem Zustand - Bestimmung der Viskosität mit einem Rotationsviskosimeter bei definiertem Geschwindigkeitsgefälle*. Berlin. DOI: 10.31030/2725724.

[22] Deutsches Institut für Normung. *DIN EN ISO 11358-1:2014-10: Kunststoffe - Thermogravimetrie (TG) von Polymeren - Teil 1: Allgemeine Grundsätze*.

[23] Deutsches Institut für Normung. *DIN EN ISO 11357-2:2014-07: Kunststoffe - Dynamische Differenz-Thermoanalyse (DSC) - Teil 2: Bestimmung der Glasübergangstemperatur und der Glasübergangsstufenhöhe*.

[24] Deutsches Institut für Normung. *DIN EN ISO 6721-1:2019-09: Kunststoffe - Bestimmung dynamisch-mechanischer Eigenschaften - Teil 1: Allgemeine Grundlagen*.

[25] J. Zheng, Z. M. Png, S. H. Ng, G. X. Tham, E. Ye, S. S. Goh, X. J. Loh, and Z. Li. “Vitrimers: Current research trends and their emerging applications”. In: *Materials Today* 51 (2021), pp. 586–625. ISSN: 1369-7021. DOI: 10.1016/j.mattod.2021.07.003.

[26] Deutsches Institut für Normung. *DIN EN ISO 527-2:2012-06, Kunststoffe - Bestimmung der Zugeigenschaften- Teil 2: Prüfbedingungen für Form- und Extrusionsmassen*. Berlin. DOI: 10.31030/1860304.

[27] Deutsches Institut für Normung. *DIN EN ISO 527-4:1997-07: Kunststoffe - Bestimmung der Zugeigenschaften - Teil 4: Prüfbedingungen für isotrop und anisotrop faserverstärkte Kunststoffverbundwerkstoffe*.

[28] Deutsches Institut für Normung. *DIN EN ISO 527-5:2010-01: Kunststoffe - Bestimmung der Zugeigenschaften - Teil 5: Prüfbedingungen für unidirektional faserverstärkte Kunststoffverbundwerkstoffe*. Berlin. DOI: 10.31030/1560314.

[29] Deutsches Institut für Normung. *DIN EN ISO 14125:2011-05: Faserverstärkte Kunststoffe - Bestimmung der Biegeeigenschaften*.

[30] Deutsches Institut für Normung. *DIN EN ISO 14126:2000-12: Faserverstärkte Kunststoffe - Bestimmung der Druckeigenschaften in der Laminatebene*. Berlin. DOI: 10.31030/9495241.

[31] American Society for Testing and Materials. *ASTM D5045-99: Standard Test Methods for Plane-Strain Fracture Toughness and Strain Energy Release Rate of Plastic Materials*.

[32] Deutsches Institut für Normung. *DIN EN ISO 4589:2017-08: Kunststoffe - Bestimmung des Brennverhaltens durch den Sauerstoff-Index*. Berlin. DOI: 10.31030/2607872.

[33] Underwriters Laboratories. *UL 94 - Standard for Safety: Tests for Flammability of Plastic Materials for Parts in Devices and Appliances*. Northbrook, IL, USA.

[34] S. Vyazovkin and C. A. Wight. "Isothermal and non-isothermal kinetics of thermally stimulated reactions of solids". In: *International Reviews in Physical Chemistry* 17.3 (1998), pp. 407–433. DOI: 10.1080/014423598230108.

[35] K. J. Laidler. "A glossary of terms used in chemical kinetics, including reaction dynamics (IUPAC Recommendations 1996)". In: *Pure and Applied Chemistry* 68.1 (1996), pp. 149–192. DOI: 10.1351/pac199668010149.

[36] M. J. Starink. "On the applicability of isoconversion methods for obtaining the activation energy of reactions within a temperature-dependent equilibrium state". In: *Journal of Materials Science* 32.24 (1997), pp. 6505–6512. DOI: 10.1023/A:1018655026036.

[37] A. Pratap, T. Lilly Shanker Rao, K. N. Lad, and H. D. Dhurandhar. "Isoconversional vs. Model fitting methods". In: *Journal of Thermal Analysis and Calorimetry* 89.2 (2007), pp. 399–405. DOI: 10.1007/s10973-006-8160-7.

[38] H. L. Friedman. "Kinetics of thermal degradation of char-forming plastics from thermogravimetry. Application to a phenolic plastic". In: *Journal of Polymer Science Part C: Polymer Symposia* 6.1 (1964), pp. 183–195. ISSN: 0449-2994. DOI: 10.1002/polc.5070060121.

[39] T. Akahira and T. Sunose. "Method of determining activation deterioration constant of electrical insulating materials". In: *Res Rep Chiba Inst Technol* 16 (1971), pp. 22–31.

[40] C. D. Doyle. "Estimating isothermal life from thermogravimetric data". In: *Journal of Applied Polymer Science* 6.24 (1962), pp. 639–642. DOI: 10.1002/app.1962.070062406.

[41] J. H. Flynn and L. A. Wall. "A quick, direct method for the determination of activation energy from thermogravimetric data". In: *Journal of Polymer Science Part B: Polymer Letters* 4.5 (1966), pp. 323–328. ISSN: 0449-2986. DOI: 10.1002/pol.1966.110040504.

[42] L. Granado, S. Kempa, S. Bremmert, L. J. Gregoriades, F. Brüning, E. Anglaret, and N. Fréty. "Isothermal DSC Study of the Curing Kinetics of an Epoxy/Silica Composite for Microelectronics". In: *Journal of Microelectronics and Electronic Packaging* 14.2 (2017), pp. 45–50. DOI: 10.4071/imaps.359903.

[43] J. Opfermann and E. Kaisersberger. "An advantageous variant of the Ozawa-Flynn-Wall analysis". In: *Thermochimica Acta* 203 (1992), pp. 167–175. DOI: 10.1016/0040-6031(92)85193-Y.

[44] R. Font and M. A. Garrido. "Friedman and n-reaction order methods applied to pine needles and polyurethane thermal decompositions". In: *Thermochimica Acta* 660 (2018), pp. 124–133. ISSN: 0040-6031. DOI: 10.1016/j.tca.2018.01.002.

[45] J. J. P. Barros, I. D. d. S. Silva, N. G. Jaques, and R. M. R. Wellen. "Approaches on the non-isothermal curing kinetics of epoxy/PCL blends". In: *Journal of Materials Research and Technology* 9.6 (2020), pp. 13539–13554. DOI: 10.1016/j.jmrt.2020.09.081.

[46] M. A. Bashir. “Cure Kinetics of Commercial Epoxy-Amine Products with Iso-Conversional Methods”. In: *Coatings* 13.3 (2023), p. 592. DOI: 10.3390/coatings13030592.

[47] P. Ravi. “Model free isoconversional procedure for evaluating the effective activation energy values of thermally stimulated processes in dinitroimidazoles”. In: *The Journal of chemical physics* 140.20 (2014), p. 204201. DOI: 10.1063/1.4878410.

[48] M. R. Kamal and S. Sourour. “Kinetics and thermal characterization of thermoset cure”. In: *Polymer Engineering and Science* 13.1 (1973), pp. 59–64. ISSN: 0032-3888. DOI: 10.1002/pen.760130110.

[49] H. Qiao, M. Chen, B. Chen, H. Zhang, and B. Zheng. “Understanding the curing kinetics of boron-based hyperbranched polysiloxane reinforced and toughened epoxy resin by rheology”. In: *Chemical Engineering Journal* 467 (2023), p. 143542. DOI: 10.1016/j.cej.2023.143542.

[50] H. E. Kissinger. “Variation of Peak Temperature With Heating Rate in Differential Thermal Analysis”. In: *Journal of Research of the National Bureau of Standards* 57.4 (1956). DOI: 10.6028/jres.057.026.

[51] H. E. Kissinger. “Reaction Kinetics in Differential Thermal Analysis”. In: *Analytical Chemistry* 29.11 (1957), pp. 1702–1706. ISSN: 0003-2700. DOI: 10.1021/ac60131a045.

[52] R. L. Blaine and H. E. Kissinger. “Homer Kissinger and the Kissinger equation”. In: *Thermochimica Acta* 540 (2012), pp. 1–6. DOI: 10.1016/j.tca.2012.04.008.

[53] T. Ozawa. “A New Method of Analyzing Thermogravimetric Data”. In: *Bulletin of the Chemical Society of Japan* 38.11 (1965), pp. 1881–1886. DOI: 10.1246/bcsj.38.1881.

[54] N. Koga. “Ozawa’s kinetic method for analyzing thermoanalytical curves”. In: *Journal of Thermal Analysis and Calorimetry* 113.3 (2013), pp. 1527–1541. DOI: 10.1007/s10973-012-2882-5.

[55] M. R. Keenan. “Autocatalytic cure kinetics from DSC measurements: Zero initial cure rate”. In: *Journal of Applied Polymer Science* 33.5 (1987), pp. 1725–1734. ISSN: 0021-8995. DOI: 10.1002/app.1987.070330525.

[56] S. Montserrat and J. Málek. “A kinetic analysis of the curing reaction of an epoxy resin”. In: *Thermochimica Acta* 228 (1993), pp. 47–60. ISSN: 0040-6031. DOI: 10.1016/0040-6031(93)80273-D.

[57] T. Vidil, F. Tournilhac, S. Musso, A. Robisson, and L. Leibler. "Control of reactions and network structures of epoxy thermosets". In: *Progress in Polymer Science* 62 (2016), pp. 126–179. ISSN: 0079-6700. DOI: 10.1016/j.progpolymsci.2016.06.003.

[58] J. Chen, I. M. Hutchings, T. Deng, M. S. Bradley, and K. K. Koziol. "The effect of carbon nanotube orientation on erosive wear resistance of CNT-epoxy based composites". In: *Carbon* 73 (2014), pp. 421–431. ISSN: 0008-6223. DOI: 10.1016/j.carbon.2014.02.083.

[59] A. Redmann, P. Oehlmann, T. Scheffler, L. Kagermeier, and T. A. Osswald. "Thermal curing kinetics optimization of epoxy resin in Digital Light Synthesis". In: *Additive Manufacturing* 32 (2020), p. 101018. DOI: 10.1016/j.addma.2019.101018.

[60] M. R. Petersen, Chen, M. Roll, S. J. Jung, and M. Yossef. "Mechanical properties of fire-retardant glass fiber-reinforced polymer materials with alumina tri-hydrate filler". In: *Composites Part B: Engineering* 78 (2015), pp. 109–121. ISSN: 1359-8368. DOI: 10.1016/j.compositesb.2015.03.071.

[61] J. Z. Liang, J. Q. Feng, C. P. Tsui, C. Y. Tang, D. F. Liu, S. D. Zhang, and W. F. Huang. "Mechanical properties and flame-retardant of PP/MRP/$Mg(OH)_2$/$Al(OH)_3$ composites". In: *Composites Part B: Engineering* 71 (2015), pp. 74–81. ISSN: 1359-8368. DOI: 10.1016/j.compositesb.2014.10.054.

[62] F. Ameen, M. Atif, K. Mahmood, and U. F. Yousuf. "Qualitative and quantitative impact of filler on thermomechanical properties of epoxy composites". In: *Polymers for Advanced Technologies* 32.8 (2021), pp. 2813–2828. ISSN: 1042-7147. DOI: 10.1002/pat.5304.

[63] M. Choudhary, T. Singh, M. Dwivedi, and A. Patnaik. "Waste marble dust–filled glass fiber–reinforced polymer composite Part I: Physical, thermomechanical, and erosive wear properties". In: *Polymer Composites* 40.10 (2019), pp. 4113–4124. ISSN: 0272-8397. DOI: 10.1002/pc.25272.

[64] H. Sharma *et al.* "Critical review on advancements on the fiber-reinforced composites: Role of fiber/matrix modification on the performance of the fibrous composites". In: *Journal of Materials Research and Technology* 26 (2023), pp. 2975–3002. ISSN: 2238-7854. DOI: 10.1016/j.jmrt.2023.08.036.

[65] S. Trubachev *et al.* “Flame-Retardant Glass Fiber-Reinforced Epoxy Resins with Phosphorus-Containing Bio-Based Benzoxazines and Graphene”. In: *Polymers* 16.16 (2024). DOI: 10.3390/polym16162333.

[66] J.-X. Yang, Y. Sun, W.-M. Song, and Y. Liu. “A novel phosphorus/boron-containing flame retardant for improving the flame retardancy of ramie fiber reinforced epoxy composites”. In: *Construction and Building Materials* 451 (2024), p. 138814. ISSN: 0950-0618. DOI: 10.1016/j.conbuildmat.2024.138814.

[67] Z. Mi, F. Chu, W. Hu, Y. Hu, and L. Song. “Eco-friendly preparation of advanced epoxy composites and their pyrolysis and flame retardant mechanisms”. In: *Polymer Degradation and Stability* 224 (2024), p. 110749. ISSN: 0141-3910. DOI: 10.1016/j.polymdegradstab.2024.110749.

[68] M. S. Murad, A. K. Hamzat, E. Asmatulu, and R. Asmatulu. “Flame-retardant fiber composites: synergistic effects of additives on mechanical, thermal, chemical, and structural properties”. In: *Advanced Composites and Hybrid Materials* 8.1 (2025). ISSN: 2522-0128. DOI: 10.1007/s42114-024-01111-1.

[69] Z. Zhao, J. Qu, Y. Geng, R. Li, J. Qiu, M. Liu, X. Chen, S. Li, and C. Jiao. “Facile preparation of microcapsuled P-N@MXene flame retardant using layer-by-layer assembly strategy towards enhanced fire safety of epoxy resin”. In: *Polymer Degradation and Stability* 234 (2025), p. 111219. ISSN: 0141-3910. DOI: 10.1016/j.polymdegradstab.2025.111219.

[70] C. Liu, J. Tao, T. Wu, H.-B. Zhao, C. Yu, and W. Rao. “Construction of hierarchical SiO_2 microcapsule towards flame retardation, low toxicity and mechanical enhancement of epoxy resins”. In: *Chemosphere* 342 (2023), p. 140184. DOI: 10.1016/j.chemosphere.2023.140184.

[71] M. Zhao, N. Guo, K. Wang, Q. Qu, Q. Zhang, C. Wang, and H. Xin. “Facial functionalization carbon fiber with MnO_2 nanosheets for high–performance epoxy composites with excellent flame retardancy and mechanical properties”. In: *Polymer Composites* 46.8 (2025), pp. 7569–7580. ISSN: 0272-8397. DOI: 10.1002/pc.29450.

[72] N. D. Muralidharan, J. Subramanian, S. K. Rajamanickam, P. Krishnasamy, S. M. K. Thiagamani, and A. Khan. “Flame retardant characteristics of natural fibre reinforced polymer composites: A thematic review”.

In: *Polymer Composites* 45.14 (2024), pp. 12530–12558. ISSN: 0272-8397. DOI: 10.1002/pc.28699.

[73] M. Yu, Y. Chu, W. Xie, L. Fang, X. Liu, O. Zhang, M. Ren, and J. Sun. "An interlayer flame retardant method to effectively fire retardant and reinforce CF/EP composites by nanofiber film intercalation". In: *Chemical Engineering Journal* 467 (2023), p. 143545. ISSN: 1385-8947. DOI: 10.1016/j.cej.2023.143545.

[74] X.-H. Shi, X.-L. Li, Y.-M. Li, Z. Li, and D.-Y. Wang. "Flame-retardant strategy and mechanism of fiber reinforced polymeric composite: A review". In: *Composites Part B: Engineering* 233 (2022), p. 109663. ISSN: 1359-8368. DOI: 10.1016/j.compositesb.2022.109663.

[75] Á. Pomázi and A. Toldy. "Multifunctional Gelcoats for Fiber Reinforced Composites". In: *Coatings* 9.3 (2019), p. 173. DOI: 10.3390/coatings9030173.

[76] Á. Pomázi, M. Krecz, and A. Toldy. "Thermal behaviour and fire and mechanical performance of carbon fibre-reinforced epoxy composites coated with flame-retardant epoxy gelcoats". In: *Journal of Thermal Analysis and Calorimetry* 148.7 (2023), pp. 2685–2702. ISSN: 1388-6150. DOI: 10.1007/s10973-022-11710-z.

[77] L. Zhang, H. Ren, L. Wu, Z. Liu, A. Xie, X. Yao, J. Ju, and M. Liu. "Recent advances in gel coatings: from lab to industry". In: *Journal of Materials Chemistry A* 12.30 (2024), pp. 18901–18920. ISSN: 2050-7488. DOI: 10.1039/D4TA02586E.

[78] P. Joseph and S. Tretsiakova-McNally. "Melt-Flow Behaviours of Thermoplastic Materials under Fire Conditions: Recent Experimental Studies and Some Theoretical Approaches". In: *Materials (Basel, Switzerland)* 8.12 (2015), pp. 8793–8803. ISSN: 1996-1944. DOI: 10.3390/ma8125492.

[79] D. van Krevelen. "Chapter 21 - Thermal Decomposition". In: *Properties of Polymers (Third Edition)*. Ed. by D. van Krevelen. Third Edition. Amsterdam: Elsevier, 1997, pp. 641–653. ISBN: 978-0-444-82877-4. DOI: 10.1016/B978-0-444-82877-4.50028-7.

[80] Clariant Plastics & Coatings GmbH. *Fire initiation and combustion process*. 2024, [Accessed on January 28, 2026]. URL: https://www.flameretardants-online.com/fires/fire-initiation.

[81] B. Schartel, B. Perret, B. Dittrich, M. Ciesielski, J. Krämer, P. Müller, V. Altstädt, L. Zang, and M. Döring. "Flame Retardancy of Polymers: The Role of Specific Reactions in the Condensed Phase". In: *Macromolecular Materials and Engineering* 301.1 (2016), pp. 9–35. ISSN: 1438-7492. DOI: 10.1002/mame.201500250.

[82] M.-X. Xu, J.-Y. Di, Y.-C. Wu, X.-X. Meng, Haiwen-Ji, H. Jiang, J.-H. Li, and Q. Lu. "Insights into the pyrolysis mechanisms of epoxy resin polymers based on the combination of experiments and ReaxFF-MD simulation". In: *Chemical Engineering Journal* 473 (2023), p. 145404. ISSN: 1385-8947. DOI: 10.1016/j.cej.2023.145404.

[83] M. Rakotomalala, S. Wagner, and M. Döring. "Recent Developments in Halogen Free Flame Retardants for Epoxy Resins for Electrical and Electronic Applications". In: *Materials (Basel, Switzerland)* 3.8 (2010), pp. 4300–4327. ISSN: 1996-1944. DOI: 10.3390/ma3084300.

[84] J. Vogt. "Thermal analysis of epoxy-resins: Identification of decomposition products". In: *Thermochimica Acta* 85 (1985), pp. 411–414. ISSN: 0040-6031. DOI: 10.1016/0040-6031(85)85611-2.

[85] J. Troitzsch and E. Antonatus, eds. *Plastics flammability handbook: Principles, regulations, testing, and approval*. 4th edition. Hanser eLibrary. Munich and Cincinnati: Hanser, 2021. ISBN: 978-1-56990-763-4. DOI: 10.3139/9781569907634?locatt=mode:legacy.

[86] M. Zhi, Q. Liu, H. Chen, X. Chen, S. Feng, and Y. He. "Thermal Stability and Flame Retardancy Properties of Epoxy Resin Modified with Functionalized Graphene Oxide Containing Phosphorus and Silicon Elements". In: *ACS omega* 4.6 (2019), pp. 10975–10984. DOI: 10.1021/acsomega.9b00852.

[87] M. Zhi, X. Yang, R. Fan, S. Yue, L. Zheng, Q. Liu, and Y. He. "A comprehensive review of reactive flame-retardant epoxy resin: fundamentals, recent developments, and perspectives". In: *Polymer Degradation and Stability* 201 (2022), p. 109976. ISSN: 0141-3910. DOI: 10.1016/j.polymdegradstab.2022.109976.

[88] M. Ciesielski, B. Burk, C. Heinzmann, and M. Döring. "Fire-retardant high-performance epoxy-based materials". In: *Novel fire retardant polymers and composite materials*. Ed. by D.-Y. Wang. Woodhead Publishing series in composites science and engineering. Duxford, United Kingdom:

Woodhead Publishing is an imprint of Elsevier, 2017, pp. 3–51. ISBN: 978-0-08-100977-2. DOI: 10.1016/B978-0-08-100136-3.00002-9.

[89] A. Aljamal, G. Marosi, and B. Szolnoki. "Investigation of the modes of action for phosphorous flame retardants in a fully waterborne sugar-based epoxy resin". In: *Journal of Thermal Analysis and Calorimetry* 148.2 (2023), pp. 281–292. ISSN: 1388-6150. DOI: 10.1007/s10973-022-11736-3.

[90] J. Sag. "Phosphorhaltige Flammschutzmittel aus biobasierten Plattformchemikalien". Doctoral Thesis. Technische Universität Darmstadt, 2022. DOI: 10.26083/TUPRINTS-00020227.

[91] C. Cheng, Y. Lu, W. Ma, S. Li, J. Yan, and S. Du. "Preparation and characterization of polydopamine/melamine microencapsulated red phosphorus and its flame retardance in epoxy resin". In: *RSC advances* 11.33 (2021), pp. 20391–20402. DOI: 10.1039/D1RA03164C.

[92] Y. Zhao, Y. Li, J. Li, Y. Xiao, W. Mu, Z. Wang, L. Song, and J. Yu. "Flame Retardancy of Epoxy Resins Modified with Few-Layer Black Phosphorus". In: *Polymers* 15.7 (2023). DOI: 10.3390/polym15071655.

[93] H.-Q. Yin, D.-D. Yuan, and X.-F. Cai. "Red phosphorus acts as second acid source to form a novel intumescent-contractive flame-retardant system on ABS". In: *Journal of Thermal Analysis and Calorimetry* 111.1 (2013), pp. 499–506. ISSN: 1388-6150. DOI: 10.1007/s10973-012-2536-7.

[94] R. Zheng, M. Li, Y. Chen, F. Hao, and B. Xu. "Fire behavior and mechanical properties of phosphorus-containing silica gel coated ammonium polyphosphate as fire retardants in thermoplastic polyurethane (TPU)". In: *Journal of Polymer Research* 30.10 (2023). ISSN: 1022-9760. DOI: 10.1007/s10965-023-03778-4.

[95] Y. Liu, Z. Tang, and J. Zhu. "Synergistic flame retardant effect of aluminum hydroxide and ammonium polyphosphate on epoxy resin". In: *Journal of Applied Polymer Science* 139.46 (2022). ISSN: 0021-8995. DOI: 10.1002/app.53168.

[96] X. He, W. Zhang, D. Yi, and R. Yang. "Flame retardancy of ammonium polyphosphate–montmorillonite nanocompounds on epoxy resin". In: *Journal of Fire Sciences* 34.3 (2016), pp. 212–225. ISSN: 0734-9041. DOI: 10.1177/0734904116637213.

[97] J. Yang, Y. Hua, J. Sun, X. Wang, X. Gu, and S. Zhang. "A Boron–Containing Ammonium Polyphosphate for Epoxy Resins with Enhanced Flame Retardancy and Reduced Smoke Release". In: *Advanced Engineering Materials* 25.13 (2023). ISSN: 1438-1656. DOI: 10.1002/adem.202300011.

[98] X. Bi *et al.* "A core–shell-structured APP@COFs hybrid for enhanced flame retardancy and mechanical property of epoxy resin (EP)". In: *Advanced Composites and Hybrid Materials* 5.3 (2022), pp. 1743–1755. ISSN: 2522-0128. DOI: 10.1007/s42114-021-00411-0.

[99] K.-T. Hsiao and D. Heider. "Vacuum assisted resin transfer molding (VARTM) in polymer matrix composites". In: *Manufacturing Techniques for Polymer Matrix Composites (PMCs)*. Ed. by S. G. Advani and K.-T. Hsiao. Woodhead Publishing Series in Composites Science and Engineering. Woodhead Publishing, 2012, pp. 310–347. ISBN: 978-0-85709-067-6. DOI: 10.1533/9780857096258.3.310.

[100] M. Bodaghi, R. Costa, R. Gomes, J. Silva, N. Correia, and F. Silva. "Experimental comparative study of the variants of high-temperature vacuum-assisted resin transfer moulding". In: *Composites Part A: Applied Science and Manufacturing* 129 (2020), p. 105708. ISSN: 1359-835X. DOI: 10.1016/j.compositesa.2019.105708.

[101] W. Xiao, P. He, G. Hu, and B. He. "Study on the Flame-retardance and Thermal Stability of the Acid Anhydride-cured Epoxy Resin Flame-retarded by Triphenyl Phosphate and Hydrated Alumina". In: *Journal of Fire Sciences* 19.5 (2001), pp. 369–377. ISSN: 0734-9041. DOI: 10.1106/R4HN-GT2G-EWAR-733C.

[102] S. V. Levchik and E. D. Weil. "Thermal decomposition, combustion and flame–retardancy of epoxy resins—a review of the recent literature". In: *Polymer International* 53.12 (2004), pp. 1901–1929. ISSN: 0959-8103. DOI: 10.1002/pi.1473.

[103] B. S. Hayes and J. C. Seferis. "Modification of thermosetting resins and composites through preformed polymer particles: A review". In: *Polymer Composites* 22.4 (2001), pp. 451–467. ISSN: 0272-8397. DOI: 10.1002/pc.10551.

[104] A. J. Kinloch, K. Masania, A. C. Taylor, S. Sprenger, and D. Egan. "The fracture of glass-fibre-reinforced epoxy composites using nanoparticle-modified matrices". In: *Journal of Materials Science* 43.3 (2008), pp. 1151–1154. ISSN: 0022-2461. DOI: 10.1007/s10853-007-2390-3.

[105] D. Lefevre, S. Comas-Cardona, C. Binétruy, and P. Krawczak. "Modelling the flow of particle-filled resin through a fibrous preform in liquid composite molding technologies". In: *Composites Part A: Applied Science and Manufacturing* 38.10 (2007), pp. 2154–2163. ISSN: 1359-835X. DOI: 10.1016/j.compositesa.2007.06.008.

[106] G. Giannakopoulos, K. Masania, and A. C. Taylor. "Toughening of epoxy using core–shell particles". In: *Journal of Materials Science* 46.2 (2011), pp. 327–338. ISSN: 0022-2461. DOI: 10.1007/s10853-010-4816-6.

[107] E. F. Da Reia Costa, A. A. Skordos, I. K. Partridge, and A. Rezai. "RTM processing and electrical performance of carbon nanotube modified epoxy/fibre composites". In: *Composites Part A: Applied Science and Manufacturing* 43.4 (2012), pp. 593–602. ISSN: 1359-835X. DOI: 10.1016/j.compositesa.2011.12.019.

[108] B. M. Louis, J. Maldonado, F. Klunker, and P. Ermanni. "Particle distribution from in–plane resin flow in a resin transfer molding process". In: *Polymer Engineering & Science* 59.1 (2019), pp. 22–34. ISSN: 0032-3888. DOI: 10.1002/pen.24860.

[109] D. Lefevre, S. Comas-Cardona, C. Binetruy, and P. Krawczak. "Coupling filtration and flow during liquid composite molding: Experimental investigation and simulation". In: *Composites Science and Technology* 69.13 (2009), pp. 2127–2134. ISSN: 0266-3538. DOI: 10.1016/j.compscitech.2009.05.008.

[110] Z. Fan and S. G. Advani. "Capillary effect of multi-walled carbon nanotubes suspension in composite processing". In: *Journal of nanoscience and nanotechnology* 8.4 (2008), pp. 1669–1678. ISSN: 1533-4880.

[111] American Society for Testing and Materials. *ASTM D2863: Test Method for Measuring the Minimum Oxygen Concentration to Support Candle-Like Combustion of Plastics (Oxygen Index)*. West Conshohocken, PA. DOI: 10.1520/D2863-23E01.

[112] International Organization for Standardization. *ISO 5660-1: Reaction to fire tests - Heat release, smoke production and mass loss rate: Part 1: Heat release rate (cone calorimeter method)*.

[113] Federal Aviation Administration, U.S. Department of Transportation. *Aircraft materials fire test handbook*. 2019.

[114] Deutsches Institut für Normung. *DIN EN 60695-11-10: Prüfungen zur Beurteilung der Brandgefahr: Prüfflammen - Prüfverfahren mit einer 50-W-Prüfflamme horizontal und vertikal (mit Berichtigung 2015-10)*. 2014.

[115] D. Budelmann, C. Schmidt, and D. Meiners. "Prepreg tack: A review of mechanisms, measurement, and manufacturing implication". In: *Polymer Composites* 41.9 (2020), pp. 3440–3458. ISSN: 0272-8397. DOI: 10.1002/pc.25642.

[116] O. d. A. Raponi, R. d. A. Raponi, G. B. Barban, R. M. Di Benedetto, and A. C. Ancelotti Junior. "Development of a Simple Dielectric Analysis Module for Online Cure Monitoring of a Commercial Epoxy Resin Formulation". In: *Materials Research* 20.suppl 2 (2017), pp. 291–297. ISSN: 1516-1439. DOI: 10.1590/1980-5373-MR-2017-0067.

[117] W. Xu, Y. Gu, M. Li, X. Ma, D. Zhang, and Z. Zhang. "Co-curing process combining resin film infusion with prepreg and co-cured interlaminar properties of carbon fiber composites". In: *Journal of Composite Materials* 48.14 (2014), pp. 1709–1724. ISSN: 0021-9983. DOI: 10.1177/0021998313490536.

[118] C. Di Fratta, D. Mario, V. Gabathuler, M. Zogg, and P. Ermanni. "Approach to Optimizing a Combined Out-of-Autoclave (OOA) Prepreg/Liquid Composite Molding (LCM) Process for Integrated Structures". In: *Sampe Journal* 48 (2012), pp. 40–46.

[119] R. Kaps and M. Wiedemann. "Combined Prepreg and Resin Infusion Technologies". In: *Adaptive, tolerant and efficient composite structures*. Ed. by M. Wiedemann. Research Topics in Aerospace. Berlin and Heidelberg: Springer, 2013, pp. 349–361. ISBN: 978-3-642-29189-0. DOI: 10.1007/978-3-642-29190-6_28.

[120] J. Körbelin. "Damage tolerance of high-performance composites". Doctoral Thesis. Hamburg: Hamburg University of Technology, 2022. DOI: 10.15480/882.4276.

[121] J. J. Andrew and H. N. Dhakal. "Sustainable biobased composites for advanced applications: recent trends and future opportunities – A critical review". In: *Composites Part C: Open Access* 7 (2022), p. 100220. ISSN: 2666-6820. DOI: 10.1016/j.jcomc.2021.100220.

[122] H. Q. Pham and M. J. Marks. "Epoxy Resins". In: *Ullmann's Encyclopedia of Industrial Chemistry* (2005). ISSN: 1435-6007. DOI: 10.1002/14356007.a09_547.pub2.

[123] S. Kumar, S. K. Samal, S. Mohanty, and S. K. Nayak. "Recent Development of Biobased Epoxy Resins: A Review". In: *Polymer-Plastics Technology and Engineering* 57.3 (2018), pp. 133–155. ISSN: 0360-2559. DOI: 10.1080/03602559.2016.1253742.

[124] M. Galià, L. M. de Espinosa, J. C. Ronda, G. Lligadas, and V. Cádiz. "Vegetable oil–based thermosetting polymers". In: *European Journal of Lipid Science and Technology* 112.1 (2010), pp. 87–96. ISSN: 1438-7697. DOI: 10.1002/ejlt.200900096.

[125] Y. Xia and R. C. Larock. "Vegetable oil-based polymeric materials: synthesis, properties, and applications". In: *Green Chemistry* 12.11 (2010), p. 1893. ISSN: 1463-9262. DOI: 10.1039/C0GC00264J.

[126] M. Alam, D. Akram, E. Sharmin, F. Zafar, and S. Ahmad. "Vegetable oil based eco-friendly coating materials: A review article". In: *Arabian Journal of Chemistry* 7.4 (2014), pp. 469–479. ISSN: 1878-5352. DOI: 10.1016/j.arabjc.2013.12.023.

[127] S. Miao, P. Wang, Z. Su, and S. Zhang. "Vegetable-oil-based polymers as future polymeric biomaterials". In: *Acta biomaterialia* 10.4 (2014), pp. 1692–1704. DOI: 10.1016/j.actbio.2013.08.040.

[128] F. G. Calvo-Flores and J. A. Dobado. "Lignin as renewable raw material". In: *ChemSusChem* 3.11 (2010), pp. 1227–1235. DOI: 10.1002/cssc.201000157.

[129] N.-E. El Mansouri, Q. Yuan, and F. Huang. "Synthesis and characterization of kraft lignin-based epoxy resins." In: *BioResources* 6.3 (2011).

[130] C. Asada, S. Basnet, M. Otsuka, C. Sasaki, and Y. Nakamura. "Epoxy resin synthesis using low molecular weight lignin separated from various lignocellulosic materials". In: *International journal of biological macromolecules* 74 (2015), pp. 413–419. DOI: 10.1016/j.ijbiomac.2014.12.039.

[131] H.-Z. Chen, Z.-Y. Li, X.-Y. Liu, Y.-M. Tian, L. Yang, and Z.-C. Wang. "Depolymerization of renewable resources – lignin by sodium hydroxide as a catalyst and its applications to epoxy resin". In: *Journal of Applied Polymer Science* 132.26 (2015). ISSN: 0021-8995. DOI: 10.1002/app.42176.

[132] F. Ferdosian, Z. Yuan, M. Anderson, and C. Xu. "Synthesis of lignin-based epoxy resins: optimization of reaction parameters using response surface methodology". In: *RSC advances* 4.60 (2014), pp. 31745–31753. DOI: 10.1039/C4RA03978E.

[133] E. Savonnet, E. Grau, S. Grelier, B. Defoort, and H. Cramail. "Divanillin-Based Epoxy Precursors as DGEBA Substitutes for Biobased Epoxy Thermosets". In: *ACS Sustainable Chemistry & Engineering* 6.8 (2018), pp. 11008–11017. ISSN: 2168-0485. DOI: 10.1021/acssuschemeng.8b02419.

[134] H. Jiang, L. Sun, Y. Zhang, Q. Liu, C. Ru, W. Zhang, and C. Zhao. "Novel biobased epoxy resin thermosets derived from eugenol and vanillin". In: *Polymer Degradation and Stability* 160 (2019), pp. 45–52. ISSN: 0141-3910. DOI: 10.1016/j.polymdegradstab.2018.12.007.

[135] C. Li, X. Liu, J. Zhu, C. Zhang, and J. Guo. "Synthesis, Characterization of a Rosin-based Epoxy Monomer and its Comparison with a Petroleum-based Counterpart". In: *Journal of Macromolecular Science, Part A* 50.3 (2013), pp. 321–329. ISSN: 1060-1325. DOI: 10.1080/10601325.2013.755879.

[136] A. M. Atta, R. Mansour, M. I. Abdou, and A. M. Sayed. "Epoxy resins from rosin acids: synthesis and characterization". In: *Polymers for Advanced Technologies* 15.9 (2004), pp. 514–522. ISSN: 1042-7147. DOI: 10.1002/pat.507.

[137] K. Huang, J. Zhang, M. Li, J. Xia, and Y. Zhou. "Exploration of the complementary properties of biobased epoxies derived from rosin diacid and dimer fatty acid for balanced performance". In: *Industrial Crops and Products* 49 (2013), pp. 497–506. ISSN: 0926-6690. DOI: 10.1016/j.indcrop.2013.05.024.

[138] H. Zhang, W. Li, J. Xu, S. Shang, and Z. Song. "Synthesis and characterization of bio-based epoxy thermosets using rosin-based epoxy monomer". In: *Iranian Polymer Journal* 30.7 (2021), pp. 643–654. ISSN: 1026-1265. DOI: 10.1007/s13726-021-00918-9.

[139] R. Liu, J. Zhu, J. Luo, and X. Liu. "Synthesis and application of novel UV-curable hyperbranched methacrylates from renewable natural tannic acid". In: *Progress in Organic Coatings* 77.1 (2014), pp. 30–37. ISSN: 0300-9440. DOI: 10.1016/j.porgcoat.2013.07.015.

[140] P. Niedermann, G. Szebenyi, and A. Toldy. "Novel high glass temperature sugar-based epoxy resins: Characterization and comparison to mineral oil-based aliphatic and aromatic resins". In: *Express Polymer Letters* 9.2 (2015), pp. 85–94. ISSN: 1788-618X. DOI: 10.3144/expresspolymlett.2015.10.

[141] M. Shibata, S. Yoshihara, M. Yashiro, and Y. Ohno. "Thermal and mechanical properties of sorbitol–based epoxy resin cured with quercetin and the biocomposites with wood flour". In: *Journal of Applied Polymer Science* 128.5 (2013), pp. 2753–2758. ISSN: 0021-8995. DOI: 10.1002/app.38438.

[142] F. Jaillet, E. Darroman, A. Ratsimihety, R. Auvergne, B. Boutevin, and S. Caillol. "New biobased epoxy materials from cardanol". In: *European Journal of Lipid Science and Technology* 116.1 (2014), pp. 63–73. ISSN: 1438-7697. DOI: 10.1002/ejlt.201300193.

[143] S. Kanehashi, K. Yokoyama, R. Masuda, T. Kidesaki, K. Nagai, and T. Miyakoshi. "Preparation and characterization of cardanol–based epoxy resin for coating at room temperature curing". In: *Journal of Applied Polymer Science* 130.4 (2013), pp. 2468–2478. ISSN: 0021-8995. DOI: 10.1002/app.39382.

[144] A.-S. Mora, M. Decostanzi, G. David, and S. Caillol. "Cardanol–Based Epoxy Monomers for High Thermal Properties Thermosets". In: *European Journal of Lipid Science and Technology* 121.8 (2019). ISSN: 1438-7697. DOI: 10.1002/ejlt.201800421.

[145] D. J. Kalita, I. Tarnavchyk, B. J. Chisholm, and D. C. Webster. "Novel bio-based epoxy resins from eugenol as an alternative to BPA epoxy and high throughput screening of the cured coatings". In: *Polymer* 233 (2021), p. 124191. ISSN: 0032-3861. DOI: 10.1016/j.polymer.2021.124191.

[146] B. Kumar, D. O. Agumba, D. H. Pham, H. C. Kim, and J. Kim. "Recent progress in bio–based eugenol resins: From synthetic strategies to structural properties and coating applications". In: *Journal of Applied Polymer Science* 139.2 (2022). ISSN: 0021-8995. DOI: 10.1002/app.51532.

[147] S. Ma, X. Liu, Y. Jiang, L. Fan, J. Feng, and J. Zhu. "Synthesis and properties of phosphorus-containing bio-based epoxy resin from itaconic acid". In: *Science China Chemistry* 57.3 (2014), pp. 379–388. ISSN: 1674-7291. DOI: 10.1007/s11426-013-5025-3.

[148] F. Gonçalves, P. Ferreira, and P. Alves. "Synthesis and characterization of itaconic-based epoxy resin: Chemical and thermal properties of partially biobased epoxy resins". In: *Polymer* 235 (2021), p. 124285. ISSN: 0032-3861. DOI: 10.1016/j.polymer.2021.124285.

[149] M. D. Garrison, M. A. Savolainen, A. P. Chafin, J. E. Baca, A. M. Bons, and B. G. Harvey. "Synthesis and Characterization of High-Performance, Bio-Based Epoxy–Amine Networks Derived from Resveratrol". In: *ACS Sustainable Chemistry & Engineering* 8.37 (2020), pp. 14137–14149. ISSN: 2168-0485. DOI: 10.1021/acssuschemeng.0c04816.

[150] Y. Tian, M. Ke, X. Wang, G. Wu, J. Zhang, and J. Cheng. "A resveratrol-based epoxy resin with ultrahigh Tg and good processability". In: *European Polymer Journal* 147 (2021), p. 110282. ISSN: 0014-3057. DOI: 10.1016/j.eurpolymj.2021.110282.

[151] K. Aalto-Korte, K. Suuronen, O. Kuuliala, M.-L. Henriks-Eckerman, and R. Jolanki. "Contact allergy to epoxy hardeners". In: *Contact dermatitis* 71.3 (2014), pp. 145–153. DOI: 10.1111/cod.12280.

[152] N. Bangsgaard *et al.* "Contact allergy to epoxy resin: risk occupations and consequences". In: *Contact dermatitis* 67.2 (2012), pp. 73–77. DOI: 10.1111/j.1600-0536.2012.02072.x.

[153] T. Lejding, K. Källberg, O. Bergendorff, S. Jacobsson, C. Svedman, and M. Bruze. "Epoxy allergy, investigation of a modern industry". In: *Contact dermatitis* 88.5 (2023), pp. 383–388. DOI: 10.1111/cod.14293.

[154] T. Spee, J. G. Timmerman, R. Rühl, K. Kersting, D. J. J. Heederik, and L. A. M. Smit. "Determinants of epoxy allergy in the construction industry: a case-control study". In: *Contact dermatitis* 74.5 (2016), pp. 259–266. DOI: 10.1111/cod.12529.

[155] J. E. van Dam, B. de Klerk-Engels, P. C. Struik, and R. Rabbinge. "Securing renewable resource supplies for changing market demands in a bio-based economy". In: *Industrial Crops and Products* 21.1 (2005), pp. 129–144. ISSN: 0926-6690. DOI: 10.1016/j.indcrop.2004.02.003.

[156] J. Franko, L. G. Jackson, A. Hubbs, M. Kashon, B. J. Meade, and S. E. Anderson. "Evaluation of furfuryl alcohol sensitization potential following dermal and pulmonary exposure: enhancement of airway responsiveness". In: *Toxicological sciences : an official journal of the Society of Toxicology* 125.1 (2012), pp. 105–115. DOI: 10.1093/toxsci/kfr271.

[157] S. P. M. Ventura, P. de Morais, J. A. S. Coelho, T. Sintra, J. A. P. Coutinho, and C. A. M. Afonso. "Evaluating the toxicity of biomass derived platform chemicals". In: *Green Chemistry* 18.17 (2016), pp. 4733–4742. ISSN: 1463-9262. DOI: 10.1039/C6GC01211F.

[158] T. Saurabh, M. Patnaik, S. Bhagt, and V. Renge. "Epoxidation of Vegetable oils: A review". In: *International Journal of Advanced Engineering Technology* 2 (2011), pp. 491–501.

[159] D. L. Motoc, J. M. Ferri, S. Ferrandiz-Bou, D. Garcia-Garcia, and R. Balart. "Dynamic-Mechanical and Decomposition Properties of Flax/Basalt Hybrid Laminates Based on an Epoxidized Linseed Oil Polymer". In: *Polymers* 13.4 (2021). DOI: 10.3390/polym13040479.

[160] J. Tang *et al.* "Preparation and Properties of Plant-Oil-Based Epoxy Acrylate-Like Resins for UV-Curable Coatings". In: *Polymers* 12.9 (2020). DOI: 10.3390/polym12092165.

[161] C. Noè, M. Hakkarainen, S. Malburet, A. Graillot, K. Adekunle, M. Skrifvars, and M. Sangermano. "Frontal–Photopolymerization of Fully Biobased Epoxy Composites". In: *Macromolecular Materials and Engineering* 307.6 (2022). ISSN: 1438-7492. DOI: 10.1002/mame.202100864.

[162] D. Radojčić, J. Hong, and Z. S. Petrović. "From Natural Oils to Epoxy Resins: A New Paradigm in Renewable Performance Materials". In: *Journal of Polymers and the Environment* 30.2 (2022), pp. 765–775. ISSN: 1566-2543. DOI: 10.1007/s10924-021-02228-w.

[163] M. A. R. Meier, J. O. Metzger, and U. S. Schubert. "Plant oil renewable resources as green alternatives in polymer science". In: *Chemical Society reviews* 36.11 (2007), pp. 1788–1802. ISSN: 0306-0012. DOI: 10.1039/B703294C.

[164] B. Matthäus and M. Musazcan Özcan. "Oil Content, Fatty Acid Composition and Distributions of Vitamin-E-Active Compounds of Some Fruit Seed Oils". In: *Antioxidants (Basel, Switzerland)* 4.1 (2015), pp. 124–133. ISSN: 2076-3921. DOI: 10.3390/antiox4010124.

[165] N. Ghasemi Rad, Z. Karami, M. J. Zohuriaan–Mehr, A. Salimi, and K. Kabiri. "Linseed oil–based reactive diluents preparation to improve tetra–functional epoxy resin properties". In: *Polymers for Advanced Technologies* 30.9 (2019), pp. 2361–2369. ISSN: 1042-7147. DOI: 10.1002/pat.4680.

[166] M. Schwaiger, C. Waly, M. Huszar, G. Oreski, M. Feuchter, F. Arbeiter, and K. Resch-Fauster. "Bioinspired fracture toughness enhancement of a fully bio-based epoxy resin". In: *Polymer Testing* 124 (2023), p. 108098. ISSN: 0142-9418. DOI: 10.1016/j.polymertesting.2023.108098.

[167] R. Wang and T. P. Schuman. "Vegetable oil-derived epoxy monomers and polymer blends: A comparative study with review". In: *Express Polymer Letters* 7.3 (2013), pp. 272–292. ISSN: 1788-618X. DOI: 10.3144/expresspolymlett.2013.25.

[168] C. Noè, M. Hakkarainen, and M. Sangermano. "Cationic UV-Curing of Epoxidized Biobased Resins". In: *Polymers* 13.1 (2020). DOI: 10.3390/polym13010089.

[169] B. Adler. *Native Epoxide und Epoxidharze - ein Beitrag zur ökologischen Chemie*. Berlin, Heidelberg: Springer Berlin Heidelberg, 2017. ISBN: 978-3-662-55614-6.

[170] K. Thiele, N. Eversmann, A. Krombholz, and D. Pufky-Heinrich. "Bio-Based Epoxy Resins Based on Linseed Oil Cured with Naturally Occurring Acids". In: *Polymers* 11.9 (2019). DOI: 10.3390/polym11091409.

[171] E. A. Baroncini, S. Kumar Yadav, G. R. Palmese, and J. F. Stanzione. "Recent advances in bio–based epoxy resins and bio–based epoxy curing agents". In: *Journal of Applied Polymer Science* 133.45 (2016). ISSN: 0021-8995. DOI: 10.1002/app.44103.

[172] J.-M. Pin, N. Sbirrazzuoli, and A. Mija. "From epoxidized linseed oil to bioresin: an overall approach of epoxy/anhydride cross-linking". In: *ChemSusChem* 8.7 (2015), pp. 1232–1243. DOI: 10.1002/cssc.201403262.

[173] C. Ding, P. S. Shuttleworth, S. Makin, J. H. Clark, and A. S. Matharu. "New insights into the curing of epoxidized linseed oil with dicarboxylic acids". In: *Green Chemistry* 17.7 (2015), pp. 4000–4008. ISSN: 1463-9262. DOI: 10.1039/C5GC00912J.

[174] S. Briede, O. Platnieks, A. Barkane, I. Sivacovs, A. Leitans, J. Lungevics, and S. Gaidukovs. "Tailored Biobased Resins from Acrylated Vegetable Oils for Application in Wood Coatings". In: *Coatings* 13.3 (2023), p. 657. DOI: 10.3390/coatings13030657.

[175] S. K. Sahoo, V. Khandelwal, and G. Manik. "Development of completely bio–based epoxy networks derived from epoxidized linseed and castor oil cured with citric acid". In: *Polymers for Advanced Technologies* 29.7 (2018), pp. 2080–2090. ISSN: 1042-7147. DOI: 10.1002/pat.4316.

[176] X. Kong, T. S. Omonov, and J. M. Curtis. "The development of canola oil based bio–resins". In: *Lipid Technology* 24.1 (2012), pp. 7–10. ISSN: 0956-666X. DOI: 10.1002/lite.201200167.

[177] S.-J. Park, F.-L. Jin, and J.-R. Lee. "Effect of Biodegradable Epoxidized Castor Oil on Physicochemical and Mechanical Properties of Epoxy Resins". In: *Macromolecular Chemistry and Physics* 205.15 (2004), pp. 2048–2054. ISSN: 1022-1352. DOI: 10.1002/macp.200400214.

[178] A. Kadam, M. Pawar, O. Yemul, V. Thamke, and K. Kodam. "Biodegradable biobased epoxy resin from karanja oil". In: *Polymer* 72 (2015), pp. 82–92. ISSN: 0032-3861. DOI: 10.1016/j.polymer.2015.07.002.

[179] V. V. Goud, N. C. Pradhan, and A. V. Patwardhan. "Epoxidation of karanja (Pongamia glabra) oil by H_2O_2". In: *Journal of the American Oil Chemists' Society* 83.7 (2006), pp. 635–640. ISSN: 0003-021X. DOI: 10.1007/s11746-006-1250-7.

[180] G. Francucci, F. Cardona, and N. W. Manthey. "Cure kinetics of an acrylated epoxidized hemp oil–based bioresin system". In: *Journal of Applied Polymer Science* 128.3 (2013), pp. 2030–2037. ISSN: 0021-8995. DOI: 10.1002/app.38380.

[181] S. Dinda, A. V. Patwardhan, V. V. Goud, and N. C. Pradhan. "Epoxidation of cottonseed oil by aqueous hydrogen peroxide catalysed by liquid inorganic acids". In: *Bioresource technology* 99.9 (2008), pp. 3737–3744. ISSN: 0960-8524. DOI: 10.1016/j.biortech.2007.07.015.

[182] O. Kreye, T. Tóth, and M. A. Meier. "Copolymers derived from rapeseed derivatives via ADMET and thiol-ene addition". In: *European Polymer Journal* 47.9 (2011), pp. 1804–1816. ISSN: 0014-3057. DOI: 10.1016/j.eurpolymj.2011.06.012.

[183] S. Arumugam and G. Sriram. “Synthesis and characterization of rapeseed oil bio-lubricant dispersed with nano copper oxide: Its effect on wear and frictional behavior of piston ring–cylinder liner combination”. In: *Proceedings of the Institution of Mechanical Engineers, Part J: Journal of Engineering Tribology* 228.11 (2014), pp. 1308–1318. ISSN: 1350-6501. DOI: 10.1177/1350650114535384.

[184] A. J. Clark and S. S. Hoong. “Copolymers of tetrahydrofuran and epoxidized vegetable oils: application to elastomeric polyurethanes”. In: *Polym. Chem.* 5.9 (2014), pp. 3238–3244. ISSN: 1759-9954. DOI: 10.1039/C3PY01527K.

[185] K. Huang, Y. Zhang, M. Li, J. Lian, X. Yang, and J. Xia. “Preparation of a light color cardanol-based curing agent and epoxy resin composite: Cure-induced phase separation and its effect on properties”. In: *Progress in Organic Coatings* 74.1 (2012), pp. 240–247. ISSN: 0300-9440. DOI: 10.1016/j.porgcoat.2011.12.015.

[186] S. Maiti, S. S. Ray, and A. K. Kundu. “Rosin: a renewable resource for polymers and polymer chemicals”. In: *Progress in Polymer Science* 14.3 (1989), pp. 297–338. ISSN: 0079-6700. DOI: 10.1016/0079-6700(89)90005-1.

[187] M. Chrysanthos, J. Galy, and J.-P. Pascault. “Preparation and properties of bio-based epoxy networks derived from isosorbide diglycidyl ether”. In: *Polymer* 52.16 (2011), pp. 3611–3620. ISSN: 0032-3861. DOI: 10.1016/j.polymer.2011.06.001.

[188] Y. Tachibana, J. Torii, K.-i. Kasuya, M. Funabashi, and M. Kunioka. “Hardening process and properties of an epoxy resin with bio-based hardener derived from furfural”. In: *RSC advances* 4.99 (2014), pp. 55723–55731. DOI: 10.1039/C4RA11636D.

[189] M. Stemmelen, F. Pessel, V. Lapinte, S. Caillol, J.-P. Habas, and J.-J. Robin. “A fully biobased epoxy resin from vegetable oils: From the synthesis of the precursors by thiol–ene reaction to the study of the final material”. In: *Journal of Polymer Science Part A: Polymer Chemistry* 49.11 (2011), pp. 2434–2444. ISSN: 0887-624X. DOI: 10.1002/pola.24674.

[190] S. Ma, Y. Jiang, X. Liu, L. Fan, and J. Zhu. “Bio-based tetrafunctional crosslink agent from gallic acid and its enhanced soybean oil-based UV-cured coatings with high performance”. In: *RSC Advances* 4.44 (2014), p. 23036. DOI: 10.1039/c4ra01311e.

[191] J. Hong, D. Radojčić, M. Ionescu, Z. S. Petrović, and E. Eastwood. "Advanced materials from corn: isosorbide-based epoxy resins". In: *Polym. Chem.* 5.18 (2014), pp. 5360–5368. ISSN: 1759-9954. DOI: 10.1039/C4PY00514G.

[192] F. I. Altuna, V. Pettarin, and R. J. J. Williams. "Self-healable polymer networks based on the cross-linking of epoxidised soybean oil by an aqueous citric acid solution". In: *Green Chemistry* 15.12 (2013), p. 3360. ISSN: 1463-9262. DOI: 10.1039/c3gc41384e.

[193] P. Gogoi, M. Boruah, S. Sharma, and S. K. Dolui. "Blends of Epoxidized Alkyd Resins Based on Jatropha Oil and the Epoxidized Oil Cured with Aqueous Citric Acid Solution: A Green Technology Approach". In: *ACS Sustainable Chemistry & Engineering* 3.2 (2015), pp. 261–268. ISSN: 2168-0485. DOI: 10.1021/sc500627u.

[194] C. di Mauro, A. Genua, and A. Mija. "Fully bio-based reprocessable thermosetting resins based on epoxidized vegetable oils cured with itaconic acid". In: *Industrial Crops and Products* 185 (2022), p. 115116. ISSN: 0926-6690. DOI: 10.1016/j.indcrop.2022.115116.

[195] F. Rothenhäusler and H. Ruckdaeschel. "Amino Acids as Bio-Based Curing Agents for Epoxy Resin: Correlation of Network Structure and Mechanical Properties". In: *Polymers* 15.2 (2023). DOI: 10.3390/polym15020385.

[196] F. Rothenhäusler and H. Ruckdaeschel. "l-Arginine as Bio-Based Curing Agent for Epoxy Resins: Temperature-Dependence of Mechanical Properties". In: *Polymers* 14.21 (2022), p. 4696. DOI: 10.3390/polym14214696.

[197] M. D'Este, M. Alvarado-Morales, and I. Angelidaki. "Amino acids production focusing on fermentation technologies - A review". In: *Biotechnology Advances* 36.1 (2018), pp. 14–25. DOI: 10.1016/j.biotechadv.2017.09.001.

[198] Dr. med. Werner G. Gehring. *Arginin: Lebensmittel: Arginin-Gehalt in mg pro 100 g Lebensmittel*. Ed. by DocMedicus Verlag. 2024 [Accessed on January 28, 2026]. URL: https://www.vitalstoff-lexikon.de/Aminosaeuren/Arginin/Lebensmittel.

[199] Dr. med. Werner G. Gehring. *Phenylalanin: Lebensmittel. Phenylalanin-Gehalt in mg pro 100 g Lebensmittel.* Ed. by DocMedicus Verlag. 2024 [Accessed on January 28, 2026]. URL: https://www.vitalstoff-lexikon.de/Aminosaeuren/Phenylalanin/Lebensmittel.

[200] Dr. med. Werner G. Gehring. *Tryptophan: Lebensmittel: Tryptophan-Gehalt in mg pro 100 g Lebensmittel.* Ed. by DocMedicus Verlag. 2024 [Accessed on January 28, 2026]. URL: https://www.vitalstoff-lexikon.de/Aminosaeuren/Tryptophan/Lebensmittel.

[201] D. Gibhardt, C. Buggisch, D. Meyer, and B. Fiedler. "Hygrothermal Aging History of Amine-Epoxy Resins: Effects on Thermo-Mechanical Properties". In: *Frontiers in Materials* 9 (2022). DOI: 10.3389/fmats.2022.826076.

[202] Y. Kwon, B.-s. Yim, J.-m. Kim, and J. Kim. "Mechanical and wetting properties of epoxy resins: Amine-containing epoxy-terminated siloxane oligomer with or without reductant". In: *Microelectronics Reliability* 51.4 (2011), pp. 819–825. DOI: 10.1016/j.microrel.2010.11.001.

[203] L. Q. Reyes, J. Zhang, B. Dao, D. L. Nguyen, and R. J. Varley. "Subtle variations in the structure of crosslinked epoxy networks and the impact upon mechanical and thermal properties". In: *Journal of Applied Polymer Science* 137.29 (2020), p. 48874. DOI: 10.1002/app.48874.

[204] L. Núñez-Regueira, M. Villanueva, and I. Fraga-Rivas. "Effect of a reactive diluent on the curing and dynamomechanical properties of an epoxy-diamine system". In: *Journal of Thermal Analysis and Calorimetry* 86.2 (2006), pp. 463–468. DOI: 10.1007/s10973-005-7191-9.

[205] S. Ma, W. Liu, C. Hu, Z. Wang, and C. Tang. "Toughening of epoxy resin system using a novel dendritic polysiloxane". In: *Macromolecular Research* 18.4 (2010), pp. 392–398. ISSN: 2092-7673. DOI: 10.1007/s13233-010-0408-1.

[206] H. Wen, X. Zhang, R. Xia, Z. Yang, and Y. Wu. "Thermal Decomposition Properties of Epoxy Resin in SF_6/N_2 Mixture". In: *Materials (Basel, Switzerland)* 12.1 (2018). ISSN: 1996-1944. DOI: 10.3390/ma12010075.

[207] V. B. Gupta, L. T. Drzal, C. Y.-C. Lee, and M. J. Rich. "The temperature–dependence of some mechanical properties of a cured epoxy resin system". In: *Polymer Engineering and Science* 25.13 (1985), pp. 812–823. ISSN: 0032-3888. DOI: 10.1002/pen.760251305.

[208] A. Shokuhfar and B. Arab. "The effect of cross linking density on the mechanical properties and structure of the epoxy polymers: molecular dynamics simulation". In: *Journal of Molecular Modeling* 19.9 (2013), pp. 3719–3731. DOI: 10.1007/s00894-013-1906-9.

[209] C. Leopold, T. Augustin, T. Schwebler, J. Lehmann, W. V. Liebig, and B. Fiedler. "Influence of carbon nanoparticle modification on the mechanical and electrical properties of epoxy in small volumes". In: *Journal of Colloid and Interface Science* 506 (2017), pp. 620–632. DOI: 10.1016/j.jcis.2017.07.085.

[210] K. C. Radford. "The mechanical properties of an epoxy resin with a second phase dispersion". In: *Journal of Materials Science* 6.10 (1971), pp. 1286–1291. ISSN: 0022-2461. DOI: 10.1007/BF00552042.

[211] W. J. Cantwell and H. H. Kausch. "Fracture behaviour of epoxy resins". In: *Chemistry and Technology of Epoxy Resins*. Dordrecht: Springer Netherlands, 1993, pp. 144–174. ISBN: 978-94-011-2932-9.

[212] M. Fang, Z. Zhang, J. Li, H. Zhang, H. Lu, and Y. Yang. "Constructing hierarchically structured interphases for strong and tough epoxy nanocomposites by amine-rich graphene surfaces". In: *Journal of Materials Chemistry* 20.43 (2010), p. 9635. ISSN: 0959-9428. DOI: 10.1039/c0jm01620a.

[213] S. Morsch, Z. Kefallinou, Y. Liu, S. B. Lyon, and S. R. Gibbon. "Controlling the nanostructure of epoxy resins: Reaction selectivity and stoichiometry". In: *Polymer* 143 (2018), pp. 10–18. ISSN: 0032-3861. DOI: 10.1016/j.polymer.2018.03.065.

[214] W. Liu, W. Huang, N. Song, Y. Wu, X. Zhao, and K. Chen. "Effect of stoichiometry on chemical structure, dielectric and mechanical properties of epoxy resin under gamma irradiation". In: *Radiation Physics and Chemistry* 202 (2023), p. 110551. ISSN: 0969-806X. DOI: 10.1016/j.radphyschem.2022.110551.

[215] F. Ullmann and B. Elvers, eds. *Ullmann's polymers and plastics: Products and processes*. Wiley-VCH, 2016. ISBN: 978-3-527-33823-8.

[216] H. Li, G. Chen, H. Su, D. Li, L. Sun, and J. Yang. "Effect of the stoichiometric ratio on the crosslinked network structure and cryogenic properties of epoxy resins cured at low temperature". In: *European Polymer Journal* 112 (2019), pp. 792–798. ISSN: 0014-3057. DOI: 10.1016/j.eurpolymj.2018.10.051.

[217] J. D'Almeida and S. N. Monteiro. "The effect of the resin/hardener ratio on the compressive behavior of an epoxy system". In: *Polymer Testing* 15.4 (1996), pp. 329–339. ISSN: 0142-9418. DOI: 10.1016/0142-9418(95)00037-2.

[218] M. I. B. Tavares, J. R. M. D'Almeida, and S. N. Monteiro. "^{13}C solid-state NMR analysis of the DGEBA/TETA epoxy system". In: *Journal of Applied Polymer Science* 78.13 (2000), pp. 2358–2362. ISSN: 0021-8995. DOI: 10.1002/1097-4628(20001220)78:13<2358::AID-APP120>3.0.CO;2-T.

[219] J. R. M. D'Almeida, G. W. de Menezes, and S. N. Monteiro. "Ageing of the DGEBA/TETA epoxy system with off-stoichiometric compositions". In: *Materials Research* 6.3 (2003), pp. 415–420. DOI: 10.1590/S1516-14392003000300017.

[220] F. Rothenhäusler and H. Ruckdaeschel. "Influence of the stoichiometric ratio on the in–situ formation of crystals and the mechanical properties of epoxy resin cured with L–tyrosine". In: *Polymer Engineering & Science* 63.12 (2023), pp. 4007–4018. ISSN: 0032-3888. DOI: 10.1002/pen.26501.

[221] Y. Li, F. Xiao, and C. P. Wong. "Novel, environmentally friendly crosslinking system of an epoxy using an amino acid: Tryptophan–cured diglycidyl ether of bisphenol A epoxy". In: *Journal of Polymer Science Part A: Polymer Chemistry* 45.2 (2007), pp. 181–190. ISSN: 0887-624X. DOI: 10.1002/pola.21742.

[222] J. G. Williams. "The beta relaxation in epoxy resin–based networks". In: *Journal of Applied Polymer Science* 23.12 (1979), pp. 3433–3444. ISSN: 0021-8995. DOI: 10.1002/app.1979.070231201.

[223] G. Nikolic, S. Zlatkovic, M. Cakic, S. Cakic, C. Lacnjevac, and Z. Rajic. "Fast Fourier transform IR characterization of epoxy GY systems crosslinked with aliphatic and cycloaliphatic EH polyamine adducts". In: *Sensors (Basel, Switzerland)* 10.1 (2010), pp. 684–696. DOI: 10.3390/s100100684.

[224] A.-S. Mora, R. Tayouo, B. Boutevin, G. David, and S. Caillol. "A perspective approach on the amine reactivity and the hydrogen bonds effect on epoxy-amine systems". In: *European Polymer Journal* 123 (2020), p. 109460. ISSN: 0014-3057. DOI: 10.1016/j.eurpolymj.2019.109460.

[225] T. Kolev. “Solid-state IR-LD spectroscopic and theoretical analysis of arginine-containing peptides”. In: *Biopolymers* 83.1 (2006), pp. 39–45. ISSN: 0006-3525. DOI: 10.1002/bip.20525.

[226] F. Dai, Q. Zhuang, G. Huang, H. Deng, and X. Zhang. “Infrared Spectrum Characteristics and Quantification of OH Groups in Coal”. In: *ACS omega* 8.19 (2023), pp. 17064–17076. DOI: 10.1021/acsomega.3c01336.

[227] A. Antoniou, M. Rosemeier, K. Tazefidan, A. Krimmer, and G. Wolken-Möhlmann. “Impact of Site-Specific Thermal Residual Stress on the Fatigue of Wind-Turbine Blades”. In: *AIAA Journal* 58.11 (2020), pp. 4781–4793. ISSN: 0001-1452. DOI: 10.2514/1.J059388.

[228] H. Wang, Y. Liu, J. Zhang, T. Li, Z. Hu, and Y. Yu. “Effect of curing conversion on the water sorption, corrosion resistance and thermomechanical properties of epoxy resin”. In: *RSC Advances* 5.15 (2015), pp. 11358–11370. DOI: 10.1039/C4RA13678K.

[229] V. B. Gupta and C. Brahatheeswaran. “Molecular packing and free volume in crosslinked epoxy networks”. In: *Polymer* 32.10 (1991), pp. 1875–1884. ISSN: 0032-3861. DOI: 10.1016/0032-3861(91)90379-W.

[230] M. Ogata, N. Kinjo, and T. Kawata. “Effects of crosslinking on physical properties of phenol–formaldehyde novolac cured epoxy resins”. In: *Journal of Applied Polymer Science* 48.4 (1993), pp. 583–601. ISSN: 0021-8995. DOI: 10.1002/app.1993.070480403.

[231] S. Li, J. He, S. Han, F. Chen, Y. Zhang, Y. Chen, and H. Zou. “Hydrogen bond-driven rigid filling strategy: Regulation of epoxy resin network structure and properties by anchored groups”. In: *Polymer* 329 (2025), p. 128511. ISSN: 0032-3861. DOI: 10.1016/j.polymer.2025.128511.

[232] A. M. A. M. Altaweel, H. B. Ravikumar, and C. Ranganathaiah. “Influence of free volume on the mechanical properties of epoxy based composites: A correlation study”. In: *physica status solidi c* 6.11 (2009), pp. 2401–2403. ISSN: 1862-6351. DOI: 10.1002/pssc.200982070.

[233] K. Karunakaran, S. S. Singh, and R. Kitey. “Investigating the role of filler shape on the dynamic mechanical properties of glass–filled epoxy composites”. In: *Polymer Composites* 43.10 (2022), pp. 6912–6925. ISSN: 0272-8397. DOI: 10.1002/pc.26737.

[234] B. Fiedler, M. Hojo, S. Ochiai, K. Schulte, and M. Ando. "Failure behavior of an epoxy matrix under different kinds of static loading". In: *Composites Science and Technology* 61.11 (2001), pp. 1615–1624. ISSN: 0266-3538. DOI: 10.1016/S0266-3538(01)00057-4.

[235] O. V. Startsev, Y. M. Vapirov, M. P. Lebedev, and A. K. Kychkin. "Comparison of Glass-Transition Temperatures for Epoxy Polymers Obtained by Methods of Thermal Analysis". In: *Mechanics of Composite Materials* 56.2 (2020), pp. 227–240. ISSN: 0191-5665. DOI: 10.1007/s11029-020-09875-5.

[236] A. X. H. Yong, G. D. Sims, S. J. P. Gnaniah, S. L. Ogin, and P. A. Smith. "Heating rate effects on thermal analysis measurement of Tg in composite materials". In: *Advanced Manufacturing: Polymer & Composites Science* 3.2 (2017), pp. 43–51. ISSN: 2055-0340. DOI: 10.1080/20550340.2017.1315908.

[237] K. Hristova and W. C. Wimley. "A look at arginine in membranes". In: *The Journal of membrane biology* 239.1-2 (2011), pp. 49–56. DOI: 10.1007/s00232-010-9323-9.

[238] E. Courvoisier, P. A. Williams, G. K. Lim, C. E. Hughes, and K. D. M. Harris. "The crystal structure of L-arginine". In: *Chemical communications (Cambridge, England)* 48.22 (2012), pp. 2761–2763. DOI: 10.1039/C2CC17203H.

[239] S. Yoshizawa, T. Arakawa, and K. Shiraki. "Effect of counter ions of arginine as an additive for the solubilization of protein and aromatic compounds". In: *International journal of biological macromolecules* 91 (2016), pp. 471–476. DOI: 10.1016/j.ijbiomac.2016.05.085.

[240] R. Ramsdale-Capper and J. P. Foreman. "Internal antiplasticisation in highly crosslinked amine cured multifunctional epoxy resins". In: *Polymer* 146 (2018), pp. 321–330. ISSN: 0032-3861. DOI: 10.1016/j.polymer.2018.05.048.

[241] J. M. Morancho, X. Ramis, X. Fernández-Francos, J. M. Salla, A. O. Konuray, and À. Serra. "Curing of off-stoichiometric amine–epoxy thermosets". In: *Journal of Thermal Analysis and Calorimetry* 133.1 (2018), pp. 519–527. ISSN: 1388-6150. DOI: 10.1007/s10973-018-7158-2.

[242] G. Ranoux, G. Tataru, and X. Coqueret. "Cationic Curing of Epoxy–Aromatic Matrices for Advanced Composites: The Assets of Radiation Processing". In: *Applied Sciences* 12.5 (2022), p. 2355. DOI: 10.3390/app12052355.

[243] J. A. McGowen and L. J. Mathias. "Cationic polymerization of diglycidly ether of bisphenol a resins initiated by benzylsulfonium salts". In: *Polymer Composites* 18.3 (1997), pp. 348–367. ISSN: 0272-8397. DOI: 10.1002/pc.10287.

[244] B. E. F. Ekbrant, A. L. Skov, and A. E. Daugaard. "Epoxy-Rich Systems with Preference for Etherification over Amine-Epoxy Reactions for Tertiary Amine Accelerators". In: *Macromolecules* 54.9 (2021), pp. 4280–4287. ISSN: 0024-9297. DOI: 10.1021/acs.macromol.0c02630.

[245] D. Gibhardt. "Environmental effects on composites durability with regard to fibers, matrix, and interphase". PhD thesis. Hamburg University of Technology, 2024. DOI: 10.15480/882.9468.

[246] J. Drummer, D. Gibhardt, J. Körbelin, and B. Fiedler. "General influence of the environmental temperature on the matrix strength under tensile and compressive loading - A comprehensive study on high performance matrices". In: *Composites Science and Technology* 230 (2022), p. 109486. DOI: 10.1016/j.compscitech.2022.109486.

[247] G. M. Odegard and A. Bandyopadhyay. "Physical aging of epoxy polymers and their composites". In: *Journal of Polymer Science Part B: Polymer Physics* 49.24 (2011), pp. 1695–1716. ISSN: 0887-6266. DOI: 10.1002/polb.22384.

[248] A. Le Guen-Geffroy, P.-Y. Le Gac, B. Habert, and P. Davies. "Physical ageing of epoxy in a wet environment: Coupling between plasticization and physical ageing". In: *Polymer Degradation and Stability* 168 (2019), p. 108947. ISSN: 0141-3910. DOI: 10.1016/j.polymdegradstab.2019.108947.

[249] E. S.-W. Kong. "Physical aging in epoxy matrices and composites". In: *Epoxy resins and composites*. Ed. by K. Dušek. Vol. 80. Advances in polymer science. Berlin: Springer, 1986, pp. 125–171. ISBN: 978-3-540-16423-4. DOI: 10.1007/3-540-16423-5_14.

[250] A. I. Gagani, A. B. Monsås, A. E. Krauklis, and A. T. Echtermeyer. "The effect of temperature and water immersion on the interlaminar shear fatigue of glass fiber epoxy composites using the I-beam method". In: *Composites Science and Technology* 181 (2019), p. 107703. ISSN: 0266-3538. DOI: 10.1016/j.compscitech.2019.107703.

[251] C. Humeau, P. Davies, and F. Jacquemin. "An experimental study of water diffusion in carbon/epoxy composites under static tensile stress". In: *Composites Part A: Applied Science and Manufacturing* 107 (2018), pp. 94–104. ISSN: 1359-835X. DOI: 10.1016/j.compositesa.2017.12.016.

[252] A. Ilioni, P.-Y. Le Gac, C. Badulescu, D. Thévenet, and P. Davies. "Prediction of Mechanical Behaviour of a Bulk Epoxy Adhesive in a Marine Environment". In: *The Journal of Adhesion* 95.1 (2019), pp. 64–84. ISSN: 0021-8464. DOI: 10.1080/00218464.2017.1377616.

[253] M. Bordes, P. Davies, J.-Y. Cognard, L. Sohier, V. Sauvant-Moynot, and J. Galy. "Prediction of long term strength of adhesively bonded steel/epoxy joints in sea water". In: *International Journal of Adhesion and Adhesives* 29.6 (2009), pp. 595–608. ISSN: 0143-7496. DOI: 10.1016/j.ijadhadh.2009.02.013.

[254] V. Jaksic, C. R. Kennedy, D. M. Grogan, S. B. Leen, and C. M. Ó. Brádaigh. *Influence of Composite Fatigue Properties on marine Tidal Turbine Blade Design: In: Durability of Composites in a Marine Environment 2. Editors P. Davies and Y. D. Rajapakse.* Cham: Springer International Publishing, 2018. ISBN: 978-3-319-65145-3. DOI: 10.1007/978-3-319-65145-3.

[255] Y. Zheng, R. D. Priestley, and G. B. McKenna. "Physical aging of an epoxy subsequent to relative humidity jumps through the glass concentration". In: *Journal of Polymer Science Part B: Polymer Physics* 42.11 (2004), pp. 2107–2121. ISSN: 0887-6266. DOI: 10.1002/polb.20084.

[256] J. Zhou and J. P. Lucas. "Hygrothermal effects of epoxy resin. Part II: variations of glass transition temperature". In: *Polymer* 40.20 (1999), pp. 5513–5522. ISSN: 0032-3861. DOI: 10.1016/S0032-3861(98)00791-5.

[257] V. O. Startsev, M. P. Lebedev, K. A. Khrulev, M. V. Molokov, A. S. Frolov, and T. A. Nizina. "Effect of outdoor exposure on the moisture diffusion and mechanical properties of epoxy polymers". In: *Polymer Testing*

65 (2018), pp. 281–296. ISSN: 0142-9418. DOI: 10.1016/j.polymertesting.2017.12.007.

[258] V. Bellenger, J. Verdu, and E. Morel. "Structure-properties relationships for densely cross-linked epoxide-amine systems based on epoxide or amine mixtures". In: *Journal of Materials Science* 24.1 (1989), pp. 63–68. ISSN: 0022-2461. DOI: 10.1007/BF00660933.

[259] J. B. Enns and J. K. Gillham. "Effect of the extent of cure on the modulus, glass transition, water absorptio, and density of an amine-cured epoxy". In: *Journal of Applied Polymer Science* 28.9 (1983), pp. 2831–2846. DOI: 10.1002/app.1983.070280914.

[260] P. Musto, G. Ragosta, G. Scarinzi, and L. Mascia. "Probing the molecular interactions in the diffusion of water through epoxy and epoxy–bismaleimide networks". In: *Journal of Polymer Science Part B: Polymer Physics* 40.10 (2002), pp. 922–938. ISSN: 0887-6266. DOI: 10.1002/polb.10147.

[261] J. Zhou and J. P. Lucas. "Hygrothermal effects of epoxy resin. Part I: the nature of water in epoxy". In: *Polymer* 40.20 (1999), pp. 5505–5512. ISSN: 0032-3861. DOI: 10.1016/S0032-3861(98)00790-3.

[262] E. Gaudichet–Maurin, F. Thominette, and J. Verdu. "Water sorption characteristics in moderately hydrophilic polymers, Part 1: Effect of polar groups concentration and temperature in water sorption in aromatic polysulfones". In: *Journal of Applied Polymer Science* 109.5 (2008), pp. 3279–3285. ISSN: 0021-8995. DOI: 10.1002/app.24873.

[263] A. F. Abdelkader and J. R. White. "Water absorption in epoxy resins: The effects of the crosslinking agent and curing temperature". In: *Journal of Applied Polymer Science* 98.6 (2005), pp. 2544–2549. ISSN: 0021-8995. DOI: 10.1002/app.22400.

[264] G. Capiel, J. Uicich, D. Fasce, and P. E. Montemartini. "Diffusion and hydrolysis effects during water aging on an epoxy-anhydride system". In: *Polymer Degradation and Stability* 153 (2018), pp. 165–171. ISSN: 0141-3910. DOI: 10.1016/j.polymdegradstab.2018.04.030.

[265] A. Berens and H. Hopfenberg. "Diffusion and relaxation in glassy polymer powders: 2. Separation of diffusion and relaxation parameters". In: *Polymer* 19.5 (1978), pp. 489–496. ISSN: 0032-3861. DOI: 10.1016/0032-3861(78)90269-0.

[266] L.-R. Bao, A. F. Yee, and C. Y.-C. Lee. "Moisture absorption and hygrothermal aging in a bismaleimide resin". In: *Polymer* 42.17 (2001), pp. 7327–7333. ISSN: 0032-3861. DOI: 10.1016/S0032-3861(01)00238-5.

[267] O. Starkova, S. Chandrasekaran, T. Schnoor, J. Sevcenko, and K. Schulte. "Anomalous water diffusion in epoxy/carbon nanoparticle composites". In: *Polymer Degradation and Stability* 164 (2019), pp. 127–135. ISSN: 0141-3910. DOI: 10.1016/j.polymdegradstab.2019.04.010.

[268] A. E. Krauklis, C. W. Karl, I. B. C. M. Rocha, J. Burlakovs, R. Ozola-Davidane, A. I. Gagani, and O. Starkova. "Modelling of Environmental Ageing of Polymers and Polymer Composites-Modular and Multiscale Methods". In: *Polymers* 14.1 (2022). DOI: 10.3390/polym14010216.

[269] M. R. Loos, L. A. F. Coelho, S. H. Pezzin, and S. C. Amico. "The effect of acetone addition on the properties of epoxy". In: *Polímeros* 18.1 (2008), pp. 76–80. DOI: 10.1590/S0104-14282008000100015.

[270] V. d. C. Rodrigues, D. Hirayama, and A. C. Ancelotti Junior. "The effects of residual organic solvent on epoxy: modeling of kinetic parameters by DSC and Borchardt-Daniels method". In: *Polímeros* 31.1 (2021). DOI: 10.1590/0104-1428.09820.

[271] Y. Ji, Y. Chen, X. Han, X. Hu, B. Yuan, and Y. Qiao. "Effect of acetone on mechanical properties of epoxy used for surface treatment before adhesive bonding". In: *Polymer Testing* 86 (2020), p. 106492. ISSN: 0142-9418. DOI: 10.1016/j.polymertesting.2020.106492.

[272] M. L. Kaplan. "Solvent Penetration in Cured Epoxy Networks". In: *Polymer Engineering and Science* 31.10 (1991).

[273] S. Zheng and P. A. Lucas. "Understanding Chemical Resistance in Epoxy System (Evonik Corporation)". In: *Coatings World* (2020), pp. 35–45.

[274] T. Aziz, F. Haq, A. Farid, L. Cheng, L. F. Chuah, A. Bokhari, M. Mubashir, D. Y. Y. Tang, and P. L. Show. "The epoxy resin system: function and role of curing agents". In: *Carbon Letters* 34.1 (2024), pp. 477–494. ISSN: 1976-4251. DOI: 10.1007/s42823-023-00547-7.

[275] C. Galant, B. Fayolle, M. Kuntz, and J. Verdu. "Thermal and radio-oxidation of epoxy coatings". In: *Progress in Organic Coatings* 69.4 (2010), pp. 322–329. ISSN: 0300-9440. DOI: 10.1016/j.porgcoat.2010.07.005.

[276] A. E. Krauklis and A. T. Echtermeyer. “Mechanism of Yellowing: Carbonyl Formation during Hygrothermal Aging in a Common Amine Epoxy”. In: *Polymers* 10.9 (2018). DOI: 10.3390/polym10091017.

[277] E. Ernault, E. Richaud, and B. Fayolle. “Thermal oxidation of epoxies: Influence of diamine hardener”. In: *Polymer Degradation and Stability* 134 (2016), pp. 76–86. ISSN: 0141-3910. DOI: 10.1016/j.polymdegradstab.2016.09.030.

[278] B. Mailhot, S. Morlat–Thérias, M. Ouahioune, and J.-.-L. Gardette. “Study of the Degradation of an Epoxy/Amine Resin, 1”. In: *Macromolecular Chemistry and Physics* 206.5 (2005), pp. 575–584. ISSN: 1022-1352. DOI: 10.1002/macp.200400395.

[279] B. De’Nève and M. Shanahan. “Water absorption by an epoxy resin and its effect on the mechanical properties and infra-red spectra”. In: *Polymer* 34.24 (1993), pp. 5099–5105. ISSN: 0032-3861. DOI: 10.1016/0032-3861(93)90254-8.

[280] D. Gibhardt, C. Fleschhut, and B. Fiedler. “The influence of different glass fiber/epoxy matrix combinations on the durability under severe moisture impact”. In: *IOP Conference Series: Materials Science and Engineering* 942.1 (2020), p. 012009. ISSN: 1757-8981. DOI: 10.1088/1757-899X/942/1/012009.

[281] B. A. Hernandez-Sanchez, D. Miller, and D. Samborsky. *2018 SNL/MSU/DOE COMPOSITE MATERIAL FATIGUE DATABASE - Environmental Version 28E*. 2018. DOI: 10.2172/1481599.

[282] A. A. Khan, I. V. Singh, B. K. Mishra, and R. Chennamsetti. “An experimental investigation of fatigue performance and damage distribution mechanism in Bi-Directional GFRP composites”. In: *International Journal of Fatigue* 193 (2025), p. 108735. ISSN: 0142-1123. DOI: 10.1016/j.ijfatigue.2024.108735.

[283] D. Gibhardt, T. Tiedemann, M. Walter, N. Jegel, A. Trippel, and B. Fiedler. *Fracture toughness of composites: How material, manufacturing, environmental and testing parameters affect the results*. 12th International Conference on Composite Testing and Model Identification, Riga, Lativa, 22.05.2025.

[284] A. Siddique, S. Abid, F. Shafiq, Y. Nawab, H. Wang, B. Shi, S. Saleemi, and B. Sun. "Mode I fracture toughness of fiber-reinforced polymer composites: A review". In: *Journal of Industrial Textiles* 50.8 (2021), pp. 1165–1192. ISSN: 1528-0837. DOI: 10.1177/1528083719858767.

[285] S.-J. Park, F.-L. Jin, and J.-R. Lee. "Thermal and mechanical properties of tetrafunctional epoxy resin toughened with epoxidized soybean oil". In: *Materials Science and Engineering: A* 374.1-2 (2004), pp. 109–114. ISSN: 0921-5093. DOI: 10.1016/j.msea.2004.01.002.

[286] Y. Chen, L. Yang, J. Wu, L. Ma, D. E. Finlow, S. Lin, and K. Song. "Thermal and mechanical properties of epoxy resin toughened with epoxidized soybean oil". In: *Journal of Thermal Analysis and Calorimetry* 113.2 (2013), pp. 939–945. ISSN: 1388-6150. DOI: 10.1007/s10973-012-2859-4.

[287] J. Janesch, A. Solt-Rindler, L. Dumschat, O. Vay, A. Mija, W. Gindl-Altmutter, T. Rosenau, W. Raffeiner, and C. Hansmann. "Flexible Biobased Thermosets from Epoxidized Plant Oils: A Study of Aliphatic Cross-Linking Agents". In: *ACS applied polymer materials* 7.6 (2025), pp. 3686–3697. DOI: 10.1021/acsapm.4c03944.

[288] W. Wang, Z. Hu, and W. Lei. "Research Progress on Vegetable Oil-Based UV-Curing Resins". In: *Polymers* 17.14 (2025). DOI: 10.3390/polym17141890.

[289] A. Todorovic, K. Resch–Fauster, A. R. Mahendran, G. Oreski, and W. Kern. "Curing of epoxidized linseed oil: Investigation of the curing reaction with different hardener types". In: *Journal of Applied Polymer Science* 138.16 (2021). ISSN: 0021-8995. DOI: 10.1002/app.50239.

[290] M. Shimbo, N. Nishitani, and T. Takahama. "Mechanical properties of acid–cured epoxide resins with different network structures". In: *Journal of Applied Polymer Science* 29.5 (1984), pp. 1709–1721. ISSN: 0021-8995. DOI: 10.1002/app.1984.070290524.

[291] C. Ding and A. S. Matharu. "Recent Developments on Biobased Curing Agents: A Review of Their Preparation and Use". In: *ACS Sustainable Chemistry & Engineering* 2.10 (2014), pp. 2217–2236. DOI: 10.1021/sc500478f.

[292] A. Apelblat. *Citric acid*. Cham: Springer, 2014. ISBN: 978-3-319-11232-9. DOI: 10.1007/978-3-319-11233-6.

[293] E. M. Woo and J. C. Seferis. “Cure kinetics of epoxy/anhydride thermosetting matrix systems”. In: *Journal of Applied Polymer Science* 40.7-8 (1990), pp. 1237–1256. ISSN: 0021-8995. DOI: 10.1002/app.1990.070400713.

[294] A. Solanki, V. Anand, V. Choudhary, and I. K. Varma. “Effect of structure on thermal behavior of homopolymers and copolymers of itaconimides”. In: *Journal of Macromolecular Science, Part C* 41.4 (2001), pp. 253–284. ISSN: 1532-1797. DOI: 10.1081/MC-100107859.

[295] D. van Krevelen. “Some basic aspects of flame resistance of polymeric materials”. In: *Polymer* 16.8 (1975), pp. 615–620. ISSN: 0032-3861. DOI: 10.1016/0032-3861(75)90157-3.

[296] J. Zhou, Z. Heng, H. Zhang, Y. Chen, H. Zou, and M. Liang. “High residue bio-based structural-functional integration epoxy and intrinsic flame retardant mechanism study”. In: *RSC advances* 9.71 (2019), pp. 41603–41615. DOI: 10.1039/C9RA08098H.

[297] J. C. Markwart, A. Battig, M. M. Velencoso, D. Pollok, B. Schartel, and F. R. Wurm. “Aromatic vs. Aliphatic Hyperbranched Polyphosphoesters as Flame Retardants in Epoxy Resins”. In: *Molecules (Basel, Switzerland)* 24.21 (2019). DOI: 10.3390/molecules24213901.

[298] C.-D. Varganici, L. Rosu, A. Bifulco, D. Rosu, F. Mustata, and S. Gaan. “Recent advances in flame retardant epoxy systems from reactive DOPO–based phosphorus additives”. In: *Polymer Degradation and Stability* 202 (2022), p. 110020. ISSN: 0141-3910. DOI: 10.1016/j.polymdegradstab.2022.110020.

[299] H. Wang *et al.* “Environmental Friendly Intumescent Flame Retardant Gives Epoxy Resin Excellent Fire Resistance and Mechanical Properties”. In: *Macromolecular Research* 30.8 (2022), pp. 536–546. ISSN: 1598-5032. DOI: 10.1007/s13233-022-0059-z.

[300] S. Zhou, R. Tao, P. Dai, Z. Luo, and M. He. “Two–step fabrication of lignin–based flame retardant for enhancing the thermal and fire retardancy properties of epoxy resin composites”. In: *Polymer Composites* 41.5 (2020), pp. 2025–2035. ISSN: 0272-8397. DOI: 10.1002/pc.25517.

[301] C. Zhou, X. Wang, J. Wang, Z. Pan, and H. Zhou. "Epoxy resin modified with chitosan derivatives and DOPO: Improved flame retardancy, mechanical properties and transparency". In: *Polymer Degradation and Stability* 199 (2022), p. 109931. ISSN: 0141-3910. DOI: 10.1016/j.polymdegradstab.2022.109931.

[302] I. Mitterová, V. Veľková, and A. Majlingová. "Comprehensive Evaluation of a High-Resistance Fire Retardant via Simultaneous Thermal Analysis, Gas Chromatography–Mass Spectrometry, and Mass Loss Study". In: *Fire* 8.11 (2025), p. 432. DOI: 10.3390/fire8110432.

[303] G. Tang, X. Huang, H. Ding, X. Wang, S. Jiang, K. Zhou, B. Wang, W. Yang, and Y. Hu. "Combustion properties and thermal degradation behaviors of biobased polylactide composites filled with calcium hypophosphite". In: *RSC advances* 4.18 (2014), p. 8985. DOI: 10.1039/c3ra44537b.

[304] K.-S. Lim, S.-T. Bee, L. T. Sin, T.-T. Tee, C. T. Ratnam, D. Hui, and A. R. Rahmat. "A review of application of ammonium polyphosphate as intumescent flame retardant in thermoplastic composites". In: *Composites Part B: Engineering* 84 (2016), pp. 155–174. ISSN: 1359-8368. DOI: 10.1016/j.compositesb.2015.08.066.

[305] S. Rabe, Y. Chuenban, and B. Schartel. "Exploring the Modes of Action of Phosphorus-Based Flame Retardants in Polymeric Systems". In: *Materials* 10.5 (2017). ISSN: 1996-1944. DOI: 10.3390/ma10050455.

[306] M. R. Elkhayat, H. H. Zayet, M. K. Hashem, G. F. Aly, and A. A. Alkarn. "Silicosis among phosphate mine workers in Upper Egypt: a cross-sectional study". In: *The Egyptian Journal of Bronchology* 19.1 (2025). DOI: 10.1186/s43168-025-00496-x.

[307] Y. Hamed, M. Gentilucci, N. Mokadem, R. Khalil, Y. Ayadi, R. Hadji, and E. Elaloui. "Assessment and Mitigation of Groundwater Contamination from Phosphate Mining in Tunisia: Geochemical and Radiological Analysis". In: *Hydrology* 11.6 (2024), p. 84. DOI: 10.3390/hydrology11060084.

[308] X. Liang, Q. Hu, X. Wang, L. Li, Y. Dong, C. Sun, C. Hu, and X. Gu. "Thermal Kinetics of a Lignin-Based Flame Retardant". In: *Polymers* 12.9 (2020). DOI: 10.3390/polym12092123.

[309] P. Dai, M. Liang, X. Ma, Y. Luo, M. He, X. Gu, Q. Gu, I. Hussain, and Z. Luo. "Highly Efficient, Environmentally Friendly Lignin-Based Flame Retardant Used in Epoxy Resin". In: *ACS omega* 5.49 (2020), pp. 32084–32093. DOI: 10.1021/acsomega.0c05146.

[310] S. Fatullayeva, D. Tagiyev, N. Zeynalov, S. Mammadova, and E. Aliyeva. "Recent advances of chitosan-based polymers in biomedical applications and environmental protection". In: *Journal of Polymer Research* 29.7 (2022). ISSN: 1022-9760. DOI: 10.1007/s10965-022-03121-3.

[311] Y. Li, Z. Yang, J. Guan, Q. Yan, and Z. Lei. "Organic-inorganic hybrid functionalized chitosan/ammonium polyphosphate (APP): A synergistic strategy for flame-retardant and high-mechanical-strength epoxy thermosets". In: *International journal of biological macromolecules* 309.1 (2025), p. 142579. DOI: 10.1016/j.ijbiomac.2025.142579.

[312] Y. Yang, Y. Lu, W. Zhan, and Q. Kong. "Design of a Novel Chitosan Derivatives and DOPO Flame Retardant and Its Application in Epoxy Resin". In: *Macromol* 5.1 (2025), p. 9. DOI: 10.3390/macromol5010009.

[313] L. Zheng, X. Zhu, J. Wang, and W. Su. "Mechanochemical-assisted extraction and enzymatic hydrolysis of calcium phytate from defatted rice bran". In: *Chemical and Biological Technologies in Agriculture* 10.1 (2023). DOI: 10.1186/s40538-023-00424-5.

[314] W. Zhang, W. Wu, W. Meng, W. Xie, Y. Cui, J. Xu, and H. Qu. "Core-Shell Graphitic Carbon Nitride/Zinc Phytate as a Novel Efficient Flame Retardant for Fire Safety and Smoke Suppression in Epoxy Resin". In: *Polymers* 12.1 (2020). DOI: 10.3390/polym12010212.

[315] Y. Xu, F. Yan, Y. Zong, J. Li, H. Gao, Y. Liu, Y. Wang, Y. Zhu, and Q. Wang. "Proteomic and lipidomics analyses of high fatty acid AhDGAT3 transgenic soybean reveals the key lipase gene associated with the lipid internal mechanism". In: *Genome* 65.3 (2022), pp. 153–164. DOI: 10.1139/gen-2021-0043.

[316] G. Lou, Z. Ma, J. Dai, Z. Bai, S. Fu, S. Huo, L. Qian, and P. Song. "Fully Biobased Surface-Functionalized Microcrystalline Cellulose via Green Self-Assembly toward Fire-Retardant, Strong, and Tough Epoxy Biocomposites". In: *ACS Sustainable Chemistry & Engineering* 9.40 (2021), pp. 13595–13605. ISSN: 2168-0485. DOI: 10.1021/acssuschemeng.1c04718.

[317] A. Dowbysz, M. Samsonowicz, and B. Kukfisz. “Recent Advances in Bio-Based Additive Flame Retardants for Thermosetting Resins”. In: *International journal of environmental research and public health* 19.8 (2022). DOI: 10.3390/ijerph19084828.

[318] A. L. M. Daneluti and J. d. R. Matos. “Study of thermal behavior of phytic acid”. In: *Brazilian Journal of Pharmaceutical Sciences* 49.2 (2013), pp. 275–283. DOI: 10.1590/S1984-82502013000200009.

[319] K. Matsumoto, T. Tanaka, M. Sasada, N. Sano, and K. Masuyama. “A mechanism for fire retardancy realized by a combination of biofillers and ammonium polyphosphate in various polymer systems”. In: *Cellulose* 28.6 (2021), pp. 3833–3846. ISSN: 0969-0239. DOI: 10.1007/s10570-021-03747-4.

[320] M. Maqsood and G. Seide. “Biodegradable Flame Retardants for Biodegradable Polymer”. In: *Biomolecules* 10.7 (2020). DOI: 10.3390/biom10071038.

[321] V. Selvam, M. Kumar, and M. Vadivel. “Mechanical properties of epoxy/chitosan biocomposites”. In: *International Journal of Chemical Sciences* 11 (2013), pp. 1103–1109.

[322] A. Gazzola, P. A. Carraro, D. Gibhardt, M. Walter, B. Fiedler, M. Quaresimin, and M. Zappalorto. “Damage monitoring of GFRP laminates via electrical measurements: Experiments and predictions”. In: *Composites Part A: Applied Science and Manufacturing* 203 (2026), p. 109588. ISSN: 1359-835X. DOI: 10.1016/j.compositesa.2026.109588.

A. Appendix

A.2. Materials and Methods

Table A.2.1.: Schematic image and process parameters of the three-roll mill.

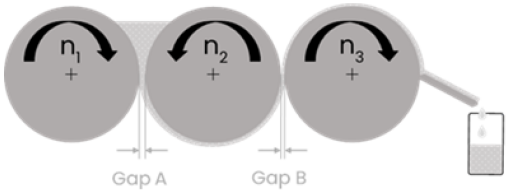

Step	Gap A (µm)	Gap B (µm)	n1 (rpm)	n2 (rpm)	n3 (rpm)
1	120	40	33	100	300
2	40	13	33	100	300
3-7	13	5	33	100	300

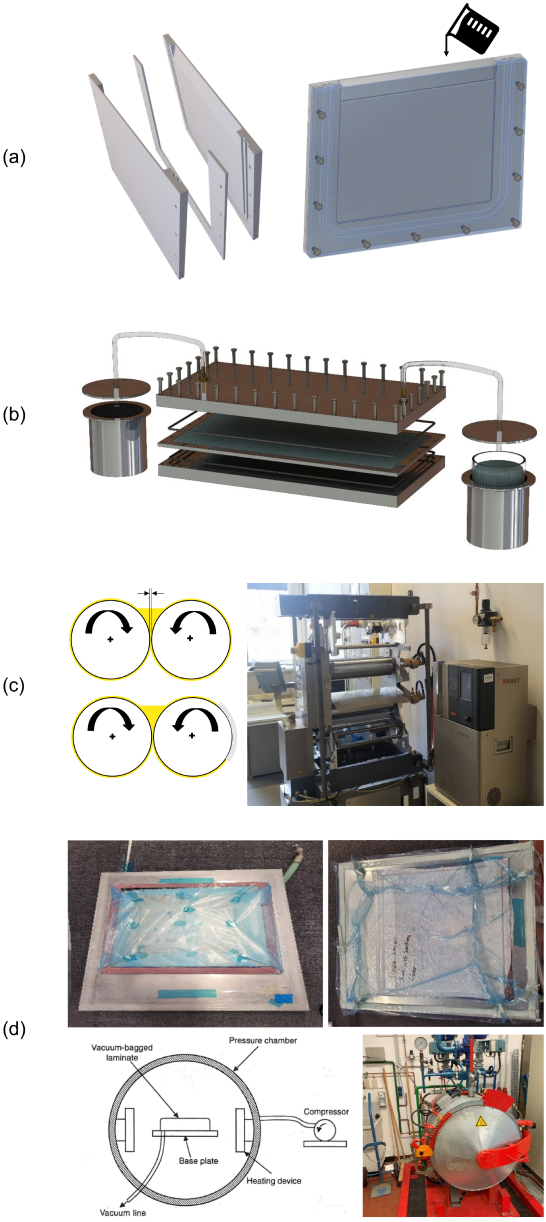

Figure A.2.1.: Manufacturing processes: (a) casting process, (b) RTM process, (c) impregnation roll mill and (d) autoclave process.

A.3. Partially Flame Retardant Composites

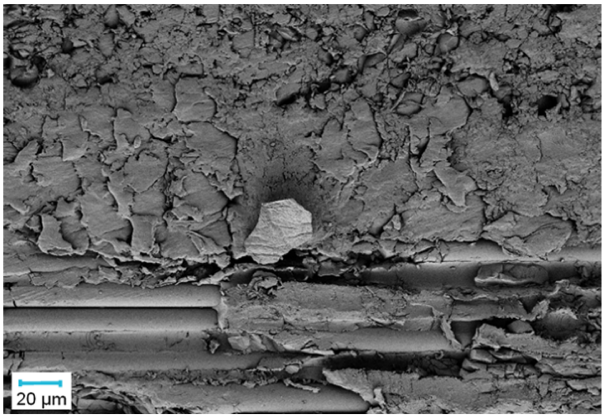

Figure A.3.1.: SEM image of a representative RP particle ($\approx D_{50}$). Due to their size, they are located at the layer boundaries and not between fibres.

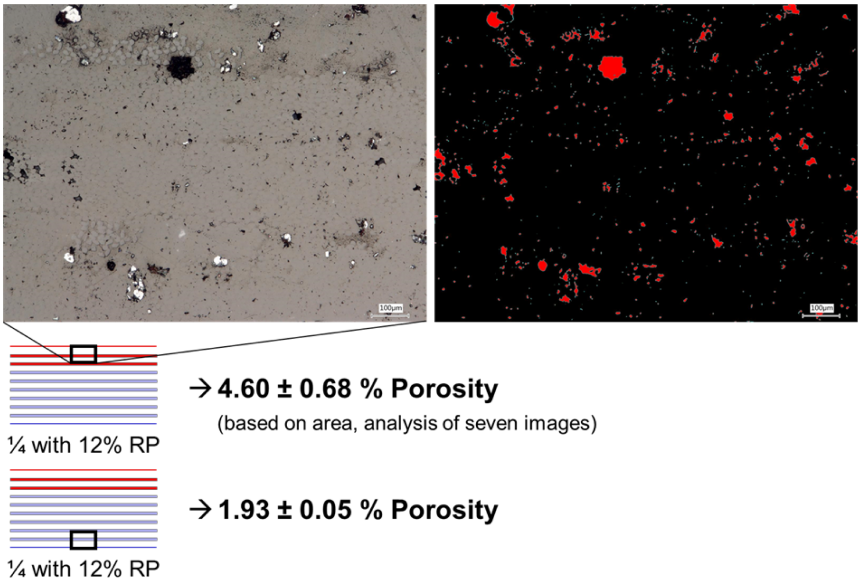

Figure A.3.2.: Porosity evaluation via image analysis.

Table A.3.1.: Densities and fibre-volume ratios for all investigated configurations.

Configuration	Density in g/cm^3	Fibre-Volume Ratio in %
without NW	1.819 ± 0.004	45.2 ± 0.4
with NW	1.825 ± 0.007	45.8 ± 0.4
*pre-cured	1.822 ± 0.008	45.5 ± 0.5
⅛ 6% RP	1.821 ± 0.010	45.3 ± 0.8
⅛ 12% RP	1.824 ± 0.007	45.7 ± 0.6
¼ 12% RP	1.829 ± 0.006	46.1 ± 0.4

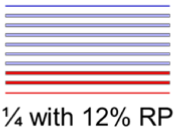

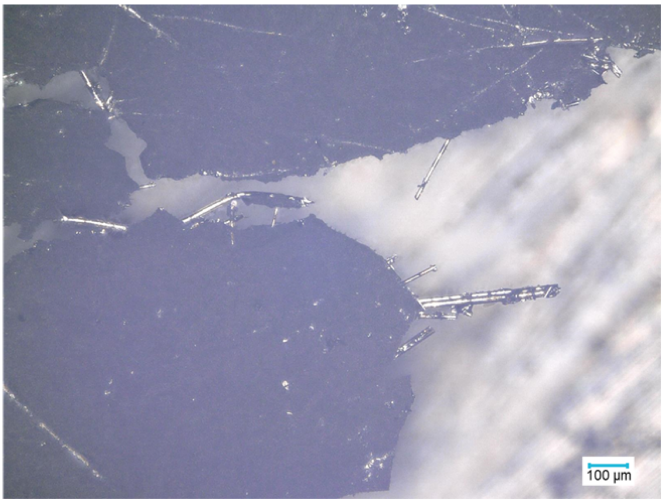

Figure A.3.3.: Char-cracking after compression test (digital microscopy).

Table A.3.2.: Compressive strengths of relevant configurations.

Configuration		Compressive strength in MPa
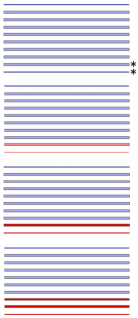	*pre-cured	390.09 ± 11.95
	⅛ 6% RP	379.84 ± 13.22
	⅛ 12% RP	400.94 ± 22.93
	¼ 12% RP	422.96 ± 15.52

A.4. Sustainable Matrix Materials

Table A.4.1.: Linearised temperature profiles and used thermokinetic methods with correlation to the experimental data.

System	Temperature profile in °C	Thermokin. method	Correlation
827/137H	20 to 45 (3 K/min); 45 (140 min); 45 to 110 (0.5 K/min); 110 (85 min); 110 to 20 (- 0.5 K/min)	FM	0.99
827/L-Arg	20 to 167 (4 K/min); 167 (60 min); 167 to 180 (0.05 K/min); 180 (70 min); 180 to 20 (- 0.5 K/min)	KAS	1.02
827/L-Arg/UR500	20 to 160 (1 K/min); 160 to 180 (0.2 K/min); 180 (90 min); 180 to 20 (- 0.5 K/min)	FM	0.91
827/L-Phe/UR500	20 to 96 (1 K/min); 96 (105 min); 96 to 180 (0.9 K/min); 180 to 20 (- 0.5 K/min)	FM	0.97
827/L-Trp/UR500	20 to 102 (4.8 K/min); 102 (123 min); 102 to 150 (0.5 K/min); 150 (200 min); 150 to 20 (- 0.5 K/min)	FM	0.98
SR810/137H	20 to 37 (0.9 K/min); 37 to 50 (0.1 K/min); 50 to 68 (0.2 K/min); 68 to 95 (0.5 K/min); 95 to 180 (1.9 K/min); 180 (100 min); 180 to 20 (- 0.5 K/min)	FM	1.00
SR810/L-Arg	20 to 160.5 (5 K/min); 160.5 (392 min); 160.5 to 20 (- 0.5 K/min)	FM	0.96

Table A.4.2.: Decomposition temperatures and respective mass losses in nitrogen atmosphere.

	M_1 (%)	$T_{d,1}$ (°C)
827/137H	92.25	380.38
827/L-Arg	90.43	376.38
827/L-Arg/UR500	91.92	425.12
827/L-Phe/UR500	88.37	424.47
827/L-Trp/UR500	89.34	429.89
SR810/137H	94.55	338.76
SR810/L-Arg	91.57	362.18

Table A.4.3.: Decomposition temperatures and respective mass losses in synthetic air atmosphere.

	M_1 (%)	$T_{d,1}$ (°C)	M_2 (%)	$T_{d,2}$ (°C)
827/137H	76.09	375.53	23.91	569.63
827/L-Arg	75.08	367.34	24.92	566.42
827/L-Arg/UR500	78.01	419.85	22.00	567.85
827/L-Phe/UR500	68.33	424.25	26.43	564.51
827/L-Trp/UR500	75.62	436.54	24.38	563.32
SR810/137H	78.70	344.00	21.30	569.04
SR810/L-Arg	74.05	342.57	25.95	568.18

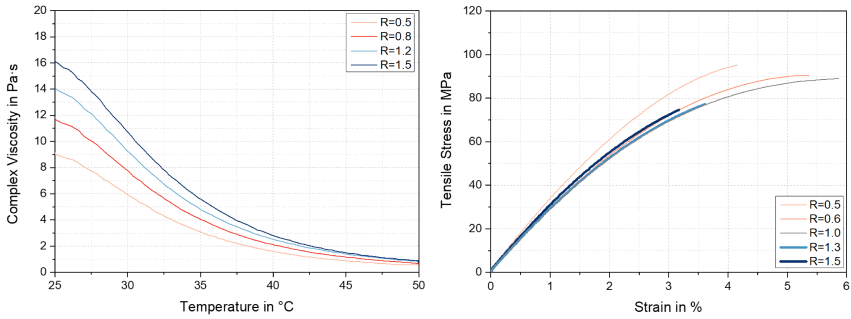

Figure A.4.1.: Temperature-dependent viscosity (left) and representative stress-strain curves (right) for selected mixing ratios.

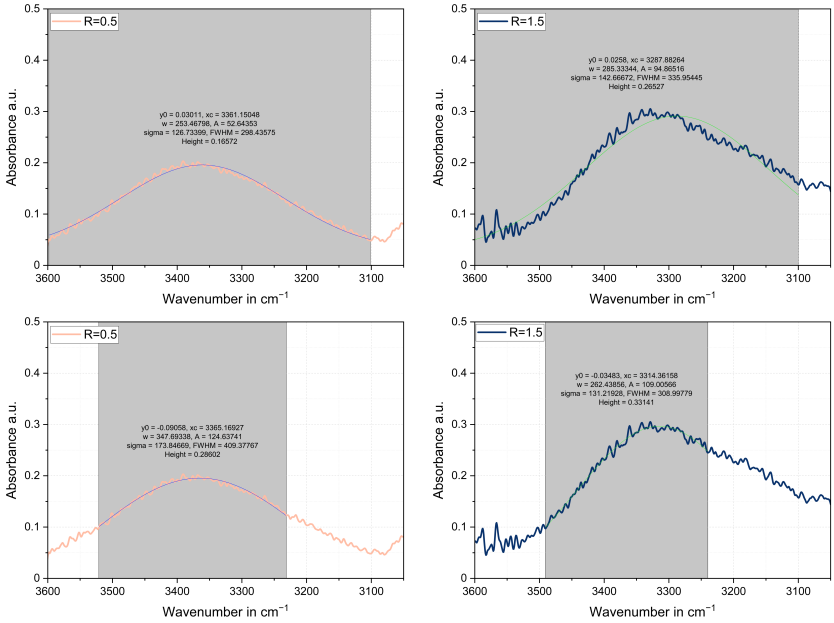

Figure A.4.2.: Determination of peak-positions via gaussian fitting to evaluate the occurring peak shift. Exemplary for R = 0.5 and R = 1.5: Top: Complete peak range as boundary. Bottom: Final Boundaries for best-fit of asymmetric peaks.

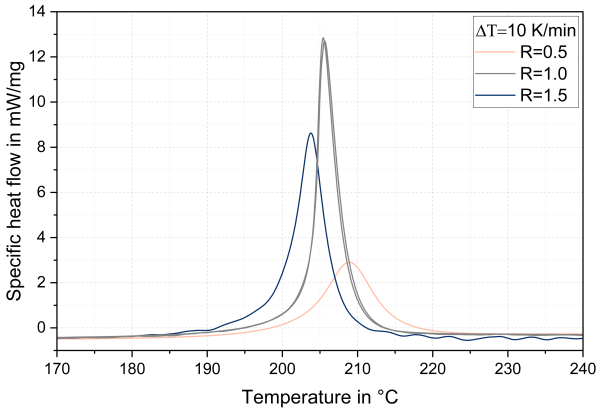

Figure A.4.3.: DSC thermograms of curing with heating rates of 10 K/min. Comparison of the configurations R = 0.5, R = 1.0 and R = 1.5.

Table A.4.4.: Mechanical properties of all configurations.

Stoichiometric Ratio R	Tensile Strength in MPa	Elongation at Break in %	Young's Modulus in GPa	Complex Modulus in GPa
0.5	95.81 ± 4.05	4.44 ± 0.54	3.42 ± 0.11	3,61 ± 0,09
0.6	92.04 ± 3.81	5.95 ± 0.72	3.09 ± 0.12	3,25 ± 0,00
0.7	88.99 ± 3.05	7.05 ± 0.76	2.79 ± 0.09	2,99 ± 0,07
0.8	90.17 ± 1.27	7.16 ± 0.34	2.81 ± 0.15	2,90 ± 0,02
0.9	87.87 ± 3.78	6.17 ± 0.51	2.80 ± 0.13	2,93 ± 0,01
1.0	87.31 ± 1.40	5.97 ± 0.75	2.90 ± 0.11	2,97 ± 0,01
1.1	72.24 ± 2.02	3.30 ± 0.23	2.92 ± 0.08	3,09 ± 0,00
1.2	74.82 ± 1.89	3.55 ± 0.19	3.01 ± 0.10	3,05 ± 0,03
1.3	74.69 ± 4.53	3.45 ± 0.30	3.07 ± 0.08	3,16 ± 0,00
1.4	73.86 ± 2.42	3.54 ± 0.25	2.98 ± 0.05	3,12 ± 0,05
1.5	73.25 ± 2.83	3.11 ± 0.09	3.27 ± 0.10	3,19 ± 0,00

Table A.4.5.: Glass-transition temperatures of all configurations.

Stoichiometric Ratio R	T_g DSC Midpoint in °C	T_g DMA Onset in °C
0.5	082.35 ± 0.75	083.11 ± 0.29
0.6	106.10 ± 0.30	108,95 ± 0.76
0.7	120.30 ± 1.00	122.09 ± 0.72
0.8	123.70 ± 1.00	128.13 ± 1.10
0.9	122.05 ± 0.05	127.65 ± 0.41
1.0	121.35 ± 0.35	127.09 ± 1.97
1.1	114.15 ± 0.05	116.96 ± 1.03
1.2	114.85 ± 0.25	118.05 ± 0.85
1.3	115.15 ± 0.15	119.38 ± 0.78
1.4	114.55 ± 0.15	117.34 ± 1.17
1.5	115.80 ± 1.50	117.81 ± 1.22

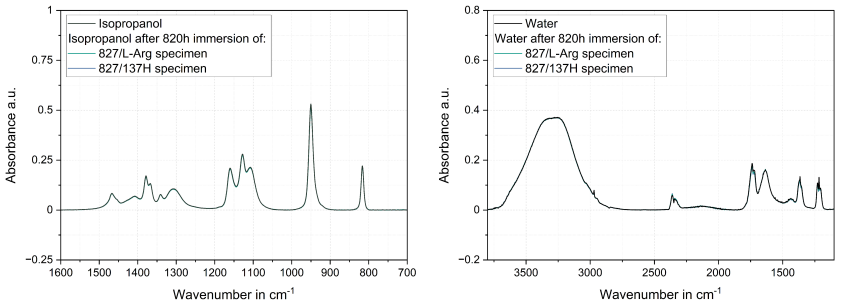

Figure A.4.4.: FTIR-spectra of isopropanol (left) and demineralised water (22 °C) without and after immersion of 827/L-Arg and 827/137H specimens.

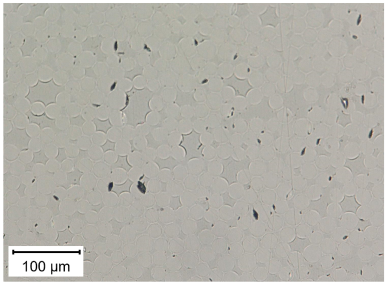

Figure A.4.5.: Microscopy image of glass fibre-reinforced 827/137H manufactured with DirectPreg process.

Table A.4.6.: Linearised temperature profiles. Thermokinetic method: FM.

System	Temperature profile in °C
ELO/CA (max. 100°C)	20 to 65 (5 K/min); 65 to 90 (1.3 K/min); 90 to 100 (0.3 K/min); 100 (380 min); 100 to 20 (-0.5 K/min)
ELO/CA (max. 120°C)	20 to 65 (5 K/min); 65 to 84.7 (1.4 K/min); 84.7 to 96.2 (0.6 K/min); 96.2 to 98.6 (0.05 K/min); 98.6 to 112.5 (1 K/min); 112.5 to 120 (2 K/min); 120 (99 min); 120 to 20 (-0.5 K/min)
ELO/CA (max. 140°C)	20 to 65 (5 K/min); 65 to 79.9 (1.5 K/min); 79.9 to 95.9 (0.8 K/min); 95.9 to 98.3 (0.1 K/min); 98.3 to 112.5 (1 K/min); 112.5 to 140 (2.2 K/min); 140 (11 min); 140 to 20 (-0.5 K/min)
ELO/CA (max. 160°C)	20 to 65 (5 K/min); 65 to 84.7 (1.4 K/min); 84.7 to 97.4 (0.6 K/min); 97.4 (29 min); 97.4 to 120.4 (1.2 K/min); 120.4 to 160 (3.2 K/min); 160 to 20 (-0.5 K/min)
ELO/CA (max. 180°C)	20 to 65 (5 K/min); 65 to 88.3 (1.3 K/min); 88.3 to 97 (0.5 K/min); 97 to 98.8 (0.05 K/min); 98.8 to 120.9 (1.3 K/min); 120.9 to 180 (3.5 K/min); 180 to 20 (-0.5 K/min)
ELO/ITA Model 1	70 to 110 (5 K/min); 110 (52 min); 110 to 118 (0.8 K/min); 118 to 140 (3 K/min); 140 (42.7 min); 140 to 20 (-0.5 K/min)
ELO/ITA Model 2	70 to 105 (5 K/min); 105 (43 min); 105 to 115 (0.4 K/min); 115 to 140 (1.5 K/min) 140 (28.4 min); 140 to 20 (-0.5 K/min)

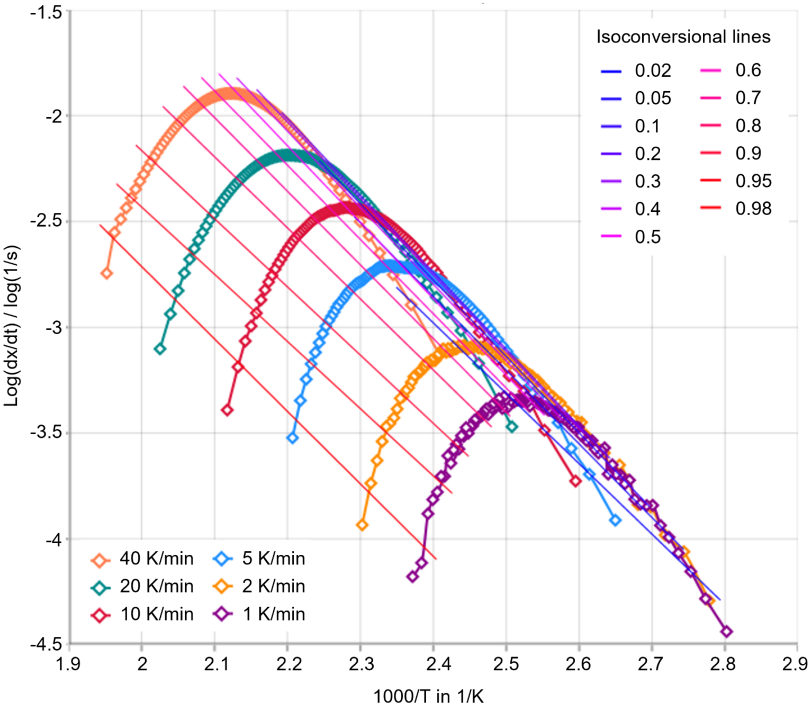

Figure A.4.6.: Friedman plot (ELO/ITA, Model 2).

A.5. Flame-Retardancy of Biomolecules

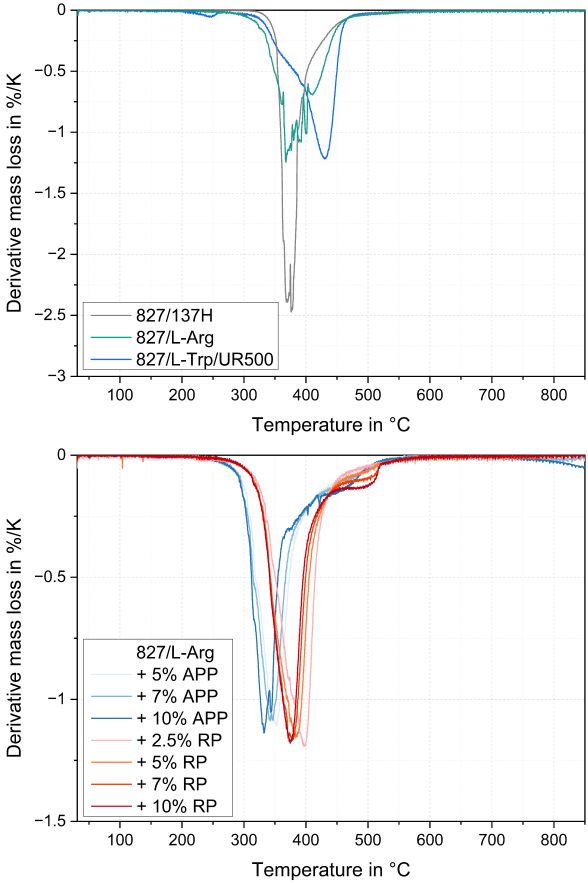

Figure A.5.1.: Temperature-dependent derivative mass loss of neat epoxies (left) and modified 827/L-Arg (bottom), nitrogen atmosphere.

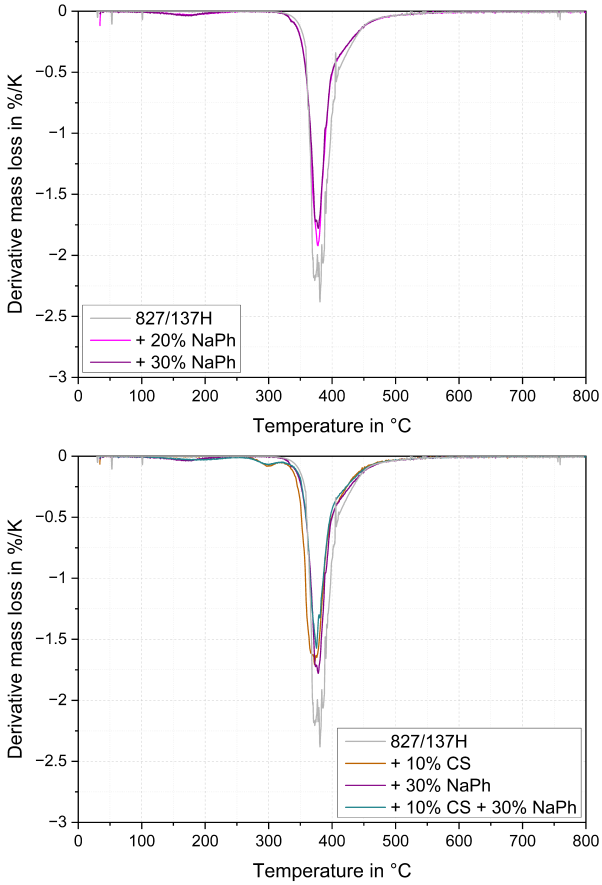

Figure A.5.2.: Derivative mass loss (DTG) for NaPh-modified 827/137H (left) and NaPh and/or CS modified 827/137H in nitrogen atmosphere.